Sperm Guidance in Zebrafish

Dissertation

zur

Erlangung des Doktorgrades (Dr. rer. nat.)

der

Mathematisch-Naturwissenschaftlichen Fakultät

der

Rheinischen Friedrich-Wilhelms-Universität Bonn

vorgelegt von

Kai Korsching

aus

Tübingen

Bonn 2023

Angefertigt mit Genehmigung der Mathematisch-Naturwissenschaftlichen Fakultät
der Rheinischen Friedrich-Wilhelms-Universität Bonn

Gutachter und Betreuer: Ulrich Benjamin Kaupp
Gutachter: Michael Famulok

Tag der Promotion: 22.02.24
Erscheinungsjahr: 2024

Abstract

The core challenge of the fertilization process is one of pathfinding: how do motile sperm cells locate the immotile oocyte? In some species, this process is well studied, e.g. sea urchin and human. Both species employ chemotaxis—the orientation along a three-dimensional gradient of a chemoattractant—to facilitate pathfinding of sperm towards the oocyte. But the molecular implementation differs considerably between the two species. Overall, great variation is found in fertilization processes even between closely related species. Zebrafish is a widely used vertebrate model system, yet very little is known about how their sperm function. In my thesis, I approached the question of pathfinding in zebrafish sperm from several angles.

First, I performed extensive bioinformatic studies in jawless, cartilaginous, and bony fishes to elucidate the presence or absence of several components of the signaling cascades involved in pathfinding. I showed a fine-grained pattern of many independent gene losses for the CatSper channel complex and soluble adenylate cyclase (sAC), both of which are considered essential for sperm motility in species as distantly related as sea urchin and human. In particular, both CatSper and sAC are clearly absent in zebrafish. Synteny analysis between the genome of zebrafish and the closely related goldfish, which possesses CatSper, showed chromosomal breakpoints as likely origin of the loss for all four subunits of the CatSper channel. By comparison with related species I could deduce that CatSper was lost at the origin of the family Danionidae, whereas sAC was already lost earlier, at the origin of the order Cypriniformes. The absence of these proteins in zebrafish means that signaling in zebrafish sperm must function in a manner yet unknown.

Second, I investigated the proteome of the egg envelope (chorion) using mass spectroscopy to identify potential chemoattractant candidates for haptotaxis (orientation along a two-dimensional gradient of a tethered chemoattractant). Zebrafish chorion possess a micropyle, an opening that allows the sperm access to the oocyte. I found no difference in the proteome between chorion samples that contained the micropyle and those that did not. The main components of the zebrafish chorion are zona pellucida (ZP) proteins. I identified 20 ZP proteins in the proteome and assigned their respective subfamilies. Interestingly, ZPB and ZPC proteins are present, which are required for the acrosome reaction in mammals, although zebrafish possess a micropyle and therefore do not use the acrosome reaction.

Third, I established a baseline of motility behavior and internal ion changes of activated but unstimulated zebrafish sperm through dark-field and fluorescence microscopy. Swimming paths vary greatly in curvature, although the majority displays lower curvature. Cytosolic calcium increases during initiation of motility, via release from internal stores. The sperm also acidify, in contrast to sea urchin, human, and mouse, where the sperm alkalizes. Next, I tested oocyte-derived stimulus on the sperm, but found no indication that zebrafish sperm employ chemotaxis.

Last, I discovered regularly spaced, dye-accumulating structures in the sperm flagellum. They may correspond to vesicular bodies of unknown function described so far only morphologically.

My results form a basis for future studies to fully elucidate signaling in zebrafish sperm.

Zusammenfassung

Die große Herausforderung im Befruchtungsvorgang ist die Wegfindung: Wie lokalisieren motile Spermienzellen die unbewegliche Oozyte? In manchen Spezies ist dieser Vorgang gut untersucht, z.B. Seeigel und Mensch. Beide Spezies verwenden Chemotaxis—die Orientierung entlang eines dreidimensionalen Lockstoffgradienten—um die Wegfindung zur Oozyte zu ermöglichen. Jedoch unterscheidet sich die molekulare Implementierung erheblich zwischen den beiden Spezies. Insgesamt beobachtet man eine große Variation in Befruchtungsvorgängen sogar zwischen nah verwandten Spezies. Zebrabärbling ist ein häufig eingesetztes Modellsystem für Vertebraten, allerdings ist nur wenig darüber bekannt, wie die Spermien ihren Weg finden. In meiner Doktorarbeit habe ich diese Frage der Wegfindung von Zebrabärblingsspermien von verschiedenen Blickwinkeln untersucht.

Zunächst führte ich ausführliche bioinformatische Studien durch, um die An- oder Abwesenheit von mehreren Komponenten der beteiligten Signalisierungskaskaden in kieferlosen, Knorpel- und Knochenfischen aufzuklären. Ich konnte ein feinkörniges Muster von vielen unabhängigen Genverlusten für den CatSper Kanalkomplex und die lösliche Adenylatcyclase (sAC) zeigen, die beide, in so entfernt verwandten Spezies wie Seeigel und Mensch, als essentiell für Spermienmotilität erachtet werden. Insbesondere besitzt Zebrabärbling weder CatSper noch sAC. Syntenieanalyse zwischen dem Genom des Zebrabärblings und des nah verwandten Goldfischs, der CatSper besitzt, zeigte chromosomale Bruchstellen als den wahrscheinlichen Ursprung für den Verlust von allen vier CatSper Kanaluntereinheiten. Durch den Vergleich mit verwandten Spezies konnte ich schließen, dass CatSper am Ursprung der Familie Danionidae verloren ging, wohingegen sAC bereits am Ursprung der Ordnung Cypriniformes verloren ging. Die Abwesenheit dieser Proteine im Zebrabärbling bedeutet, das Signalisierung in Zebrabärblingspermien auf bisher unbekannte Weise funktionieren muss.

Zweitens untersuchte ich das Proteom der Eihülle (Chorion) mittels Massenspektroskopie, um potentielle Lockstoffkandidaten für Haptotaxis (Orientierung entlang eines zweidimensionalen Gradienten von einem gebundenen Lockstoff) zu ermitteln. Das Chorion des Zebrabärblings besitzt eine Mikropyle, eine Öffnung, die den Spermien Zugang zur Oozyte erlaubt. Ich fand keinen Unterschied im Proteom zwischen Chorionproben, die die Mikropyle enthielten, und denen, die es nicht enthielten. Die primären Komponenten des Chorions sind Zona Pellucida (ZP) Proteine. Ich identifizierte 20 ZP Proteine im Proteom, die alle den bekannten ZP Unterfamilien zugeordnet werden konnten. Interessanterweise waren ZPB und ZPC Proteine vorhanden, die in Säugetieren für die Akrosomreaktion vonnöten sind, obwohl Zebrabärblinge eine Mikropyle besitzen und daher die Akrosomreaktion nicht aufweisen.

Drittens etablierte ich eine Baseline für das Motilitätsverhalten und die internen Ionenänderungen von aktivierten aber nicht stimulierten Zebrabärblingspermien mittels Dunkelfeld- und Fluoreszenzmikroskopie. Die Schwimmpfade variieren stark in der Krümmung, allerdings weist der Großteil geringere Krümmung auf. Zytosolisches Kalzium steigt während der Initiierung von Bewegung durch die Freisetzung aus internen Speichern an. Der pH der Spermien sinkt außerdem, im Unterschied zu Seeigel, Mensch und Maus, in denen die Spermien

alkalisieren. Als Nächstes testete ich Oozytenextrakte an den Spermien des Zebrabärblings, aber fand keinen Hinweis, dass sie Chemotaxis verwenden.

Schließlich entdeckte ich Farbstoff-anreichernde Strukturen im Spermienflagellum, die in regelmäßigen Abständen vorkommen. Diese könnten bisher nur morphologisch beschriebenen Vesikulärkörpern entsprechen, deren Funktion noch unbekannt ist.

Meine Ergebnisse bilden eine Grundlage für zukünftige Studien, um die Signalisierung in Spermien des Zebrabärblings vollständig aufzuklären.

Preface

Parts of this thesis' results were previously published in:

Rafati, Nima, Junfeng Chen, Amaury Herpin, Mats E. Pettersson, Fan Han, Chungang Feng, Ola Wallerman, et al. 2020. "Reconstruction of the Birth of a Male Sex Chromosome Present in Atlantic Herring." *Proceedings of the National Academy of Sciences* 117 (39): 24359–68. https://doi.org/10.1073/pnas.2009925117.

Acknowledgements

I would like to express my gratitude to the many people who have contributed in different ways to make this thesis possible.

Firstly, Prof. Dr. U. Benjamin Kaupp for trusting me with this project, supporting me as a scientist, as well as his interest and constructive feedback in the writing of this thesis. I am grateful to Dr. Reinhard Seifert for his supervision, his unfailing scientific advice, and constructive criticism. I would like to thank Prof. Dr. Benjamin Odermatt for being part of my thesis advisory committee, my exam committee, and last but not least for the donation of zebrafish. Thanks go to Christian Trötschel for carrying out MS measurements, to Dr. Heinz Körschen, Dr. René Pascal, and Dr. Louis Alvarez for their advice and support in molecular biology and fluorometric methods, and to Prof. Dr. Sigrun Korsching for introducing me to bioinformatics. I am grateful to my PhD colleagues for many fun, interesting, and also helpful discussions, especially I want to thank Lea Wobig and Elena Grahn for their support and advice. Verena Juchems and Dr. Stefan Pauls have been another much appreciated source of zebrafish for my projects. Prof. Dr. Michael Pankratz and Prof. Dr. Michael Famulok have kindly agreed to be part of my exam committee. I am thankful to Heike Krause for her excellent help in organisational matters, and more.

Last but not least I would like to express my gratitude to my family and friends for their invaluable and unwavering support in good and bad times.

Table of contents

List of abbreviations

°C	Degrees Celsius
ABC transporter	ATP-binding cassette transporter
ABHD2	Abhydrolase domain-containing protein 2
AM-ester	Acetoxy-methyl-ester
ATP	Adenosine triphosphate
BCECF	2',7'-bis-(2-carboxyethyl)-5-(and-6)-carboxyfluorescein
cAMP	Cyclic adenosine monophosphate
CatSper	Sperm-specific cation channel
CHO cells	Chinese hamster ovarian cells
CNGK channel	Cyclic nucleotide-gated potassium channel
ddH_2O	Double-distilled water
DNA	Desoxyribonucleic acid
ECACC	European Collection of Authenticated Cell Cultures
ES	Extracellular solution
EtOH	Ethanol
F	Fluorescence
F_0	Initial fluorescence
FWHM	full width at half maximum
HCN channel	Hyperpolarization-activated cyclic nucleotide–gated
Hv1 channel	Voltage-gated proton channel
Hz	Hertz
IC_{50}	Half maximal inhibitory concentration
LCM	Laser Capture Microdissection
LIN	linearity
M	Molar

MeCN	Acetonitrile
mg	Milligram
min	Minutes
ml	Milliliter
NHA1	Sodium-proton antiporter 1
OAT	Organic anion transporter
PBS	Phosphate-buffered saline
PKA	Protein kinase A
PKD2	Polycystic kidney disease 2-like 1 protein
RT	Room temperature
s	Second
s.d.	standard error
sAC	Soluble adenylyl cyclase
SDS	Sodium dodecyl sulfate
SDS-PAGE	Sodium dodecyl sulfate polyacrylamide gel electrophoresis
SLC22	Solute carrier family 22
Slo3 channel	Potassium channel of Slo family
sNHE	Sperm-specific sodium-proton-exchanger
STE	steadiness
sysH_2O	System water
t	Time
TRPP2	Transient receptor potential polycystic 2
TRPV1	Transient receptor potential cation channel subfamily V member 1
TRPV4	Transient receptor potential cation channel subfamily V member 4
VAP	Velocity Average-Path
VCL	Velocity Curvilinear
VSL	Velocity Straight Line

ZP	Zona pellucida
µl	Microliter
µm	Micrometer

1. Introduction

Fertilization constitutes a fundamental process in all sexually reproducing species. It is defined as the fusion of two haploid gametes, sperm cell and egg cell (oocyte), which allows the formation of a new diploid organism (Siu et al. 2021). The initial step in fertilization is the activation of quiescent sperm, resulting in initiation of motility. Without exception, sperm are immotile in the testis (Morisawa and Suzuki 1980; Alavi et al. 2019) and become motile upon contact with the external medium (Morisawa and Suzuki 1980; Alavi et al. 2019) or, at the latest, upon contact with the oocyte (Yanagimachi et al. 1992; Griffin et al. 1996). This activation is induced through hyper- or hypoosmotic shock in many external fertilizers such as fishes (Morisawa and Suzuki 1980; Hamamah and Gatti 1998; Cosson 2004; Wilson-Leedy, Kanuga, and Ingermann 2009). In internal fertilizers, the new environment encountered in the fertilization tract, or processes accompanying ejaculation, lead to the sperm becoming activated (Hamamah and Gatti 1998).

The next step for the sperm is to locate the oocyte. This task, while uniform in its basic simplicity across most species, has to be accomplished under vastly different circumstances: some species are internal fertilizers (such as mammals and birds), whereas others are external fertilizers (such as many fish and marine invertebrates, like sea urchin, Alvarez 2017). External fertilizers subdivide into those reproducing in freshwater and those in sea water (Ward and Kopf 1993). However, a common feature of nearly all species is that sperm are motile, whereas oocytes are immotile (Luconi and Baldi 2003). Thus, sperm cells must locate the oocyte and steer to it. In a large variety of species (fish, insects), sperm's pathfinding is complex: once the oocyte has been reached, sperm must locate the micropyle, a small opening in the egg envelope (called chorion in fish) through which sperm can access the plasma membrane for fusion (Amanze and Iyengar 1990; Yanagimachi et al. 2013). By contrast, in humans for example, the sperm can fuse with the oocyte at any point of its surface because the sperm carries an acrosomal cap which enables penetration of the egg envelope (Gupta 2021).

How do sperm deal with these pathfinding problems? Generally, cells employ a variety of guidance mechanisms—chemotaxis, haptotaxis, rheotaxis, and thermotaxis—to locate the oocyte or the micropyle. Chemotaxis describes the orientation along a three-dimensional gradient of a chemoattractant, whereas haptotaxis is the orientation along a surface-tethered chemoattractant gradient. Rheotaxis means swimming against fluid flow. Thermotaxis is the orientation along a temperature gradient.

Sperm of various species have been found to employ such mechanisms either alone or in combination (Ward et al. 1985; Fukuda et al. 2004; Publicover et al. 2008; Bönigk et al. 2009; Lishko, Botchkina, and Kirichok 2011). For example, human sperm cells employ rheotaxis for long-range guidance (Miki and Clapham 2013) and possibly chemotaxis for near-range guidance (Oren-Benaroya et al. 2008; Strünker et al. 2011), whereas sea urchin sperm only make use of chemotaxis (Ward et al. 1985). Herring sperm does

not use chemotaxis, but may use haptotaxis to reach the micropyle (Griffin et al. 1996; Yanagimachi et al. 2017). Of note: The mechanisms underlying steering to the oocyte are far from well-established and are a matter of dispute. Even when two species employ the same mechanism, it may be implemented differently. For example, the chemoattractants used in chemotaxis differ not only between sea urchin and human—short peptide and possibly a steroid, respectively (Ward et al. 1985; Oren-Benaroya et al. 2008; Strünker et al. 2011)—but even between two different sea urchin species (*Arbacia punctulata* and *Strongylocentrotus purpuratus*), which use different peptides as chemoattractants (resact and speract, respectively, Ward et al. 1985). Furthermore, the source of the chemoattractant may also differ: In sea urchin, the oocyte itself releases the chemoattractant, while in human, the cumulus cells surrounding the oocyte do (Ward et al. 1985; Oren-Benaroya et al. 2008). Moreover, the underlying signaling cascades also differ greatly.

Species-specific mechanisms in fertilization are widespread and are assumed to aid in speciation (Palumbi 2009; Gert and Pauli 2020). Indeed, reproductive proteins are known for rapid evolution, often involving positive selection (Tsaur and Wu 1997; Swanson and Vacquier 2002; Galindo, Vacquier, and Swanson 2003; Pujolar and Pogson 2011). This variation is what makes fertilization in general and sperm specifically so fascinating but on the downside also difficult to study.

1.1. Commonalities and differences in sperm signaling cascades

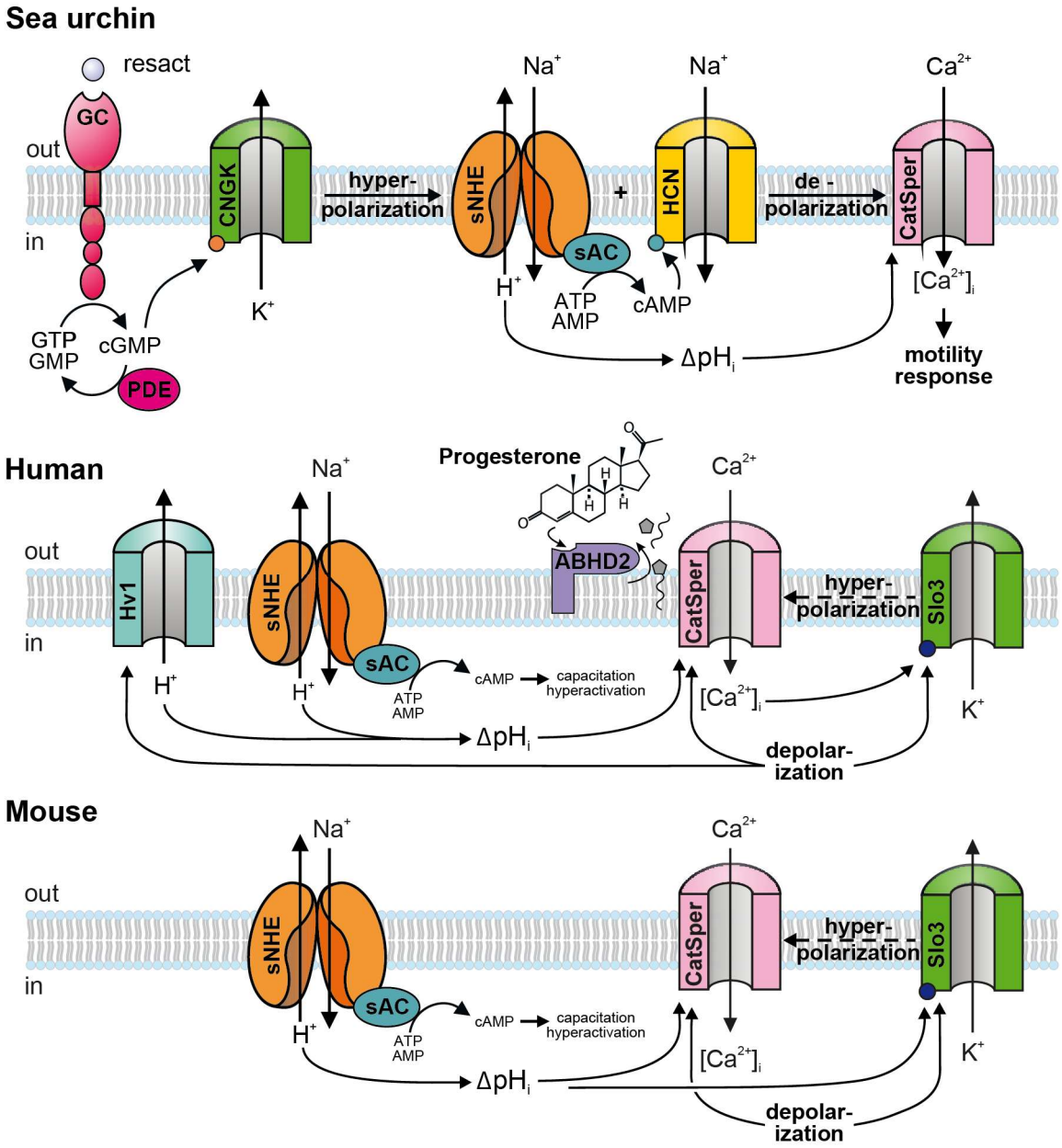

Figure 1: Sperm signaling cascades in sea urchin, human, and mouse (adapted from Kaupp and Strünker 2017). GC: guanylate cyclase. CNGK: cyclic nucleotide-gated potassium channel. Hv1: voltage-gated proton channel. sNHE: sperm-specific sodium-proton exchanger. sAC: soluble adenylate cyclase. HCN: hyperpolarization-activated, cyclic nucleotide-gated channel. CatSper: sperm-specific cation channel. Slo3: sperm-specific Slo ion channel. ABHD2: alpha/beta hydrolase domain-containing protein 2. Dotted arrows indicate inhibitory function.

The best known signaling cascade underlying chemotaxis is that from sea urchin (Figure 1), in particular *Arbacia punctulata* (Kaupp and Strünker 2017). Here, the chemoattractant resact is recognized by a membrane-bound guanylyl-cyclase receptor (GC), which generates the second messenger cGMP. The

high density of GC along the flagellum enables sea urchin sperm to detect single molecules of resact (Strünker, Alvarez, and Kaupp 2015). cGMP induces a hyperpolarization via a CNGK channel, which activates the sperm-specific sodium-proton exchanger (sNHE) leading to alkalization. The soluble adenylate cyclase (sAC), which is associated with sNHE, generates cAMP. This, in combination with the hyperpolarization, activates a hyperpolarization-activated and cyclic nucleotide-gated (HCN) channel. Sodium influx via HCN leads to depolarization. Along with the preceding alkalization, this activates the sperm-specific Ca^{2+} channel, CatSper. Opening of CatSper leads to an influx of calcium that triggers a steering response in the sea urchin sperm (Kaupp and Strünker 2017; Rafati et al. 2020).

In human sperm, a few elements of the sea urchin signaling pathway are used, but put into a different context (Figure 1). Intracellular alkalization also plays an essential role, being caused not only by sNHE but also by the proton-selective channel Hv1 (Wachten, Jikeli, and Kaupp 2017; Vyklicka and Lishko 2020; Cavarocchi et al. 2021). However, it is not yet understood how sNHE itself is activated. Hv1 is activated by depolarization, which may be caused by the temperature-sensitive TRPV4 (Mundt, Spehr, and Lishko 2018). sAC is associated with sNHE, but the cAMP it generates activates protein kinase A (PKA) instead of a HCN channel, contributing over subsequent steps to capacitation and hyperactivation of sperm. CatSper is an essential component as well. Its threshold of activation is modified by progesterone, which binds to a lipid hydrolase (ABHD2). ABHD2 reduces the inhibition of CatSper at rest and allows opening of the channel. The resulting calcium influx into the sperm triggers a steering response. The calcium influx together with the depolarization (possibly by TRPV4, Mundt, Spehr, and Lishko 2018) also generate a negative feedback by activation of the potassium channel Slo3, which hyperpolarizes the sperm by potassium efflux and thus leads to the closing of CatSper (Vyklicka and Lishko 2020).

In mouse (Figure 1), similar to human sperm, the sNHE-associated sAC generates cAMP, which contributes to capacitation and hyperactivation. Activation of sNHE itself (and possibly NHA1, another sodium-proton exchanger) leads to alkalization, although so far it is unresolved how sNHE is activated. The alkalization together with depolarization (of unknown origin) activates CatSper, which is highly pH-sensitive. Opening of CatSper generates an influx of calcium and a steering response, as it does in both sea urchin and human. Slo3 is also present in mouse sperm, but is activated by pH and depolarization instead of by calcium and depolarization, as it is in human. The activation of Slo3 leads to hyperpolarization, which contributes to the closing of CatSper (Vyklicka and Lishko 2020).

Similarities among all three signaling pathways are apparent: all three species possess sNHE, sAC, and CatSper. The internal pH rises during signaling, and the last step involves an increase in internal calcium via CatSper. This calcium increase leads to guided motility of sperm, marking internal calcium as an essential factor of sperm motility, and CatSper as keystone of the sperm signaling cascade.

However, despite CatSper's indispensable role in species as divergent as sea urchins and humans, it was reported to have been lost in Teleostei (Cai and Clapham 2008). The reliability of such statements obviously depends on the number of species being analyzed, and in fact a later study analyzing 12 ray-finned fish species has reported both presence and absence of CatSper (Romero and Nishigaki 2019b). Due to the recent availability of a multitude of sequenced fish genomes, I decided to re-investigate this question by performing a phylogenetic study with several hundred species. Here I observed a fine-grained pattern of CatSper presence and absence throughout evolution of jawless, cartilaginous, and bony fishes.

1.2. Fertilization in zebrafish

Zebrafish (Figure 2) is an established vertebrate model system for biological research. Initially, zebrafish were used to study early development due to the transparency of their larvae and development outside the mother. In recent decades, the focus has broadened considerably. Many genetic methods have been developed for zebrafish, including transgenesis, knock-out and knock-in (Lieschke and Currie 2007). The zebrafish genome project was begun in 2001 (Jekosch 2004). The current genome release GRCz11 contains over 25000 annotated protein-coding genes and over 6000 non-coding genes ("Danio_rerio - Ensembl Genome Browser 109" 2023). Despite the large evolutionary distance of over 400 million years to humans (Kumar et al. 2017), over 70–80% of human disease-related genes have an ortholog in zebrafish (Howe et al. 2013; Zang et al. 2022). Accordingly, mechanisms and therapeutic possibilities for manifold diseases have been studied in zebrafish (Lieschke and Currie 2007).

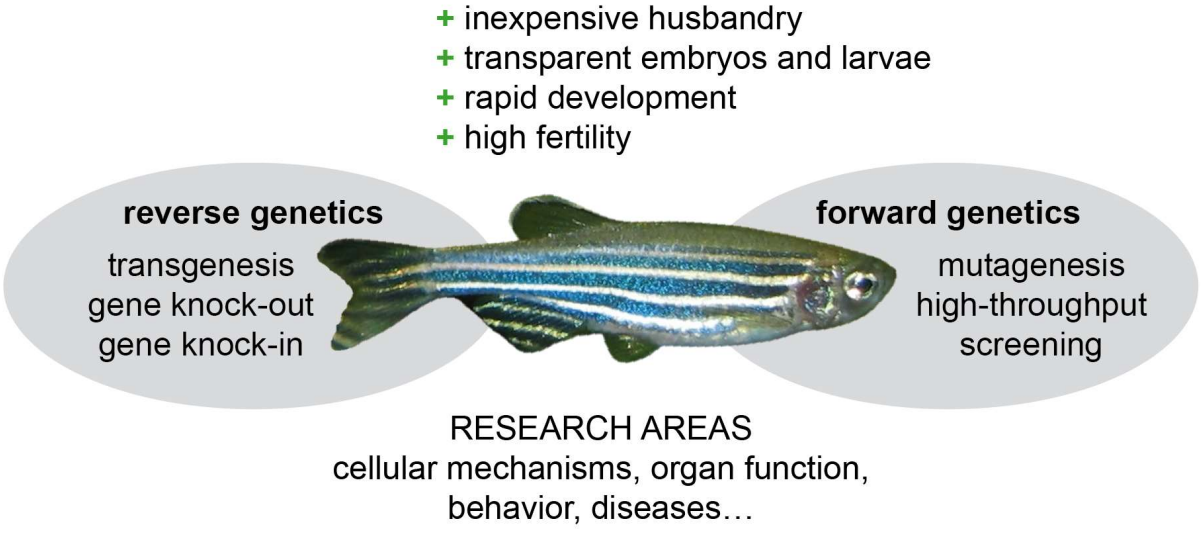

Figure 2: Advantages of zebrafish as an animal model, applicable genetic methods, and areas of research.

Zebrafish are well-suited as a model system because they are easy to keep, require less space than mice, and can spawn every few days under good conditions, producing more than 100 oocytes per

spawning session (Westerfield 2007). As such, zebrafish present a good opportunity to study sperm guidance mechanisms.

CatSper appears to be absent in zebrafish (Romero and Nishigaki 2019b). If that holds true, their sperm guidance mechanisms must necessarily differ on a molecular level than in other species that harbor CatSper (Figure 1), and present therefore a promising research topic. In the following, I will discuss what is already known about zebrafish fertilization.

Zebrafish live in freshwater and are external fertilizers (Hoo et al. 2016). Sperm motility is induced through hypoosmotic shock, which occurs upon contact with freshwater (Wilson-Leedy, Kanuga, and Ingermann 2009). Internal body fluids of the zebrafish have an osmolarity of roughly 300 mOsm, while freshwater is generally below 10 mOsm (Takai and Morisawa 1995). For comparison, sea water has between 650–1000 mOsm (Einarson 1993).

Due to being external fertilizers, there are no physical restraints on the movement of sperm as there would be for internal fertilizers. Thus, fluid flow and temperature cannot serve as potential guidance cues. Due to external fertilization, zebrafish must coordinate the release of their gametes. This release occurs during a mating dance, where male and female fish swim closely side-by-side (Zempo et al. 2021). The induction of this spawning behavior has been extensively studied in goldfish, which belong to the same order as zebrafish, Cypriniformes (Stout et al. 2016). They use reproductive hormones (steroids and prostaglandins) concomitantly as exogenous signals (pheromones) to synchronize male and female spawning behavior (Kobayashi, Sorensen, and Stacey 2002).

In zebrafish, the sperm are not deposited directly onto oocytes (Zempo et al. 2021), meaning they have to locate first the oocyte and subsequently the micropyle (Hart and Donovan 1983). Moreover, the timeframe in which fertilization is possible is short—sperm swim only roughly one minute after activation (Wilson-Leedy, Kanuga, and Ingermann 2009), and the micropyle of the oocytes becomes impermeable due to formation of a fertilization cone about a minute after contact with freshwater (Hart, Becker, and Wolenski 1992). Despite these obstacles, zebrafish are very efficient at fertilization (Gonzales Jr 2012).

Two components of the sea urchin signaling cascade have been identified in zebrafish sperm: a CNGK channel and an HCN-like channel. Both are characteristically different from their mammalian counterparts. The CNGK channel is not gated by cyclic nucleotides but by pH (Fechner et al. 2015), and the HCN-like channel conducts protons with high selectivity instead of sodium ions (Wobig et al. 2020).

However, there remain many fundamental questions to be answered: Is CatSper truly absent in zebrafish (because no genome sequence is ever 100% complete) ? What role do CNGK and HCN-like play in the signaling cascade of zebrafish sperm? Do zebrafish sperm employ additional signaling components, such as sNHE, Slo3 or sAC? Do chorion components play a role in guiding zebrafish sperm, as they do in herring sperm? Do zebrafish sperm employ a guidance mechanism at all? As a

prerequisite to examine this question, what is the swimming behavior of zebrafish sperm after activation but in the absence of oocytes?

1.3. Aim of this Thesis

The aim of my thesis was to address some of these open questions.

Firstly, phylogenetic analysis will be used to examine the evolution of CatSper and sAC, both large scale (jawless, cartilaginous and bony fish) and fine-grained (within the order of Cypriniformes of which zebrafish is a member). The latter will be combined with synteny analysis to exclude potential deficiencies of the database as possible reason for the absence of CatSper in zebrafish.

Secondly, a proteome analysis of zebrafish chorion will be performed to search for candidate guidance cues.

Thirdly, a baseline of zebrafish motility before contact with potential steering cues from the oocytes, will be established. This will comprise an analysis of swimming paths as well as examination of internal ionic changes upon activation.

Lastly, this baseline will be used as reference to test whether zebrafish sperm employ guidance mechanisms to locate the oocyte and micropyle.

2. Materials & Methods

2.2. Bioinformatics

2.2.1. Phylogenetic analyses

Phylogenetic searches for CatSper1–4 and the associated genes CatSperB, G, D, and E were carried out as described in Rafati et al. (2020).

Searches for sAC were carried out in a similar manner, described in detail in Körschen et al. (in review) as follows: All fish genomes available from NCBI (https://www.ncbi.nlm.nih.gov/genome/) as of November 2021 were used. The search was carried out in the default databases for blastp (non-redundant protein sequences, nr) and tblastn (nucleotide collection, nr/nt). For tblastn, some searches were also performed in whole-genome shotgun contigs (wgs). As query sequence, we used Homo sapiens sAC or additional annotated sACs that were more closely related to the target group. The search was restricted to the groups listed in Supplementary Table 1. For searches in wgs, candidate proteins were predicted using genewise (https://www.ebi.ac.uk/Tools/psa/genewise/) (Birney, Clamp, and Durbin 2004) with the query sequence used for tblastn. Candidates were tested using phylogenetic tree analysis including other sAC proteins from that group, a standard list of sAC (human, rat, coelacanth, and lungfish), and as outgroup, members of the family of membrane-spanning adenylate cyclases (tmAC). To construct the tree, sequences were first aligned using the MAFFT tool version 7 (https://mafft.cbrc.jp/alignment/server/) (Katoh et al. 2002; Katoh and Standley 2013). The strategy parameter was set to E-INS-I, otherwise default parameters were used. The alignment was subsequently stripped of gaps using Gap strip/squeeze v2.1.0. (https://hcv.lanl.gov/content/sequence/GAPSTREEZE/gap.html). The gap tolerance threshold was set to 80%. The tree was calculated with the PhyML online tool (http://www.atgc-montpellier.fr/phyml/) (Guindon et al. 2010), with the tree improvement method set to SPR, and the branch support set to chi-square-based aLRT. Candidate proteins, which fall with a high branch support (> 90%) into a sAC clade, were considered validated. For determining the polymorphism sites, validated sAC proteins, along with previously annotated sAC, were aligned with Homo sapiens sAC, using the MAFFT tool. The alignment was stripped of gaps using Gap strip/squeeze v2.1.0 with a gap tolerance of 50–60%. The sites of polymorphism were located by using the Homo sapiens sequence as reference.

The construction of the phylogenetic tree for zona pellucida (ZP) proteins was carried out in the same manner.

2.2.2. Synteny analysis

For the synteny analysis, it was not possible to use established synteny tools, since the goldfish genome was not included in them. Therefore, genes flanking CatSper1 in goldfish had to be identified using the NCBI genome data viewer (https://www.ncbi.nlm.nih.gov/genome/gdv/). This and subsequent steps were repeated for CatSper2–4. Gene names and location for these flanking genes were taken from NCBI to enable searching for their zebrafish orthologs by name in (https://www.ncbi.nlm.nih.gov/gene). Once the synteny region in zebrafish was identified, all genes in that region were identified as described for goldfish. A graphical representation of the sequential arrangement of the genes both in goldfish and zebrafish was created with Adobe Illustrator (Adobe, San José, CA, USA). Lastly, the gene lists for goldfish and zebrafish were compared with regard to arrangement of the genes present in both lists. This allowed the identification of break points and inversions.

2.3. Chemicals and solutions

Basic chemicals were acquired from Applichem (Darmstadt, Germany), Sigma-Aldrich (St. Louis, MO, USA), Carl Roth (Karlsruhe, Germany), Thermo Fisher (Waltham, MA, USA), or Merck Millipore (Darmstadt, Germany). Calbryte fluorescent dyes were acquired from AAT Bioquest (Pleasanton, CA, USA). Ionomycin calcium salt was purchased from Sigma-Aldrich (St. Louis, MO, USA).

All solutions were prepared with double-distilled water (ddH_2O) unless specified otherwise, and either stock solutions (for most salts) or the solid forms of the compounds (HEPES, glucose). Glucose-containing solutions were autoclaved and filtered through a 0.22 μm mesh filter. Solutions were stored at 4 °C, or aliquoted and stored at –20 °C for long-term use.

2.3.1. Solutions for sperm and chorions

Extracellular Solution (ES)	
NaCl	125–140 mM
KCl	5.4 mM
$MgCl_2$	1 mM
$CaCl_2$	1.8 mM
Glucose	10 mM
HEPES	5 mM
NaOH	to adjust to pH 7.4

PBS	
NaCl	130 mM
Na_2HPO_4	7 mM
NaH_2PO_4	3 mM
NaOH	to adjust to pH 7.4

Ringer	
NaCl	116 mM
KCl	2.9 mM
HEPES	5 mM
NaOH	to adjust to pH 7.4

TNE (Bonsignorio et al. 1996)	
Tris/HCl (pH 6.8)	10 mM
NaCl	0.6% (w/v)
EDTA	10 mM
Triton X-100	0.5% (v/v)
PMSF	10 µM
NaOH	to adjust to pH 7.2

system water (sysH_2O)	
RO water	100% (v/v)
InstantOcean	adjusted to 400 µS

Propionic acid in ES	
ES	100% (v/v))
proprionic acid	45 mM

Extracellular Solution, calcium-free	
NaCl	125 mM
KCl	5.4 mM
MgCl2	1 mM
EGTA	5 mM
HEPES	30 mM
NaOH	to adjust to pH 7.4

Coomassie Stock for Chorion staining	
DMSO	100% (v/v)
Coomassie Brilliant Blue G250	2% (w/v)

Hyperosmotic PBS	
PBS	100% (v/v)
NaCl	220 mM

2.3.2. Solutions for SDS-PAGE

Sample buffer (4x)	
Tris/HCl (pH 6.8)	200 mM
SDS	8% (w/v)
2-mercaptoethanol	4% (v/v)
glycerol (87%)	50% (v/v)
bromophenol blue	0.04% (w/v)

Running buffer (tris acetate)	
Tris	250 mM
glycine	1.92 M
SDS	1% (w/v)

Running buffer (nuMOPS, Invitrogen, Thermo Fisher, Waltham, MA, USA)	
SDS	1–3% (w/v)
N,N-dimethylformamide	0.01–0.09% (w/v)

Coomassie Stain	
Coomassie Brilliant Blue R250	0.2% (w/v)
acetic acid (96%)	10% (v/v)
EtOH	30% (v/v)

Coomassie Stain (Colloidal)	
Al2(SO4)3·16H2O	5% (w/v)
EtOH (96%)	10% (v/v)
Coomassie Brilliant Blue G250	0.02% (w/v)
H3PO4 (85%)	2% (v/v)

Destain	
NH4HCO3	40 mM
MeCN	50 % (v/v)

Destain (Colloidal)	
EtOH (96%)	10% (v/v)
H3PO4 (85%)	2% (v/v)

2.4. Animal handling and cell culture

2.4.1. Zebrafish (*Danio rerio*)

Zebrafish (strains: TU, TL, TU/TL, TL/EK) were acquired from Dr. Odermatt (Universität Bonn, Institute for Anatomy) or from the fish facility within the research center Caesar (Dr. Briggman, Department of Computational Neuroethology). In both facilities, zebrafish were kept at 28 °C in pH- and conductivity-controlled system water (sysH_2O), according to general standards (Westerfield 2007). Temporarily, zebrafish were also kept at a small fish facility within the department of Molecular Neuroscience (MNS, Dr. Kaupp, research center Caesar). There, fish were kept with a 14/10 photoperiod in large tanks (60 l) at 28 °C, with pH and conductivity control, and fed with standard flake food (Tetramin, Tetra, Melle).

For fish acquired from Dr. Odermatt, animals used for experiments mostly were euthanized and dissected on site, while the remaining fish and fish acquired from the Briggman group were first transferred to the MNS facility, and prepared there.

2.4.2. CHO cell culture

CHO (Chinese hamster ovary) K1 cells, originally sourced from the European Collection of Authenticated Cell Cultures (ECACC), were used for preliminary experiments in fluorescence imaging. The conditions and methods for the cell culture were as described in Fechner et al. (2015).

2.4.3. SDS-PAGE

SDS-PAGE (sodium dodecyl sulfate–polyacrylamide gel electrophoresis) is a method that allows separation of proteins according to their molecular mass. The basic procedure was carried out as described by Laemmli (1970), with some alterations.

Different kinds of gel were used: gradient gels (4–20% or 3–8%) purchased from invitrogen (Invitrogen, Thermo Fisher, Waltham, MA, USA) or Sigma-Aldrich (St. Louis, MO, USA), and self-cast gels of constant density. In all gels the Prestained Protein Marker VI (PanReac, Applichem, Darmstadt, Germany) was used. Samples were mixed with 4x SDS sample buffer in 3 + 1 ratio, and heated for 20 min at 70 °C, then 5 min at 95 °C.

Run conditions:

For 3–8% (Invitrogen) gels: tris-acetate running buffer, 180 V, 55 mA, ca. 1 h

For 4–20% (Sigma-Aldrich) gels: NuPAGE MOPS running buffer, 180 V, 110 mA, ca. 1 h

For 7.5% (self-cast) gels: tris-acetate running buffer, 180 V, 25 mA, ca. 1.5 h

After the run, gels were cleaned in distilled water and stained with Coomassie staining solution. In cases where staining was minimal, the gels were stained once more using a solution of colloidal Coomassie. Analysis of gel images was performed in imageJ (Schneider, Rasband, and Eliceiri 2012) using the gel plotting function.

2.5. Mass spectrometry

To prepare the SDS-PAGE gel for mass spectroscopy, the gel was briefly submerged in 50 % MeOH. For each lane, protein bands of about 9 mm thickness were cut out and collected in Eppendorf tubes, whereupon 1 ml of destaining solution was added. The gel pieces were incubated three times in the destaining solution at 37 °C and 650 rpm in a miniature shaker for 20 min each. Then, any remaining liquid was removed from the gel pieces in a vacuum-concentrator centrifuge (Univapo 150H, Uniequip, Planoocyte, Germany).

The mass spectroscopic analysis was performed as described in Brenker et al. (2014), with the following alterations. The protein sequence database used was the zebrafish (*Danio rerio*) SwissProt/UniProtKB database. Subsequent to identification of proteins, a comparative analysis between samples was performed using Microsoft Office Access 2013, a database software. For categorization of detected proteins, the NCBI (https://www.ncbi.nlm.nih.gov/guide/proteins/)as well as the UniProtKB (https://www.uniprot.org/) databases were used.

2.6. Chorion staining

The staining of chorions (both in the form of isolated chorions and whole oocytes) was performed as described in Yanagimachi et al. (2013), with the following alterations. The Coomassie stock was diluted 20-fold in either PBS or Ringer solution and used to dye the oocytes or chorions for 1–2 min. During the dyeing

process, the container was gently agitated, to ensure even dye coverage. Subsequently, oocytes or chorions were washed 3–5 times with PBS or Ringer.

2.7. Sample preparation

2.7.1. Sperm preparation

Male zebrafish were euthanized by submersion in 20 mM phosphate buffer that contained 200 mg/l tricaine for anesthesia, and were subsequently decapitated. Testis were removed by dissection and transferred into 1 ml ES. The testis were stored on ice for 5–10 min to allow the sperm to diffuse out of the tissue and into the solution. Once the solution was cloudy, it was filtered through a 40 μm mesh cell strainer to remove the testis tissue, and diluted to 5 ml ES. The sperm solution was then centrifuged at 700 g for 7 min. The supernatant was removed, leaving 100–200 μl and the sperm pellet. It was found that removing the supernatant entirely leads to a great loss of sperm cells since the pellet is not entirely solid. However, centrifuging at higher speeds would damage the sperm cells, requiring a compromise. The pellet was resuspended by gently triturating with a wide bore pipet tip (obtained by cutting off the tip), to minimise shear forces that could mechanically damage the sperm.

2.7.2. Chorion preparation

Isolated chorions were acquired through two different methods. For the first method, based on the literature (Bonsignorio et al. 1996), female zebrafish were euthanized in the same fashion as male zebrafish for sperm preparation (see above). The whole ovaries were acquired by dissection of the fish, and transferred into PBS or TNE in an Eppendorf tube. Using a glass pipet, the ovaries were rapidly triturated, which shredded the oocytes. The chorions were collected in fresh PBS or TNE. Since this process does not allow for a clean separation of the chorion and internal components of the oocyte such as yolk or cytoplasm, the isolated chorions were then subjected to several wash cycles. The chorions were shaken in wash solution (PBS or TNE) with an Eppendorf shaker at 1250 rpm for 5 min. The chorions were allowed to settle into a loose pellet by gravity, the wash solution was exchanged, and this process was repeated 5–10 times. Finally, the isolated chorions were collected in PBS or ES for storage and frozen at –20 °C.

For the second method, a pseudo crossing was set up with female and male zebrafish. Overnight, the fish were put into a breeding tank where they were able to see and smell each other, but unable to interact due to

a separator. In a normal crossing, this separator would be removed in the morning, but in this case it remained in place.

Female zebrafish were euthanized as before (see above), briefly cleaned in system water, and then transferred to a petri dish and dried off with a tissue. While immobilizing the fish, gentle stroking pressure was applied to the female's belly. If the female fish had mature oocytes that were ready to be spawned, this pressure ejected them from the body.

These mature oocytes were transferred into droplets of hyperosmotic PBS in another petri dish using a glass pipet with a widened tip; about 3–5 oocytes per droplet. Within the next 5 min, the high osmolarity of this new external solution lead to the oocytes to shrink, which separated the plasma membrane from the chorion. This allowed for removal of the chorions using forceps without damaging the plasma membrane of the oocyte, thereby minimizing possible contamination of the chorions with the internal components of the oocyte. The isolated chorions were collected in ES for storage and frozen at -20 °C.

2.7.3. Preparation of oocyte-conditioned water

For the preparation of so-called oocyte-conditioned water, mature oocytes were collected as described in 2.7.2. Chorion preparation (second method). The oocytes were transferred into an Eppendorf tube with system water. While slowly turning the Eppendorf tube, the oocytes were left in the system water for 2–4 min. Then, the oocytes were allowed to settle by gravity into a loose pellet, and the supernatant (i. e. the oocyte-conditioned water) was collected. This oocyte-conditioned water was filtered through a 40 μm mesh strainer to remove any pieces of tissue, before being stored on ice for use on that same day, or frozen at -20°C for longer storage. About 150 oocytes were to used to condition 1 ml of system water.

2.8. Dark-field imaging

To track the swimming paths of zebrafish sperm, dark-field imaging was employed, similar to what has been described in Alvarez (2012) and Saggiorato (2017). The optical set-up consisted of an inverted microscope (IX71, Olympus, Tokyo, Japan) with a long-distance dark-field condenser. A 20x objective (0.75 NA, UPLSAPO, Olympus, Tokyo, Japan) in combination with a 1.6x magnification lens was used, to a final magnification of 32x. Videos were recorded at room temperature (RT), at 25 Hz framerate, for a total of 800 frames, using a back-illuminated electron-multiplying charge-coupled device camera (DU-897D, Andor Technologies, Belfast, UK). The exposure time was set to 2 ms.

Sperm were prepared as described under 2.7.1. Sperm preparation and stored on ice for the duration of the measurements. For the experiments, custom observation chambers were used (Figure 3): in a metal holder, a 24 x 24 mm cover slip is placed. On top, another, smaller cover slip, prepared with 1–3 layers of adhesive tape strips on either side, is placed. These strips serve as spacers, creating a small chamber of 50–150 µm depth between the cover slips. Since zebrafish sperm accumulate at glass/water interfaces (Ishimoto 2017), this set-up allows for the recording of two-dimensional swimming behaviour.

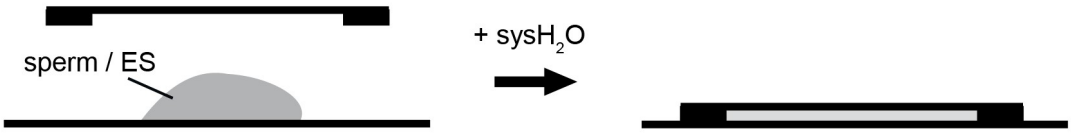

Figure 3: Observation chambers for motility measurements.

During an experiment, 1 µl of sperm in ES with a concentration of 1–5 x 10^6 / ml were placed on the lower cover slip. Then, 30 µl of system water (containing 0.5% pluronic for some experiments to minimize adhesion of sperm to the glass) were added with a pipet with a cut-off tip, very briefly mixed, then the second cover slip was added and recording began. With this method about 5 s of initial motility of the sperm are missed. Videos were analysed in Fiji (Schindelin et al. 2012) with the CASA plugin developed by Wilson-Leedy & Ingermann (2007) to extract sperm trajectories.

For experiments to determine overall motility of a sperm sample, some alterations were made to the procedure: Videos were recorded at 12 Hz for 400 frames total, with an exposure time of 50 ms. 5 µl of sperm were combined with 45 µl of activation solution (ddH_2O containing 0.5% pluronic) prior to recording.

2.9. Fluorescence imaging

2.9.1. Fluorescent dyes

Fluorescent dyes are molecules that display a change in their fluorescence upon binding to their respective ligand. For example, a calcium-sensitive fluorescent dye might show an increase in its fluorescence upon binding to calcium ions. When such dyes are brought into cells, they can indicate qualitative changes of ion concentrations within the cell (and in the case of ratiometric dyes, even quantitative changes). Various fluorescent dyes, sensitive to several ions, including protons, were used in this thesis. An overview is given in Table 1 below.

A hurdle in loading these dyes into cells is that the dye molecules are generally charged molecules, and therefore unable to diffuse through the cell membrane. To circumvent this issue one can use dyes that have

been esterized to carry acetoxy-methyl-ester groups (AM-esters) (Tsien 1981). In this form, the dye molecules carry no charge, and can diffuse through the cell membrane. Once inside the cell, the ester binding is cleaved by intracellular esterases. This cleavage results in charged dye molecules that are free to bind to their respective ligand, but at the same time, unable to diffuse across the cell membrane, which allows for a build-up of dye molecules within the cell far above the loading concentration of the dye.

However, some cells (such as CHO cells) possess anion transporters in their cell membrane (Lage 2003; Nigam et al. 2015). These transporters are able to eject even the charged dye molecules again from the cell. In these cases, it is beneficial or even necessary to use a blocker for such anion transporters, such as probenicid, within the loading solution and cell medium (Robbins et al. 2012).

Table 1: Overview of fluorescent dyes used in thesis. The maxima for excitation and emission of the respective dye are given, together with ligand and cause of fluorescence increase.

Dye	Excitation (nm)	Emission (nm)	Ligand	Fluorescence increase caused by
Calbryte520	493	515	calcium	calcium increase
Calbryte590	581	593	calcium	calcium increase
Calbryte630	607	624	calcium	calcium increase
pHrodo	560	585	protons	pH decrease
BCECF	490	535	protons	pH increase
SNARF-1[1]	488–530	580	protons	pH increase
ANG-2	517	542	sodium	sodium increase

2.9.2. Loading procedure for zebrafish sperm

Zebrafish sperm were prepared as described in 2.7.1. Sperm preparation. The sperm were diluted into 100–400 µl of ES and 100 µl of dye solution was added (ES containing the AM-ester form of the dye used and 0.05 % pluronic for those dyes for which it improves uptake). The concentrations used for the different dyes are given in Table 2 below. For all dyes, sperm were loaded at room temperature (RT) in the dark.

[1] SNARF-1 is a ratiometric dye, but only the emission wavelength that corresponds to pH increase was measured in experiments.

Table 2: Loading parameters for zebrafish sperm.

Dye	Loading Concentration	Pluronic	Loading Time
Calbryte520	200 nM	0.05%	60–90 min
Calbryte590	2 µm	0.05%	60 min
Calbryte630	2 µm	0.05%	80 min
pHrodo	1–3 µM	–	60–80 min
BCECF	1 µM	–	10 min
SNARF-1	1 µM	0.05%	60 min
ANG-2	1 µM	0.05%	60 min

After loading, the sperm were diluted with ES up to 5 ml and centrifuged at 700 g for 7 min. The supernatant was removed, and again the pellet was resuspended by careful trituration with a wide bore pipet tip. Lastly, the sperm cell concentration was determined using a Neubauer chamber, and the sperm were diluted to the appropriate working concentration for the respective experiment (usually in the range of 2×10^6–4×10^7 cells / ml).

2.9.3. Loading procedure for CHO cells

The loading procedure of CHO cells with fluorescent dyes differed depending on whether the CHO cells used were in solution or adherent to the container that was used for the experiments.

For adherent CHO cells, the cells were first washed with PBS and then loaded with dye solution (ES containing the AM-ester form of the respective dye, pluronic if necessary, and 3 mM probenicid). CHO cells were loaded at room temperature in the dark, or at 30 °C in an incubator for Calbryte520. Dye concentration and loading time is given in Table 2 below. After loading, the dye solution was removed, the cells were washed with ES containing 3 mM probenicid, and also stored in ES containing 3 mM probenicid to minimise transport of the cleaved dye out of the cells.

For CHO cells in solution the basic procedure was the same, but the washing with PBS (or ES containing 3 mM probenicid) and the removal of the dye solution was accomplished through centrifugation at 200 g for 5 min, followed by removal of the supernatant and resuspension.

Table 3: Loading parameters for CHO cells.

Dye	Loading Concentration	Pluronic	Loading Time
Calbryte520	200 nM	0.05%	60–90 min
pHrodo	3 µM	–	30 min
BCECF	1 µM	–	10 min

2.9.4. Well-plate reader

Population measurements of CHO cells or zebrafish sperm were performed using the FLuostar omega well-plate reader (BMG Labtech, Ortenberg, Germany). Well plates were either 96-well or 384-well plates. The measurement parameter was fluorescence intensity, which is detected through the bottom of the well plate. For each well, 10 measurements are taken per cycle, with the final recorded value being the mean of those 10 values. The intervall of the measurement cycle depends on the number of wells chosen for the experiment, because the wells are examined one after another, not simultaneously. Each well contained 30–50 µl of cells in solution (sperm or CHO) or adherent CHO cells, which were loaded with a fluorescent dye (see 2.9.2. Loading procedure for zebrafish sperm, 2.9.3. Loading procedure for CHO cells). The cell concentration for cells in solution was 0.5–2 x 10^6 cells/ml. Adherent cells were used when they became confluent. After 10 cycles to establish a baseline fluorescence, the stimulus was injected either manually, using an electronic multi-channel pipet, or using the Fluostar's internal injection system.

2.9.5. Rapid mixing device

Population measurements of zebrafish sperm were also carried out in a rapid mixing device (µSFM, Bio-Logic, Claix, France) in the stopped-flow mode, which allows for high time resolution and minimal time required for mixing of solutions (Figure 4). The set-up and procedure used were as described in Wobig et al. (2020), with alterations for different fluorescent dyes as indicated (see 2.9.2. Loading procedure for zebrafish sperm, Table 4). Furthermore, the light source frequency was set to 120 kHz.

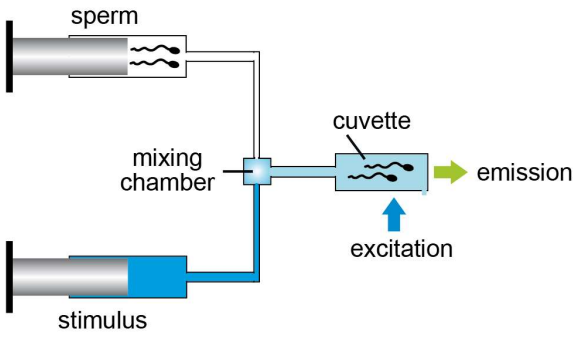

Figure 4: Set-up of rapid mixing device (scheme provided by René Pascal).

Sperm were suspended in ES and the solution was filtered through a 40 µm mesh syringe before use to avoid clumps which could interfere with the measurement. For experiments, one syringe contained the filtered sperm at a concentration of 2–4 x 10^7 / ml (chosen so that for each mixing ratio the working

concentration after mixing was 1 x 10^7 / ml). The other syringe contained system water, to activate the sperm once mixed.

2.9.6. Superfusion system

To measure fluorescence changes in single sperm cells, a gravity-assisted superfusion set-up was used. Multiple syringes are connected by tubing to a diamond-shaped open flow chamber (Figure 5). The bottom of the chamber is glass, allowing examination of the cells from below. All syringes are equipped with valves, which allows the manual control of which syringe is feeding into the chamber. During an experiment, cells adhering to the bottom of the chamber are continuously superfused with solution from the chosen syringe (at a flow rate of about 0.3 ml/min). Switching to a different syringe then enables superfusion with stimulus.

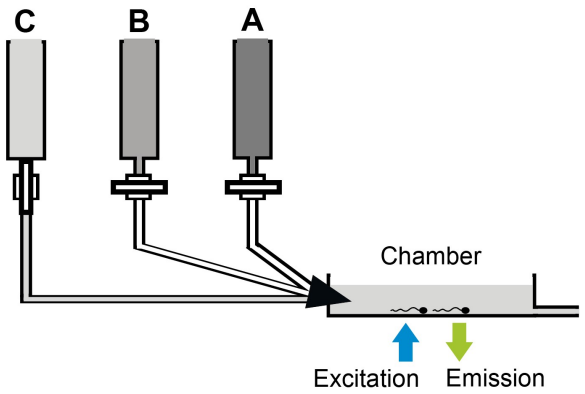

Figure 5: Gravity-assisted superfusion set-up. Syringes A to C can be filled with various solutions, such as ES, system water, or another stimulus.

Sperm were prepared and loaded with fluorescent dye according to the procedures described in 2.7.1. Sperm preparation and 2.9.2. Loading procedure for zebrafish sperm. After loading, 20 µl of sperm at a concentration of 1–5 x 10^6 / ml were placed in each chamber, 70 µl of ES were added, and the chamber was stored on ice, in the dark for 30–60 min to allow the sperm to adhere to the glass. If pluronic was present during the loading process, 60 min were used because more time was required for the sperm to adhere to the glass.

Excitation and emission wave length were set by including suitable filters in the filter cube of the fluorescence microscope, together with the appropriate dichroic mirrors (Semrock, Rochester, NY, USA, see Table 4). The excitation wave length for the fluorescent dyes was chosen as close as possible to the excitation maximum of the respective dyes, using a Spectra X light source based on solid-state lighting (Lumencor, Beaverton, OR). The emission filters were chosen to optimize efficiency of detection concomitant with good

separation from the excitation wave length. Experiments were recorded with a 60x oil-immersion objective (Olympus Apo N 60XOTIRF) and iXon Ultra DU-897U emCCD camera (iXon Ultra, Andor Technologies, Belfast, UK), using the Solis software (Andor Technologies, Belfast, UK). Videos were recorded at a framerate of 2 Hz, for a duration of 1000 frames, without binning. The number of sperm visible in the field of view were usually between 10 and 50. Videos were analysed in Fiji (Schindelin et al. 2012) using the program's internal tools, to create ROIs for each sperm in the field of view, and to track the change in brightness, i. e. fluorescence, over time.

Table 4: Light source, filters and dichroic mirrors used for fluorescent dyes.

dye	Lumencor Source	Excitation filter (nm)	Emission filter (nm)	Dichroic mirror (nm)
Calbryte520	cyan	494/20 bandpass	536/40 bandpass	495 longpass
Calbryte590	green	543/22 bandpass	593/40 bandpass	562 longpass
Calbryte630	green	562/20 bandpass	624/20 bandpass	593 longpass
pHrodo	green	543/22 bandpass	593/40 bandpass	562 longpass
BCECF	cyan	494/20 bandpass	536/40 bandpass	495 longpass
SNARF-1	teal	513/17 bandpass	632/22 bandpass	560 longpass
ANG-2	teal	513/17 bandpass	532 longpass	520 longpass

2.9.7. Data Analysis

Further analysis and data handling was performed in Microsoft Excel for the subtraction of background fluorescence (fluorescence measured without cells) and the subsequent normalization to F_0, i.e. calculation of F/F_0. Thus all fluorescence traces start at value 1. Normalization of the fluorescence signal removes the effect of variable dye concentrations between experiments. OriginPro 9 was used for baseline adjustment, if necessary, and graph creation.

3. Results

3.1. The CatSper channel in fish

The CatSper channel plays a vital role in the motility of sperm for many species. CatSper was thought to have been lost in teleost fish (Cai and Clapham 2008), but genome-wide automated gene prediction (see Scalzitti et al. 2020) has indicated the presence of CatSper genes in a few fish genomes, e.g. a teleost, goldfish, and a non-teleost fish, spotted gar (Chen et al. 2019; Braasch et al. 2016). The recent availability of several hundreds of fish genomes permitted to undertake a phylogenetic analysis to determine the extent of CatSper gene loss in the fish lineage, with a special focus on zebrafish because of its prominent status as a model system.

3.1.1. CatSper has been independently lost in multiple lineages of fish

I analyzed all fish species where genome sequences were available at the time (March 2020; 289 species) for the presence of the following CatSper genes: the core channel subunits CatSper1–4, and the auxiliary CatSper genes CatSperB, D, G, and E. As quality control, I searched for beta-actin; for further analysis, only genomes were used that provided good beta-actin hits. Since beta-actin is highly conserved, genomes without good beta-actin hits are likely of poor quality overall. Searches for CatSper were performed with tBLASTn in whole-genome shotgun databases and, when available, in transcriptome shotgun assemblies. Any potential hits were tested via phylogenetic trees that included known CatSper genes and outgroup genes (Appendix Figure 1–Appendix Figure 8).

This analysis included 271 fish species that represent only a small portion of more than 30,000 extant fish species that are currently described (Froese, Pauly, and Editors 2020) (Appendix Table 1). Nevertheless, the 271 species cover a broad spectrum from jawless fish to modern Neoteleostei and thus should provide relevant information on trends concerning the loss or retention of CatSper. In this context we need to distinguish more-derived (also designated as late-diverging) and less-derived (also early-diverging) species. In short, more-derived means more nodes in the species tree until the respective tip is reached, and vice versa for less-derived species. For example, lamprey are less-derived than sharks, because in the vertebrate species tree the shark tip is reached with 2 nodes, whereas lamprey is reached with only one node.

When considering the evolution of a gene, the observed pattern of presence and absence across the species tree needs to be explained by gene loss events (GLEs; potentially also gene gain events). Three considerations should be made when postulating GLEs: Firstly, if a pattern can be explained with fewer GLEs, then this explanation is preferred because it is assumed to more likely represent reality. Figure 6A–C

illustrates this consideration. Secondly, it must be determined whether the observed gene losses are independent from each other. As an example, Figure 6D–E shows a cladogram where this is the case. Because the gene occurs in one of the more derived clades, it must have been present in the common ancestor; thus, the gene loss must have occurred independently in the two clades, where the gene is absent. Thirdly, the number of postulated GLEs represents a lower limit estimate, unless a cladogram is detailed enough to show every species. One can always zoom in a larger clade possessing the gene in question (Figure 6F–G and may find a subclade that has lost it, necessitating to postulate an additional GLE within that subclade. Similarly, within a previously negative clade more genomes may become available and a subclade may be found that does possess the gene., This would require additional GLEs to explain the pattern.

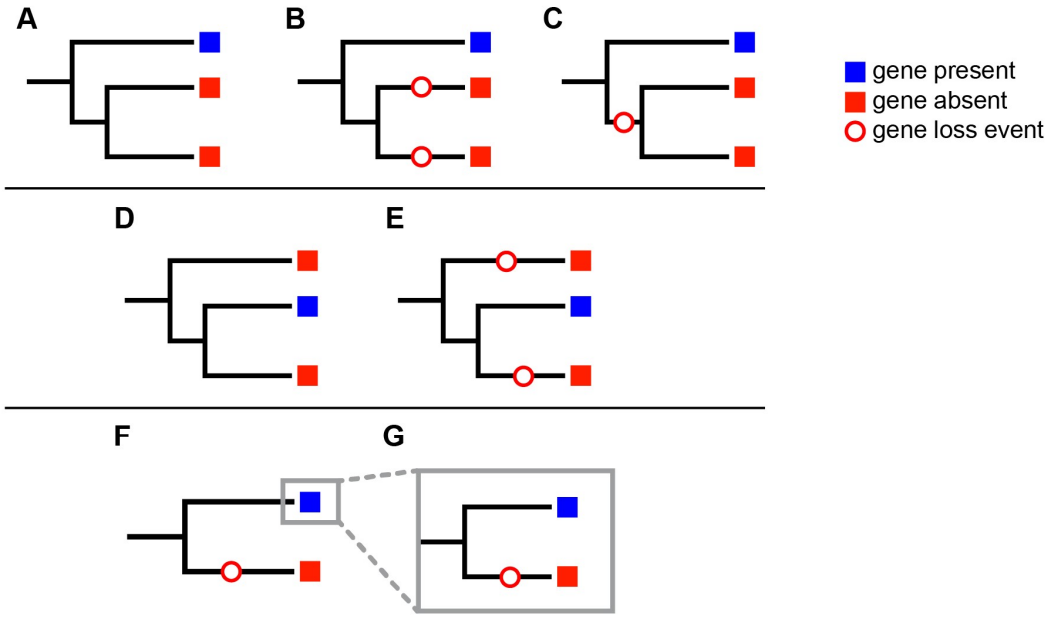

Figure 6: Schematic cladograms showing the presence (blue box) and absence (red box) of a gene in particular clades (species or species groups). A) A pattern of gene absence and presence in a species tree. **B**) A possible explanation which requires two independent GLEs. **C**) Another explanation, which requires only one GLE. Possibility C is preferred, because it requires less events. **D**) The cladogram shows again absence in 2 clades and presence in one clade, but differently arranged compared to **A**). **E**) No explanation with a single GLE is possible, the minimal number is two independent GLEs. **F**) A cladogram which requires a single GLE for explanation. **G**) A zoom-in of the 'blue' clade reveals only partial presence, i.e. an additional GLE has to be postulated. Thus, number of GLEs postulated always represents a lower limit and may increase if and when more species become available.

My phylogenetic analysis showed many fish species possessing both principal (blue boxes, Figure 7) and auxiliary (blue boxes, Figure 8, Appendix Table 2) CatSper genes, from cartilaginous fish to intermediate Neoteleostei (see Figure 7, Figure 8 for definition). For a handful of genes this confirmed previous results (e.g. goldfish and spotted gar) obtained by automated gene prediction methods (e.g. Scalzitti et al. 2020), but in addition many CatSper genes were newly found.

Several species possess only an incomplete inventory of CatSper genes (purple boxes, Figure 7, Figure 8). For example, a species possesses CatSper2–4, but not CatSper1; or only CatSperG and E, but not CatSperB and D (Figure 7, Figure 8, Appendix Table 2). In mouse and human, all of CatSper1–4 and the auxiliary CatSper subunits are required to form a functional CatSper complex (Qi et al. 2007; Jaiswal et al. 2014; Chung et al. 2011; 2017). Thus, it is likely that species with an incomplete inventory of CatSper genes are in the process of losing the CatSper complex, since the complex is presumably no longer functional. Some of the newly-identified CatSper genes are also pseudogenes (their sequences have multiple frameshifts or stop codons), indicating that these specific genes are indeed lost from a functional point of view.

In addition, many species also lack any and all CatSper genes (red boxes, Figure 7, Figure 8). These complete losses of CatSper genes are spread across the entire species tree, from early- (jawless fish) to late- (Percomorpha) diverging fish. To explain this pattern of CatSper absences, I have used the principles outlined above, and deduced a minimum number of GLEs for CatSper in the fish lineage (red circles in Figure 7, Figure 8). Since CatSper-possessing species are intermittently present in the species tree, we have to conclude that CatSper1–4 and auxiliary CatSper genes have been lost multiple times independently. Notable is the complete loss of CatSper in Percomorpha, a large clade within Neoteleostei that makes up more than half (146 species) of the examined and about half (17,000 species) of all extant fish species. Interestingly, all jawless fish examined (two lampreys and one hagfish) also do not possess any CatSper genes, suggesting the gene loss occurred in their most recent common ancestor. This was likely a very early GLE because the evolutionary distance between hagfish and lamprey is close to 500 million years (Kumar et al. 2017). More recent GLEs must have taken place in all intermediate groups, since a total or partial lack of CatSper genes is found in some group members across the board (Figure 7, Figure 8).

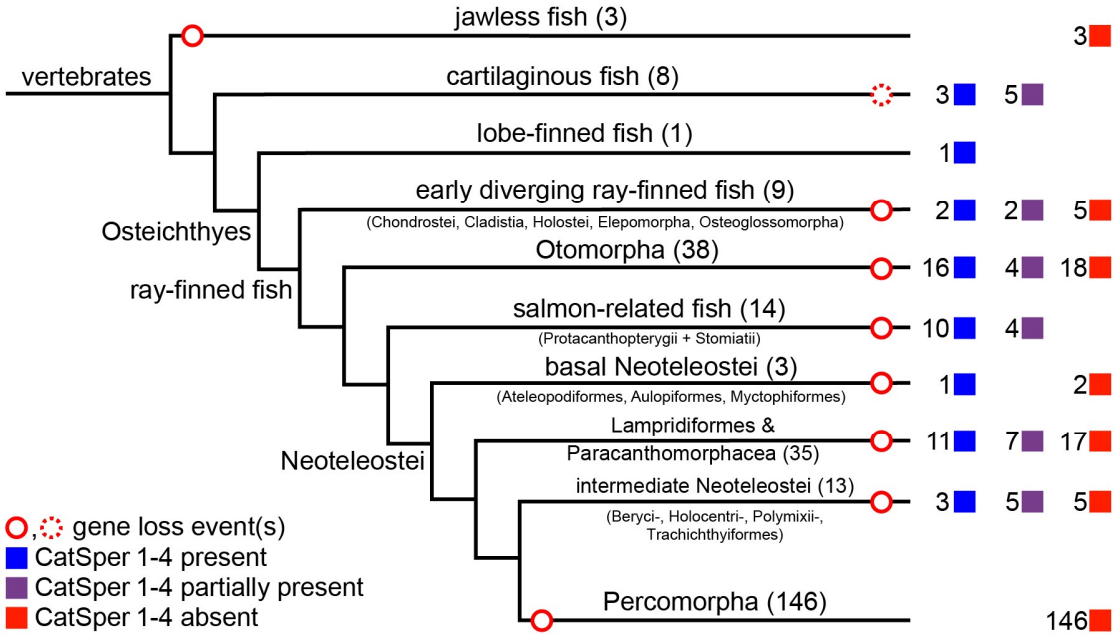

Figure 7: Presence and absence of the core channel subunits of CatSper (CatSper1–4) in different lineages of fish. The number of examined genomes is given in brackets after the name of the group (the total number of species per group is given in Appendix Table 1). Tree topology is taken from Betancur (2013). Numbers before boxes refer to number of species; color code for boxes as indicated. Empty circles indicate loss of all four CatSper1–4 genes in ≥ 1 species of the group. Dashed circles indicate loss of some of the four CatSper1–4 genes in ≥ 1 species of the group. Circles on the right-hand side of a branch indicate more recent gene loss within the group; circles on the left-hand side of a branch indicate early gene loss within the entire group.

When comparing gene loss and retention of CatSper1–4 to that of the auxiliary CatSpers, three groups show the same or a similar pattern: In jawless fish and Percomorpha, all CatSpers are completely absent (Figure 7, Figure 8). In early-diverging ray-finned fish (see Figure 7, Figure 8 for definition), only one species has a different retention for CatSper1–4 than for the auxiliary CatSpers (partial loss vs. complete loss, respectively). However, for the other fish groups, the pattern of loss and retention of CatSper genes differs considerably between CatSper1–4 (Figure 7) and the auxiliary CatSpers (Figure 8). In several species groups the auxiliary CatSper genes have been lost to a higher degree than CatSper1–4. In basal Neoteleostei, Lampridiformes, and Paracanthomorphacea, several species possess CatSper1–4, but no species possesses all auxiliary CatSper genes (Figure 7, Figure 8). In Otomorpha, salmon-related fish (Protacanthopterygii, Stomiatii), and intermediate Neoteleostei (Beryci-, Holocentri-, Polymixii-, Trachichthyiformes), more species have fully or partially lost the auxiliary CatSper genes (Figure 8) than CatSper1–4 (Figure 7). In contrast, in

cartilaginous fish, more species have retained the full complement of auxiliary CatSper genes (Figure 8) compared to those species that have retained all of CatSper1–4 (Figure 7).

These differential retention rates suggest that auxiliary CatSper genes are subject to different evolutionary pressure compared to CatSper1–4.

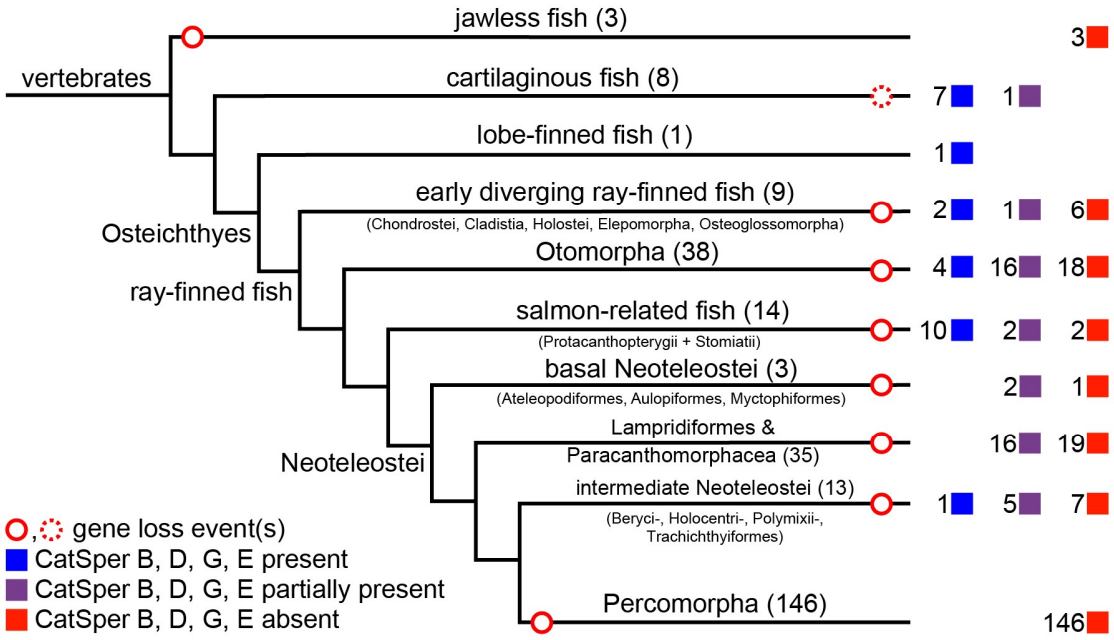

Figure 8: Presence and absence of the auxiliary CatSper genes (CatSperB, D, G, E) in different lineages of fish. The number of examined genomes is given in brackets (the total number of species per group is given in Appendix Table 1). Tree topology is taken from Betancur (2013). Numbers before boxes refer to number of species; color code for boxes as indicated. Empty circles indicate loss of all four CatSper genes in ≥ 1 species of the group. Dashed circles indicate loss of some of the four auxiliary CatSper genes in ≥ 1 species of the group. Circles on the right-hand side of a branch indicate more recent gene loss within the group; circles on the left-hand side of a branch indicate early gene loss within the entire group.

3.1.2 Zebrafish do not possess CatSper

During the search for CatSper genes, none were detected in the genome of zebrafish. However, several reasons may prevent to identify a particular gene in a genome because some regions of the genome may be inaccessible for sequencing (Treangen and Salzberg 2012; Aird et al. 2011) and the sequence quality of others may be poor, which hampers the search, especially if the gene is not well-conserved.

Therefore, I employed the following two approaches to validate the absence of CatSper in zebrafish: an examination of the presence of CatSper genes in the evolutionary neighborhood of zebrafish, and a synteny analysis of CatSper-adjacent genes in goldfish and zebrafish.

3.1.2.1. Absence of CatSper in species closely related to zebrafish suggests ancestral gene loss in the sister group to Cyprinidae

If poor quality of the zebrafish genome prevents the identification of CatSper genes, it is unlikely that similar technical flaws would happen in all species closely related to zebrafish. Thus, if zebrafish and its relatives actually do possess CatSper, one would expect to find CatSper genes in these other species. Historically, zebrafish has been classified as Cyprinidae—however, a recent comprehensive analysis of all Cypriniformes (Stout et al. 2016) suggests that they belong to a separate family, Danionidae. Goldfish, a member of Cyprinidae, does possess CatSper (Appendix Table 2). Therefore, I included all available genomes within the order Cypriniformes (22 species), which encompasses both Cyprinidae and Danionidae, in this examination.

Although most Cyprinidae species possess the core channel subunits CatSper1–4, neither the Danionidae species nor their more derived sister groups Xenocyprididae and Leuciscidae possess CatSper1–4 genes (Figure 9). This distribution of CatSper1–4 genes suggests that CatSper was lost after Danionidae diverged from Cyprinidae, but before Danionidae diverged from its more derived sister groups.

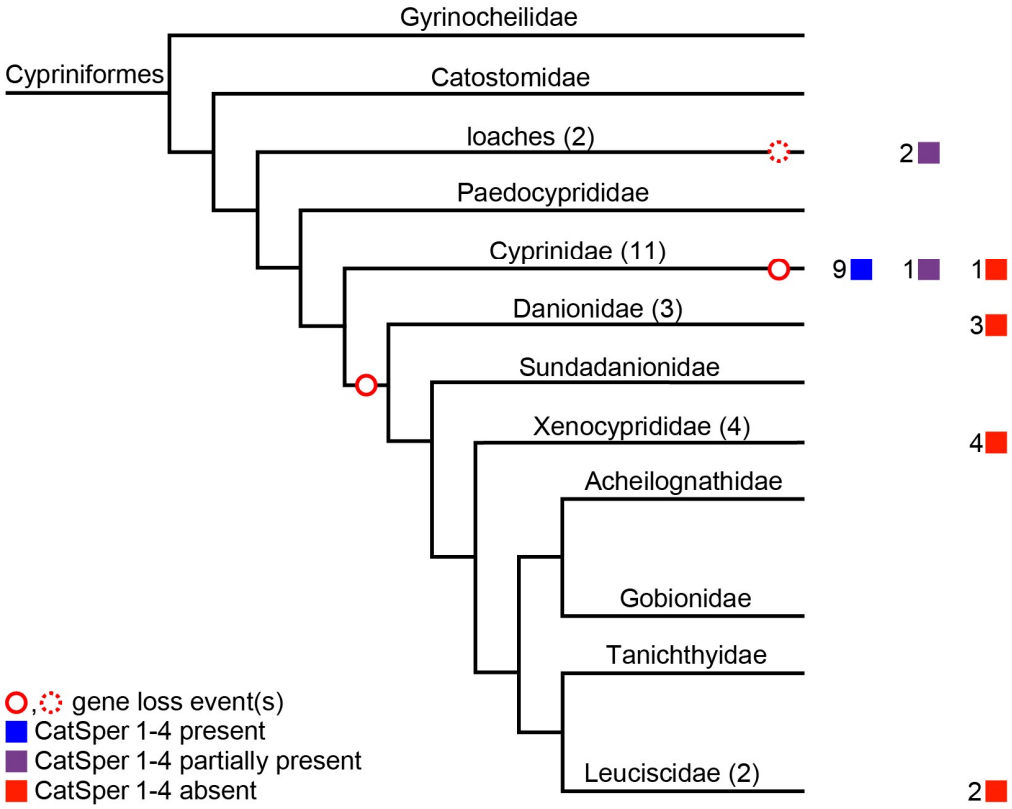

Figure 9: Presence and absence of the core channel subunits of CatSper (CatSper1–4) in Cypriniformes. The number of examined genomes is given in brackets after the name of the group (the total number of species per group is given in Appendix Table 1). Tree topology is taken from Stout et al. (2016). Numbers before boxes refer to number of species; color code for boxes as indicated. Empty circles indicate loss of all four CatSper1–4 genes in ≥ 1 species of the group. Dashed circles indicate loss of some of the four CatSper1–4 genes in ≥ 1 species of the group. Circles on the right-hand side of a branch indicate more recent gene loss within the group; circles on the left-hand side of a branch indicate early gene loss within the entire group.

The distribution of auxiliary CatSper genes differs from CatSper1–4, similar to what we observed for other fish. No species in Cypriniformes possesses CatSperB or CatSperD, whereas CatSperG and CatSperE are present in some species (Figure 10, Appendix Table 2). Interestingly, Leuciscidae and Xenocyprididae still possess some of the auxiliary CatSper genes despite having lost the CatSper1–4 genes (Figure 10). A new function of the remaining auxiliary CatSper genes may have evolved that kept them from being lost.

However, the complete absence of CatSper genes in Danionidae, both of the core channel and the associated subunits, suggests that CatSper has been lost in zebrafish.

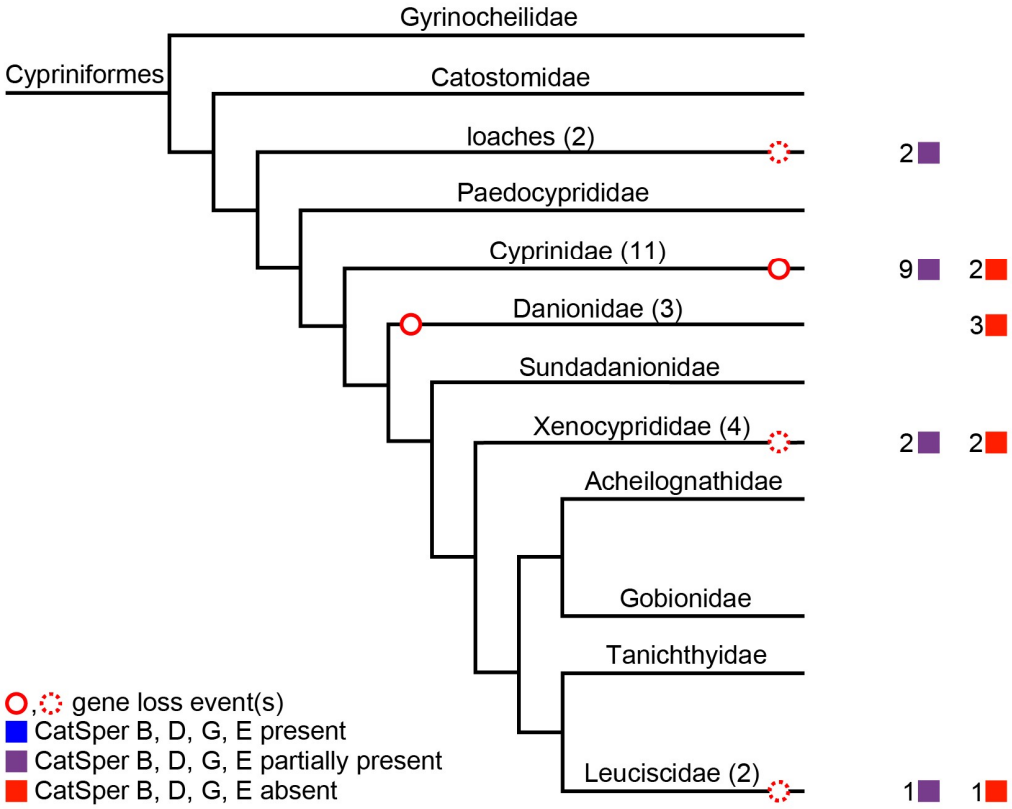

Figure 10: Presence and absence of the auxiliary CatSper genes (CatSperB, D, G, E) in Cypriniformes. The number of examined genomes is given in brackets after the name of the group (the total number of species per group is given in Appendix Table 1). Tree topology is taken from Stout et al. (2016). Numbers before boxes refer to number of species; color code for boxes as indicated. Empty circles indicate loss of all four CatSper1–4 genes in ≥ 1 species of the group. Dashed circles indicate loss of some of the four CatSper1–4 genes in ≥ 1 species of the group. Circles on the right-hand side of a branch indicate more recent gene loss within the group; circles on the left-hand side of a branch indicate early gene loss within the entire group.

3.1.2.2. Synteny analysis of goldfish and zebrafish genome confirms absence of CatSper in zebrafish

To exclude that the absence of CatSper in zebrafish might be caused by technical difficulties in sequencing the genomic region potentially containing CatSper (Treangen and Salzberg 2012; Aird et al. 2011) I performed a synteny analysis. I used goldfish as the closest relative (106 million years, Kumar et al. 2017) that possesses CatSper and has a well-annotated genome. The genes surrounding CatSper1–4 in goldfish were collected from the NCBI genome data viewer (Rangwala et al. 2021), the corresponding genes in zebrafish were searched, and their respective arrangement, location and presence or absence were compared between

the two species. If the CatSper-adjacent genes of goldfish are similarly arranged in zebrafish, it suggests that this region, where CatSper1–4 should be located, is amenable to sequencing also in the zebrafish genome. Furthermore, such an analysis can also provide clues to potential breakpoints in the region where a gene loss event may have occurred (Furuta et al. 2011; Calvete et al. 2012).

The common ancestor of goldfish and carp underwent polyploidization at least 18.5 million years ago (Li et al. 2014), resulting in duplication of all chromosomes. Many of the genes in the neighborhood of CatSper1 occur on the duplicated chromosome as well, in the same order, with some intervening genes specific to the respective chromosome. However, only one copy of the duplicated CatSper1 gene is retained. The genomic region examined around CatSper1 in goldfish is located on chromosome 21, and 2.0 Mb long. The duplicated chromosome, where many of the genes surrounding CatSper1 can also be found, is chromosome 46, where the examined segment is 2.7 Mb long (Figure 11).

I then examined the genomic location of the respective genes in zebrafish. The majority of genes surrounding CatSper1 in goldfish can be found in zebrafish in a 2.3 Mb long genomic region on chromosome 21 (37 of 64 genes surrounding CatSper1 (Figure 11). This occurrence of the same genes within one region in both species enables synteny analysis: comparing the specific arrangement and order of those shared genes.

The genes in the examined genomic region can be roughly divided into three different blocks (color-coded with magenta, yellow, and cyan in Figure 11): The middle block (yellow) consists of genes, whose sequential arrangement and direction on the chromosome is the same for goldfish chromosome 21 and zebrafish chromosome 21. The cyan block also shows the same sequential arrangement in goldfish chromosome 21 vs. zebrafish chromosome 21, but the direction of the entire block is inverted compared to goldfish (visualized by connecting lines crossing). The magenta block shows even two inversions (one for the genes arfGAP and IK cytokine, one for the rest), with the sequential order only conserved within each inversion block) and each inversion block additionally translocated (arfGAP and IK cytokine downstream of the yellow block, and the rest of the magenta block even downstream of the cyan block). Overall, the changes in arrangement and position of the genes between goldfish chromosome 21 and zebrafish chromosome 21 suggest the occurrence of at least two major translocation and three major inversion events. Both translocation and inversion create break points in the genome, which can be a source of gene loss (Furuta et al. 2011; Calvete et al. 2012). Indeed, CatSper1 in goldfish is located exactly at a breakpoint between the yellow and cyan block, suggesting it has been lost in zebrafish during such an event.

To put the changes in gene order between goldfish chromosome 21 and zebrafish chromosome 21 into perspective, we made use of the fact that the polyploidization of goldfish (18.5 million years, see above) occurred much more recently than the divergence between goldfish and zebrafish (106 million years, Kumar

et al. 2017). I compared the gene order on the duplicated goldfish chromosome both with goldfish chromosome 21 and zebrafish chromosome 21. Genes belonging to all three color blocks can be found on chromosome 46 as well, and both the relative position and direction of the three color blocks are identical between both goldfish chromosomes, indicating that no translocation or inversion events have taken place in this region since the polyploidization. Thus, the difference in gene order and arrangement between goldfish and zebrafish (Figure 11, middle and right) is considerably larger than the difference between the duplicated goldfish chromosomes (Figure 11, left and middle), as expected from the much larger evolutionary distance.

Moreover, chromosome 46 contains seven additional genes, which show synteny with zebrafish chromosome 21 (dashed connecting lines, Fig. 6). These genes are lost in goldfish chromosome 21 (gene loss is a common occurrence after polyploidization (e.g. Scannell et al. 2006), but provide further evidence for the overall synteny of the genomic regions examined.

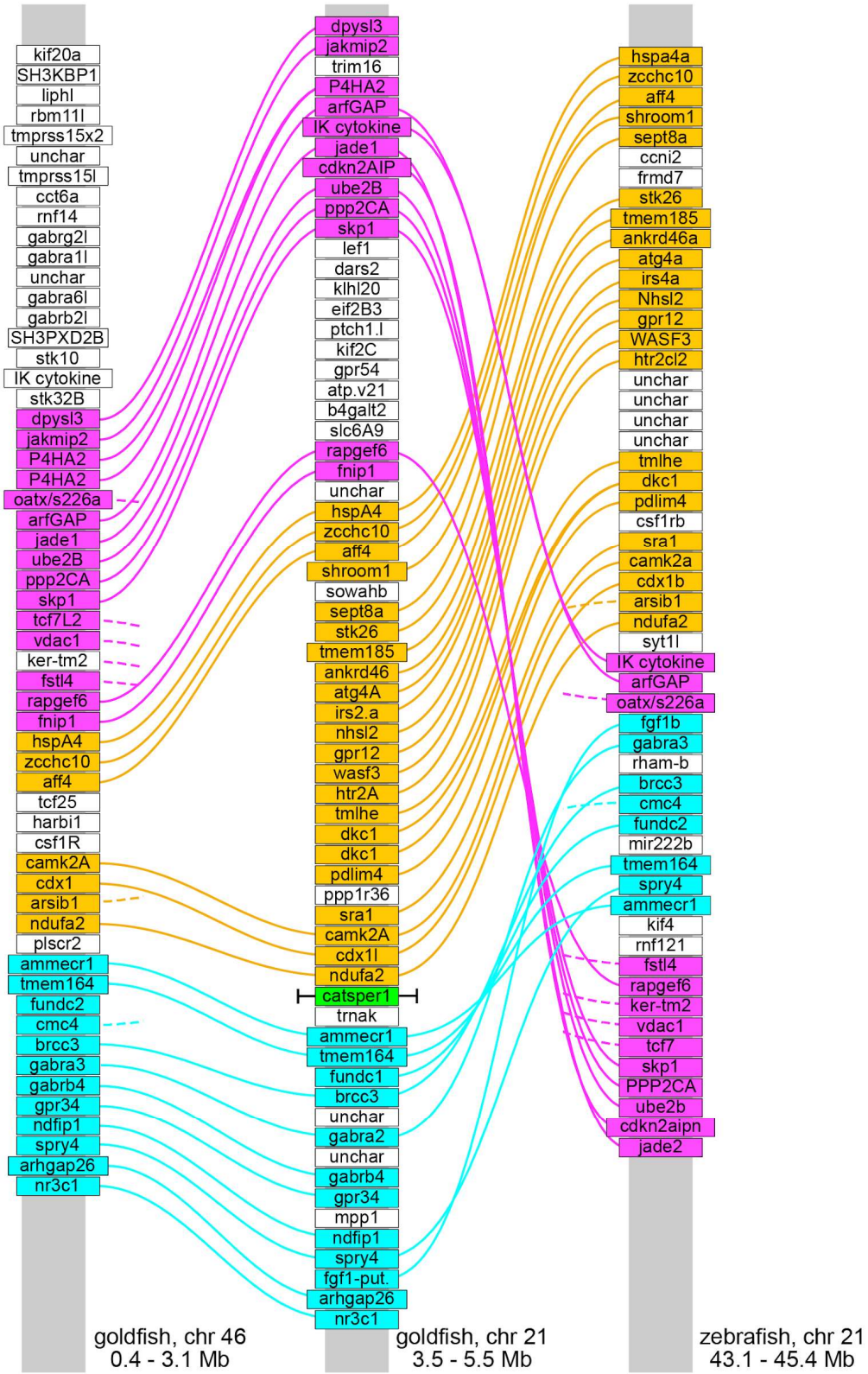
kif20a
SH3KBP1
liphl
rbm11l
tmprss15x2
unchar
tmprss15l
cct6a
rnf14
gabrg2l
gabra1l
unchar
gabra6l
gabrb2l
SH3PXD2B
stk10
IK cytokine
stk32B
dpysl3
jakmip2
P4HA2
P4HA2
oatx/s226a
arfGAP
jade1
ube2B
ppp2CA
skp1
tcf7L2
vdac1
ker-tm2
fstl4
rapgef6
fnip1
hspA4
zcchc10
aff4
tcf25
harbi1
csf1R
camk2A
cdx1
arsib1
ndufa2
plscr2
ammecr1
tmem164
fundc2
cmc4
brcc3
gabra3
gabrb4
gpr34
ndfip1
spry4
arhgap26
nr3c1
goldfish, chr 46
0.4 - 3.1 Mb
dpysl3
jakmip2
trim16
P4HA2
arfGAP
IK cytokine
jade1
cdkn2AIP
ube2B
ppp2CA
skp1
lef1
dars2
klhl20
eif2B3
ptch1.l
kif2C
gpr54
atp.v21
b4galt2
slc6A9
rapgef6
fnip1
unchar
hspA4
zcchc10
aff4
shroom1
sowahb
sept8a
stk26
tmem185
ankrd46
atg4A
irs2.a
nhsl2
gpr12
wasf3
htr2A
tmlhe
dkc1
dkc1
pdlim4
ppp1r36
sra1
camk2A
cdx1l
ndufa2
catsper1
trnak
ammecr1
tmem164
fundc1
brcc3
unchar
gabra2
unchar
gabrb4
gpr34
mpp1
ndfip1
spry4
fgf1-put.
arhgap26
nr3c1
goldfish, chr 21
3.5 - 5.5 Mb
hspa4a
zcchc10
aff4
shroom1
sept8a
ccni2
frmd7
stk26
tmem185
ankrd46a
atg4a
irs4a
Nhsl2
gpr12
WASF3
htr2cl2
unchar
unchar
unchar
unchar
tmlhe
dkc1
pdlim4
csf1rb
sra1
camk2a
cdx1b
arsib1
ndufa2
syt1l
IK cytokine
arfGAP
oatx/s226a
fgf1b
gabra3
rham-b
brcc3
cmc4
fundc2
mir222b
tmem164
spry4
ammecr1
kif4
rnf121
fstl4
rapgef6
ker-tm2
vdac1
tcf7
skp1
PPP2CA
ube2b
cdkn2aipn
jade2
zebrafish, chr 21
43.1 - 45.4 Mb

Figure 11: Synteny of the genomic region of CatSper1 in goldfish and zebrafish. Conserved blocks of genes are highlighted in yellow, magenta, and cyan. Colored lines connect orthologous genes conserved between chromosomes or species. For genes orthologous between goldfish chromosome 46 and zebrafish chromosome 21, dashed lines were used. Goldfish CatSper1 is highlighted in green and flanked by black whiskers to indicate absence of orthologous genes. Genomic distance from first to last gene is given in Mb for each chromosome (chr).

I repeated the synteny analysis for CatSper2–4 genes, which provided similar results (Appendix Figure 9–Appendix Figure 11): Blocks of the genes adjacent to CatSper2–4 in goldfish show partial synteny in zebrafish. They are translocated or their order is inverted in comparison to their order on the goldfish chromosomes, reminiscent of the situation for CatSper1. Furthermore, CatSper2, CatSper3, and CatSper4 are all located at the breakpoints between these blocks of genes (just like CatSper1), suggesting they have been lost in zebrafish by the same mechanism.

Taken together, synteny analysis suggests for CatSper1–4 that the relevant genomic regions in zebrafish can be sequenced without problems. Moreover, a plausible mechanism for gene loss in zebrafish could be inferred from the analysis. In combination with the phylogenetic findings discussed in 3.1.2.1., the synteny analysis indicates that zebrafish has truly lost CatSper.

3.1.3. Evolution of CatSper genes

The phylogenetic analysis also provides insight into the evolutionary history of CatSper genes. We observe four clades corresponding to the four Catsper genes (CatSper1–4) with near maximal branch support (Figure 12). Moreover, three of the four CatSper1–4 genes have long root branches that further support the validity of the grouping. Together, this enables unambiguous validation of CatSper1–4 candidates. This is a prerequisite to draw further conclusions concerning the evolution of the CatSper genes.

The topology of the phylogenetic tree (Figure 12) suggests that CatSper1 and CatSper3 are more closely related to one another than to CatSper2,4; vice versa, CatSper2 and CatSper4 are more closely related to one another than to CatSper1,3. These results confirm the grouping of CatSper2 and CatSper4 established by Cai and Clapham (2008; 2014) and clarifies the relationship of CatSper1 and 3 as sister clades. Previously, inconsistent grouping of CatSper1 and CatSper3 have been reported, but is difficult to evaluate due to the crucial branch supports not being given or being below 80% (Cai and Clapham 2008; Cai, Wang, and Clapham 2014). This observation suggests a potential evolutionary scenario: Originally, a single CatSper gene underwent duplication, and each duplicate was subsequently duplicated again to produce CatSper1/CatSper3, and CatSper2/CatSper4, respectively.

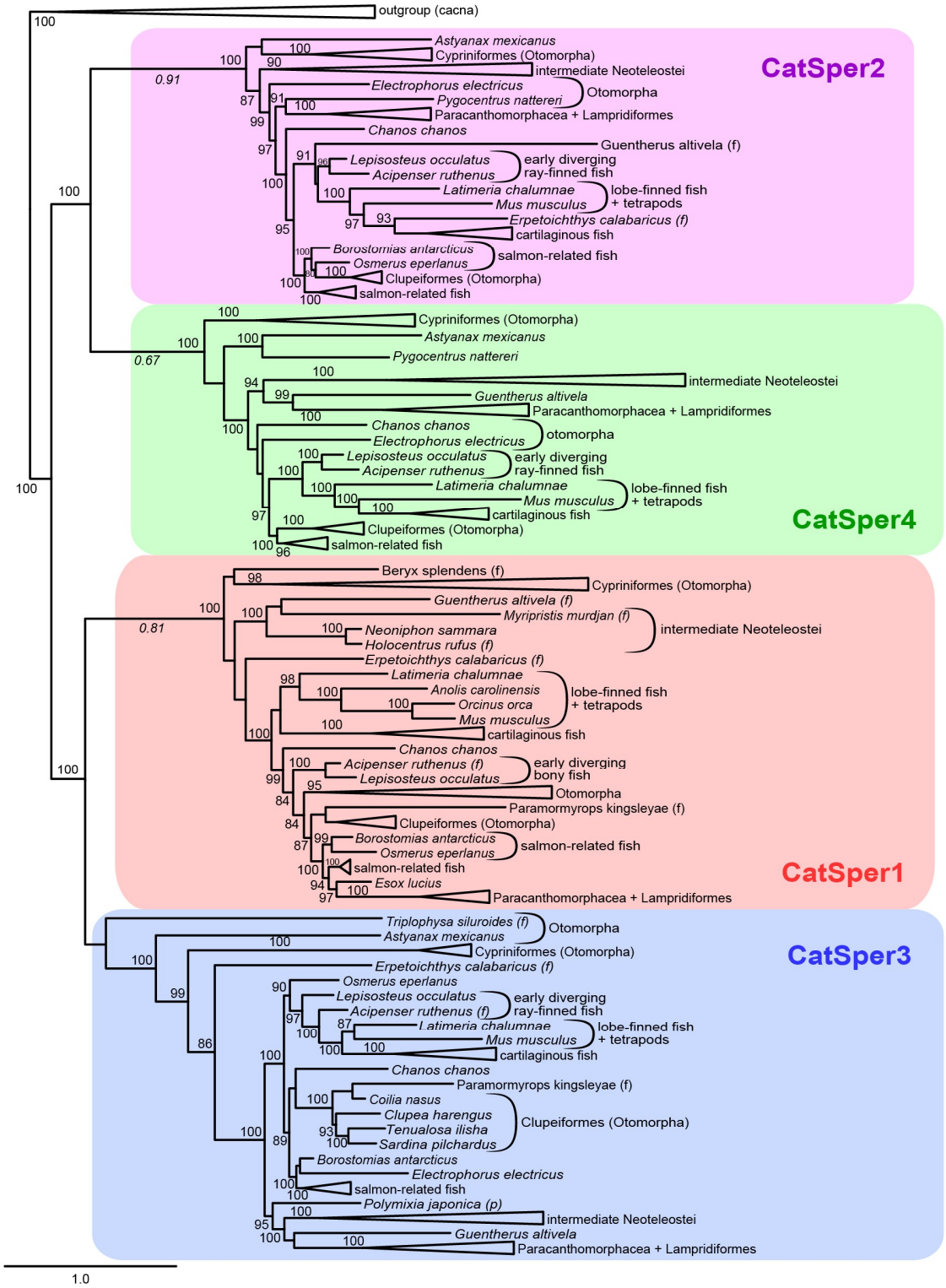

Figure 12: Phylogenic tree of new-found CatSper1–4 genes and known CatSper1–4 genes (such as *Mus musculus, Lepisosteus occulatus*), with cacna/CaV genes as outgroup. Branch support values are given in %, if above 80%, at their respective node. Branch lengths are denoted in italics below the respective

branch, where relevant. Scale bar value (1.0) denotes the replacement rate of amino acids on every position of the sequences. Genes marked (f) are fragments (< 200 amino acids); genes marked (p) are pseudogenes.

It can be informative to analyse the species relationships within each CatSper1–4 clade. In principle, orthologs from different species are expected to reflect the relationships of the respective species. Accordingly, genes from early-derived species should appear in more basal position in the phylogenetic tree, whereas genes from more derived species (i.e. the result of more divergent evolutionary processes) should appear after more bifurcation points.

To some extent this is observed for CatSper1–4. Within each CatSper1–4 grouping, certain species clades also group well together with high branch support and occasionally long root branches (Paracanthomorphacea and Lampridiformes, salmon-related fish, Cypriniformes, Clupeiformes, lobe-finned fish and tetrapods, cartilaginous fish). Clupeiformes, a subgroup of Otomorpha, also groups into a sister position to salmon-related fish (Figure 12), which reflects their taxonomic relationship (Figure 13).

However, for most species clades, their position within the phylogenetic tree for CatSper1–4 does not closely reflect their taxonomic position (Figure 12, Figure 13). The CatSper1–4 genes of cartilaginous fish, which includes sharks and rays should therefore form a sister group to the CatSper genes of all Osteichthyes (bony fish), consistently appear inside the Osteichthyes group. In addition, they appear as a sister group to the CatSper1–4 genes of lobe-finned fish and tetrapods, coelacanth (*Latimeria chalumnae*) and mouse (*Mus musculus*). The CatSper1–4 genes of early-diverging ray-finned fish, another group that would be expected to appear as a basal branch, instead has a consistent position in the middle of the phylogenetic tree. The CatSper1–4 genes of Otomorpha are even spread out over the entire tree, since the subclade Cypriniformes appears as a basal branch, whereas the Clupeiformes subclade appears in a far more derived position. CatSper genes of Paracanthomorphacea and Lampridiformes appear in the middle of the tree in CatSper2 and CatSper4, but far more derived in CatSper1 and CatSper3, neither of which is reflective of their taxonomic position (Figure 13). Intermediate Neoteleostei are the evolutionary youngest clade of fish to still possess CatSper1–4, but CatSper1,2,4 of those species appear close to a basal position in the phylogenetic tree.

Additionally, CatSper genes from single species occasionally appear far from their expected taxonomic position (for example CatSper1 of *Beryx splendens,* an intermediate Neoteleostei, and CatSper2 of *Guentherus altivela*, a basal Neoteleostei, Figure 12). Such singular deviations are most likely explained by technical causes. Fragments are known to be susceptible to inaccurate alignments, and pseudogenes do not experience selective pressure and consequently can evolve rapidly, which can change the placement in the phylogenetic tree relative to functional genes.

But most aberrations described above are surprisingly consistent between all four CatSper1–4 genes. Such robust differences between gene trees and species trees might suggest lineage-specific differences in evolutionary rates for CatSper1–4. Generally, the number of amino-acid replacements per site (as inferred from scale bar and branch lengths, Figure 12) is rather high in CatSper1–4 compared to other genes. For example, between mouse and Cypriniformes that value is 2.8–3.4. For comparison, Ca_V and Na_V channels (the channels most closely related to CatSper, see Ren et al. 2001) show a far smaller number of amino-acid replacements between human and zebrafish (for CaV ca. 0.25, Gauberg et al. 2020; for NaV ca. 0.14, Moran et al. 2015). The evolutionary distance of mouse to any Cypriniformes and of human to zebrafish is the same, (435 million years for both human-zebrafish and mouse-zebrafish, Kumar et al. 2017). CatSper1–4 consequently appear to evolve rapidly in comparison to their closest channel relatives.

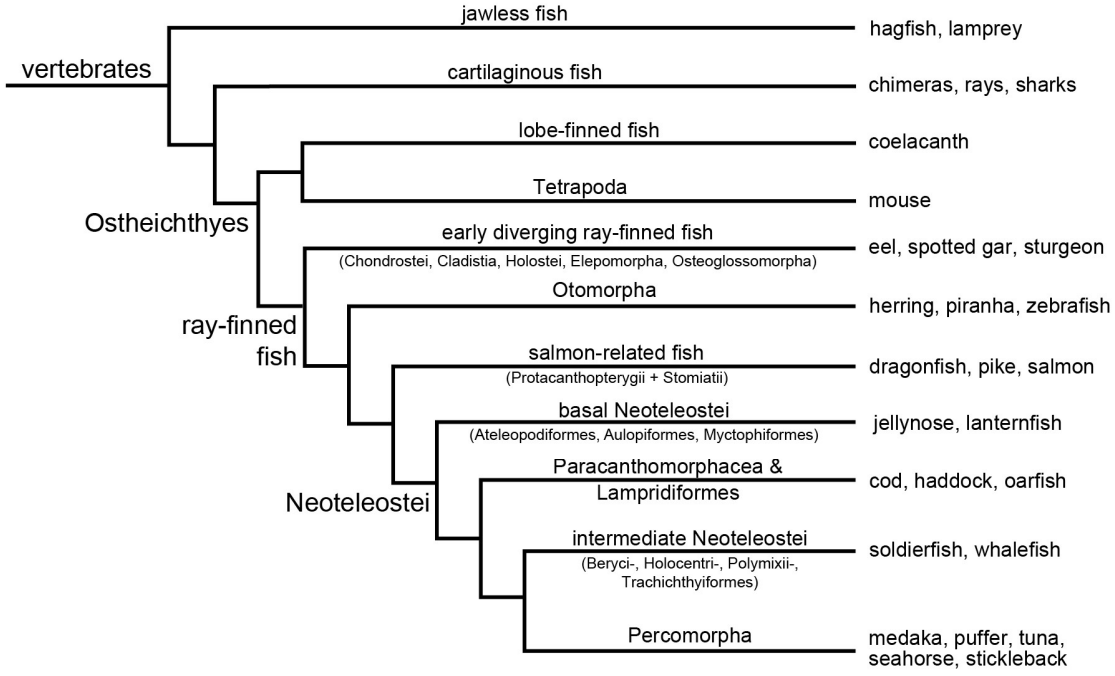

Figure 13: Taxonomy cladogram of fish lineage. Example species given on the right. Tree topology is taken from Betancur (2013).

For the auxiliary CatSper genes, the number of amino-acid replacements per sequence site is similarly high (3.3–3.6 between mouse and Cypriniformes, Figure 14). The phylogenetic analysis for the auxiliary CatSper genes also produced clearly delineated clades with high branch supports (Figure 14). Two exceptions (genes marked with *) are present, but both are pseudogenized. As explained above for CatSper1–4, pseudogenes are likely to have inaccurate alignments. Based on the phylogenetic arrangement of the auxiliary CatSper

clades, CatSperB and E are most closely related, forming a sister group to CatSperD. These three then present another sister group to CatSperG, which is the most distant group.

Within the individual clades of auxiliary CatSper genes, we find some of the same differences between taxonomic position of the species and location of the auxiliary CatSper gene from the respective species, which we have observed for CatSper1–4. This applies to the auxiliary CatSper genes of lobe-finned fish and tetrapods, salmon-related fish, and Paracanthomorphacea and Lampridiformes.

But in addition, we also find aberrant positions for some species groups for auxiliary CatSper genes that do not mimic the positions of the respective CatSper1–4 genes: For example, Clupeiformes do not have a consistent position in the phylogeny of the auxiliary CatSper genes. CatSperG genes of Clupeiformes appear basally, CatSperE genes in the middle of the tree, and CatSperD genes more derived than salmon-related fish (but Clupeiformes species are less-derived than salmon-related fish), and CatSperB genes appear as a sister group to salmon-related fish (Figure 14). Only the latter reflects their position in the phylogeny of CatSper1–4 and the position of Clupeiformes in the taxonomy (Figure 12, Figure 13). Cypriniformes possess only CatSperG and CatSperE, but in both cases this gene group appears in a more derived position (Figure 14), which differs both from the position of the CatSper1–4 genes and the taxonomic position of Cypriniformes (Figure 12, Figure 13).

The differences between phylogeny and taxonomy shared among the CatSper1–4 and auxiliary CatSper genes suggest the same underlying causes, even if those causes are currently unknown. However, additional effects are likely at play because the phylogeny of the various species clades differs between CatSper1–4 and auxiliary CatSper genes as well. Furthermore, as pointed out above, auxiliary CatSper genes are subject to more frequent gene loss than CatSper1–4 (compare Figure 7 and Figure 8, Figure 9 and Figure 10), suggesting that the auxiliary CatSper genes are subject to different evolutionary pressures. These pressures may contribute to both the observed difference in retention and in the phylogeny.

In summary, the phylogenetic analysis of CatSper shows a high rate of mutation for all CatSper genes, and furthermore suggests lineage specific-differences in their rate of evolution. For CatSper1–4, the phylogeny also suggests two subsequent rounds of gene duplication in their evolutionary history.

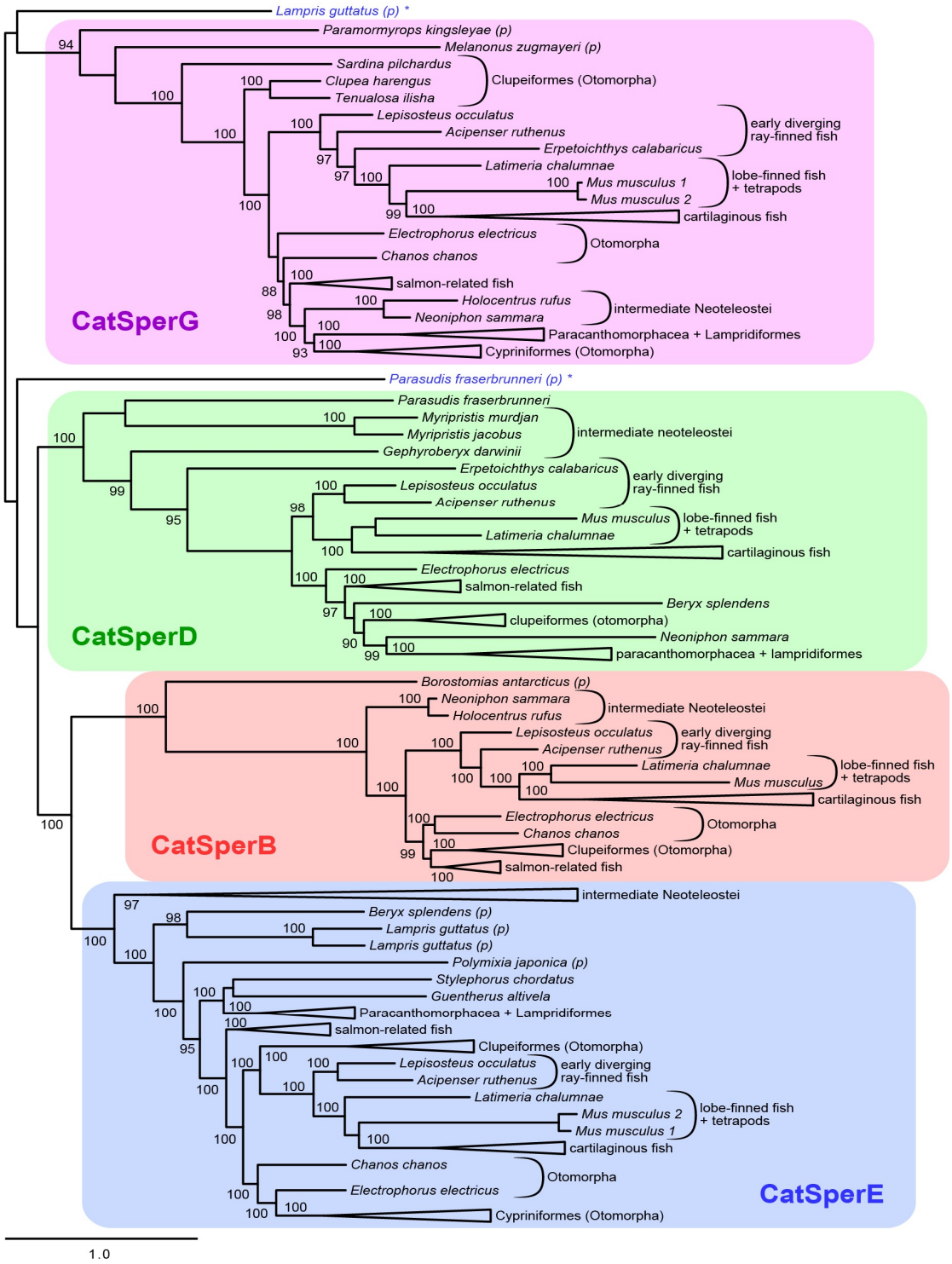

Figure 14: Phylogenic tree of new-found auxiliary CatSper genes and known auxiliary CatSper genes (such as *Mus musculus, Lepisosteus occulatus*). Branch support values are given in %, if above 80%, at their respective node. Scale bar value (1.0) denotes the replacement rate of amino acids on every position of

the sequences. Genes marked (f) are fragments (< 200 amino acids); genes marked (p) are pseudogenes. Genes marked with * were annotated as CatSperE genes.

3.2. Soluble Adenylate Cyclase in fish

Soluble adenylate cyclase (sAC) constitutes an essential part of the signalling cascade leading to CatSper activation (unlike CatSper, sAC also has other functions). It cyclizes adenosine triphosphate (ATP) to cyclic adenosine-monophosphate (cAMP), a second messenger in many contexts. In mammalian and sea urchin sperm, cAMP increase activates a sodium proton exchanger (sNHE) which over subsequent steps results in the opening of CatSper (Figure 1).

Thus it would be interesting to see, whether or to what extent the presence/absence of sAC is correlated to the presence/absence of CatSper. The method used to carry out the search is identical to the one described above for CatSper. Because the examination was carried out later (October 2021), more species genomes were available (743).

The phylogenetic analysis of sAC (Figure 15) shows that all sAC genes, both previously known and new-found, separate with maximal branch support into their own clade and are well separated from the outgroup (transmembrane adenylate cyclases). Several subclades of sAC genes are visible which correspond to phylogenetic grouping (e.g. all Clupeiformes genes cluster together, likewise all Chondrostei, which are early-derived ray-finned fish). All previously known sAC genes are well integrated at expected phylogenetic positions, e.g. the lobe-finned fish Latimeria chalumnae and Protopterus annectens group together with mammals.

sAC often is present as a single gene; however, occasionally two to four sAC genes are observed in a single species. For example, for Ictalurus punctatus (catfish) I found three additional genes beyond the already annotated one. These gene gains seem to have occured at different taxonomic levels, some appear species-specific (e.g. the newly found catfish gene 'triplet'), others appear to have happened much earlier, e.g. at the evolutionary origin of the Otomorpha group.

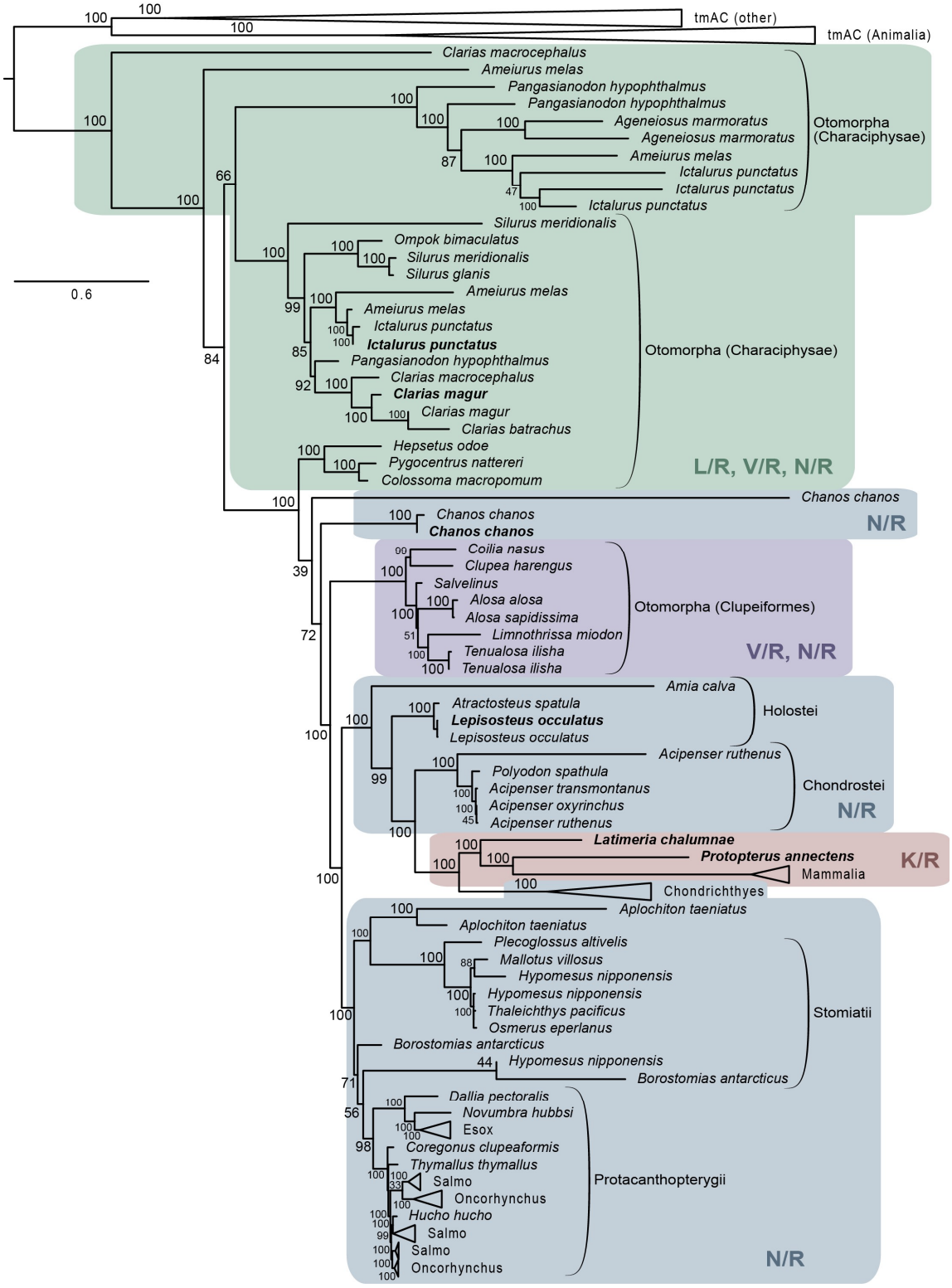

Figure 15: Phylogenic tree of new-found sAC genes and known sAC genes (such as *Latimeria chalumnae, Chanos chanos*, marked in bold italic), with transmembrane adenylate cyclase genes (tmAC) as outgroup. Branch support values are given in % at their respective node. Scale bar value (0.6)

denotes the replacement rate of amino acids on every position of the sequences. Underlaid colors indicate the polymorphism in AAs necessary for bicarbonate recognition; color code as indicated in figure.

The phylogenetic analysis shows that a considerable number of species do not posess sAC (Figure 16, Appendix Table 3). These species are distributed across the fish lineage. The earliest-diverging vertebrate clade, jawless fish, do not possess sAC. Since sAC orthologs are present in non-vertebrate chordates (Romero and Nishigaki 2019a), this is equivalent to a loss in jawless fish. Cartilaginous and lobe-finned fish all possess sAC, and several but by far not all clades within ray-finned fish do so as well. Both the earliest-diverging ray-finned clade (Cladistia) and several intervening clades (Elepomorpha, Osteoglossomorpha, Cypriniformes), as well as the most-derived clade (Neoteleostei) lack sAC entirely. The latter is especially notable because Neoteleostei comprise the largest number of fish species, both in terms of species examined, and extant species (Appendix Table 1). The absence of sAC in Cypriniformes also means that zebrafish do not possess it, just like they lack CatSper. Based on this pattern of absence and presence of sAC in fish, I postulated several independent gene loss events for sAC (Figure 16, red circles). It is noteworthy that gene losses for sAC are even more extensive than that observed for CatSper (see Figure 7). This could suggest that sAC may not constitute an essential part of the signalling cascade for sperm steering in all species that use CatSper.

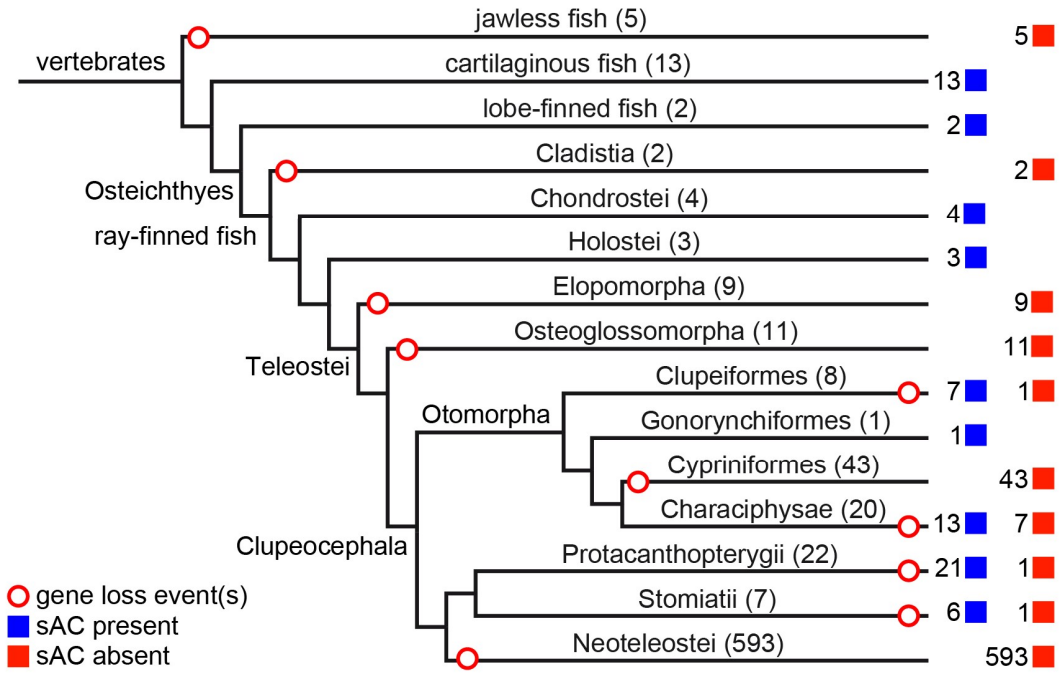

Figure 16: Presence and absence of sAC in different lineages of fish. The number of examined genomes is given in brackets after the name of the group (the total number of species per group is given in Appendix

Table 1). Tree topology is taken from Betancur (2013). Numbers before boxes refer to number of species; color code for boxes as indicated. Red circles indicate loss of sAC in ≥ 1 species of the group. Circles on the right-hand side of a branch indicate more recent gene loss within the group; circles on the left-hand side of a branch indicate early gene loss within the entire group.

Two AAs are essential to HCO3-/bicarbonate recognition in mammalian sAC: K95 and R176 (lysine and arginine, both positively charged) (Kleinboelting et al. 2014). Replacement or mutation of them impacts sAC ability to coordinate bicarbonate (Kleinboelting et al. 2014). Lobe-finned fish (coelacanth *Latimeria chalumnae*, lungfish *Protopterus annectens*) share K/R with mammalian sAC (Figure 15). However, the vast majority of sAC I found in the remaining fish lineages have N/R (lysine replaced by asparagine, which is polar but uncharged) or, more rarely, L/R (lysine replaced by leucine, which has a hydrophobic side chain) (Figure 15) (Körschen et al. 2021). This would suggest that an evolutionary divergence in sAC occurred at the bifurcation of Sarcopterygii (lobe-finned fish, which also includes mammals) and Actinopterygii (ray-finned fish). Furthermore, cartilaginous fish (a clade that is evolutionarily older than the Sarctopterygii–Actinopterygii bifurcation) also have N/R, suggesting that the K/R motif is a new development in the Sarcopterygii lineage. These data provide a foundation to select key species for functional experiments to examine to what extent bicarbonate recognition is linked to the K/R motif.

3.3. Coomassie staining of zebrafish oocytes shows variable staining in micropylar area

The chorion of fish oocytes is made up of proteins that can be stained with Coomassie Blue. Yanagimachi et al. (2013) showed that in some fish species (herring, black and barfin flounder, medaka, bitterling, and steelhead), the micropyle and the adjacent area are stained much stronger with Coomassie Blue than the rest of the chorion (see Figure 17). In black flounder oocytes, proteolytic digest with trypsin prevents staining and impairs fertilization efficiency, suggesting suggesting a protein as responsible agent (Yanagimachi et al. 2013). These observations are suggestive in that protein(s) on the chorion surface localized to the micropyle may guide or attract sperm, which facilitates fertilization in these fish. The fertilization strategies across species are quite diverse, and other species may not use this mechanism.

But regardless of the exact mechanism used, the Coomassie staining provides an easy method to identify the micropyle. This would make it possible to excise the micropyle via Laser capture microdissection (LCM), as well as pieces of plain chorion, and subsequently analyse their proteins with mass spectrometry. Here I

examined whether whole oocytes and chorions of zebrafish show a similar pattern of Coomassie Blue staining, to facilitate such a protein identification.

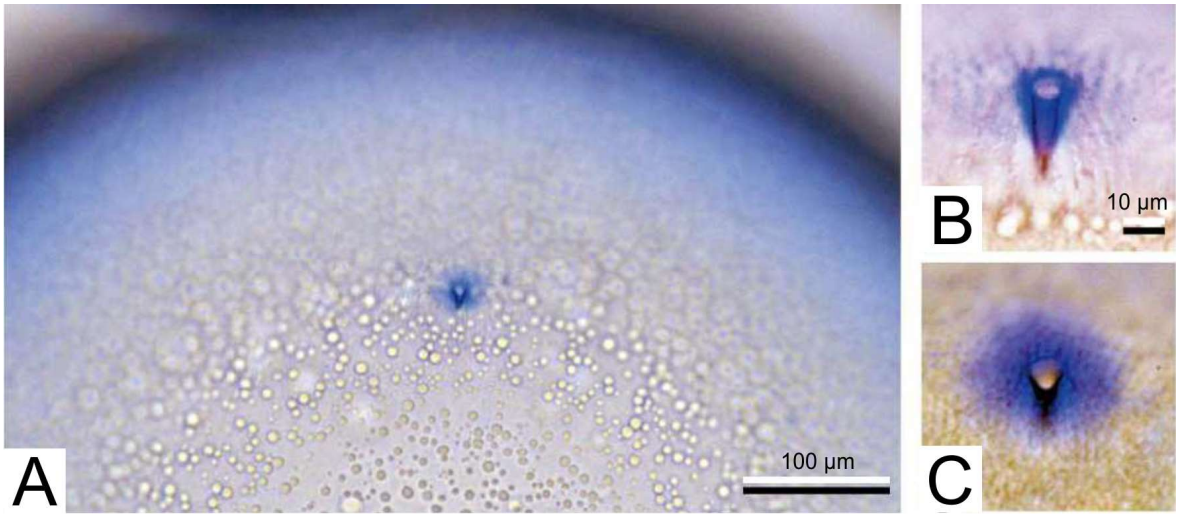

Figure 17: Black flounder oocytes stained with Coomassie Blue. Note the dark blue staining around the micropyle. A) Low and B, C) high magnification views of the micropyle (adapted from Yanagimachi et al. 2013).

Oocytes were obtained via dissection of female zebrafish. Yanagimachi et al. used Ringer solution. I also tested PBS, and obtained similar results for both solutions: in whole oocytes, Coomassie Blue lightly stains the entire chorion, and causes a more intensive staining around micropyle (Figure 18A, B) and in the micropylar channel (Figure 18C, D). In comparison to the staining pattern described by Yanagimachi et al., the contrast between micropylar staining and the staining of the remaining chorion is far lower in zebrafish (compare Figure 17 with Figure 18). This could indicate that protein(s) in the micropylar area of zebrafish are less concentrated compared to those in black flounder (Yanagimachi et al. 2013). Alternatively, Coomassie Blue may stain these proteins less avidly.

For isolated chorions, in most cases, a very weak staining was visible within the micropylar channel compared to the remaining chorion. The staining of the surrounding micropyle was not different compared to the remaining chorion (Figure 18E, F).

The variable and weaker staining of the micropylar area in the isolated chorions as compared to whole oocytes could indicate that the protein(s) are lost during the isolation process of the chorion. This process involves washing and storage in TNE (Bonsignorio, Perego et al. 1996), which contains Triton X-100, a non-ionic detergent. It is possible that exposure of the chorions to Triton X-100 affects the protein content of the micropylar area and results in a lower Coomassie Blue staining compared to whole oocytes. However, Triton X-100, unlike trypsin, does not proteolytically cleave proteins and does not denature proteins. It probably

only affects molecules on the surface of the chorion that are not covalently linked to the protein matrix of the chorion.

In conclusion, zebrafish oocytes show a differential staining with Coomassie Blue between micropylar area and the rest of the chorion, although the difference in staining is not as prominent as that in other fish species (Yanagimachi et al. 2013), and is lower in isolated chorions.

The staining of the micropylar area with Coomassie Blue facilitates the detection of the micropyle under a microscope. As mentioned, this can be leveraged for mass spectrometry of the protein composition of the chorion vs. the micropylar area; this approach will be described in the following chapters.

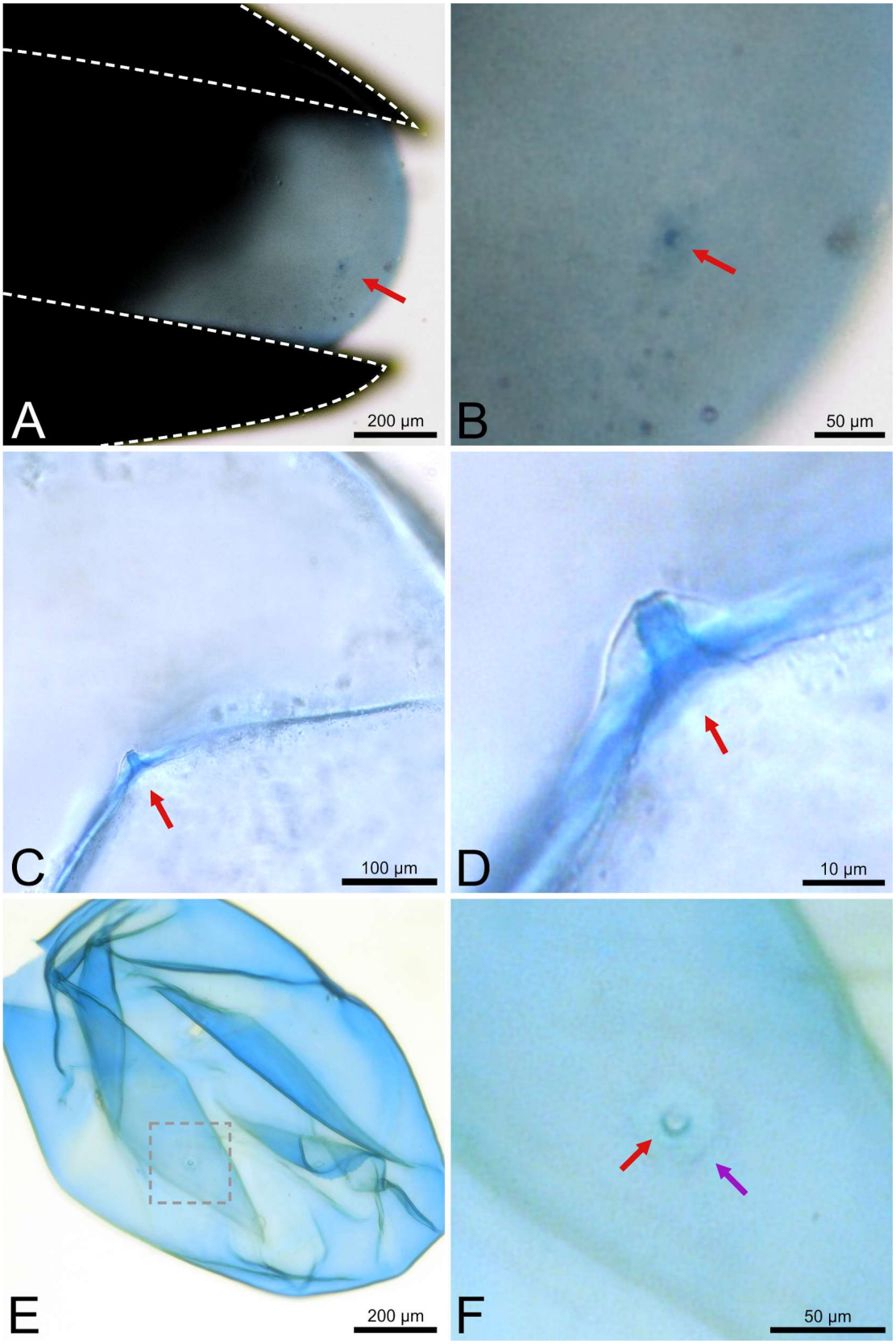
A
200 µm
B
50 µm
C
100 µm
D
10 µm
E
200 µm
F
50 µm

Figure 18: Zebrafish oocytes and isolated chorion stained with Coomassie Blue. B, D, F) Close-ups of the micropylar area of **A**, **C**, and **E**, respectively. Red arrows point to center of the micropyle. **A, B**) Oocyte prepared and stained in PBS, dashed line represents forceps used to immobilize the oocyte. Note the darker staining around the micropyle (red arrow). **C, D**) Oocyte prepared and stained in Ringer solution. Micropyle is shown in profile view through indentation of the chorion. The inside of the micropylar channel (red arrow) is strongly stained by Coomassie Blue. **E, F**) Top-down view of micropyle in isolated chorion. Dashed-line square (**E**) indicates enlargement shown in **F**. Purple arrow (**F**) points to the ring surrounding the micropylar area. The micropylar channel is visible, but the overall staining intensity is much weaker than for whole oocytes.

3.4. Protein composition of zebrafish chorion

The Coomassie Blue staining of the zebrafish chorion facilitates identification of the micropyle. It is also consistent with the hypothesis that the proteins that are localized to this area interact with sperm and may be involved in sperm guidance to the micropyle. The first step in identifying potential candidates for such a guidance function is to characterize the protein composition of the chorion, specifically the micropylar area. To that end, I employed SDS-PAGE, first to optimize the chorion preparation and, secondly, as a preliminary size separation for subsequent mass spectrometry (MS).

3.4.1. Protein content per chorion

To estimate how many chorions will be needed per experiment for later SDS-PAGE and mass spectrometry analyses, I measured the protein content per chorion using the Bradford protein assay (Bradford 1976) and the Bicinchoninic acid assay (Smith et al. 1985). The content was 2.05 ± 0.53 μg (n = 4) per chorion; this value is slightly lower than what has previously been reported (2.5 - 3 μg, Bonsignorio et al. 1996). However, as shown below, the preparation method used by Bonsignorio and coworkers leads to chorions that are contaminated with other oocyte components (Figure 20), which could result in a higher protein content.

3.4.2. Optimization of chorion isolation

Cleanly isolated chorions are a prerequisite for accurate analysis of chorion-specific proteins to determine their relative abundance with SDS-PAGE and their identity with MS.

Two different methods to isolate zebrafish chorions for SDS-PAGE have been described (Bonsignorio et al. 1996; Mold et al. 2001). The method described by Bonsignorio et al. (1996) involves homogenization of oocytes (grinding in a tissue grinder). The chorions sediment by gravity, leaving the supernatant, which contains oocyte components, and are collected with a pipet. Mold et al. (2001) use the same method to

separate chorions from oocytes but adds washing steps of both oocytes (before homogenization) and chorions (after collection). In both preparations, two protein bands are prominent at approximately 43 and 50 kDa (Figure 19, pink and cyan arrow), and a weaker band near 30 kDa (yellow arrow). In the 100 kDa region, several weaker bands can be observed; in Bonsignorio's preparation, these bands are more prominent (Figure 19, gray bar). However, whether these bands represent chorion-specific proteins is far from certain, because the authors did not show control lanes from oocytes devoid of chorions. A comparison to a sample of the supernatant of the preparation, containing the contaminant proteins from the remains of the oocytes, could help elucidate this issue.

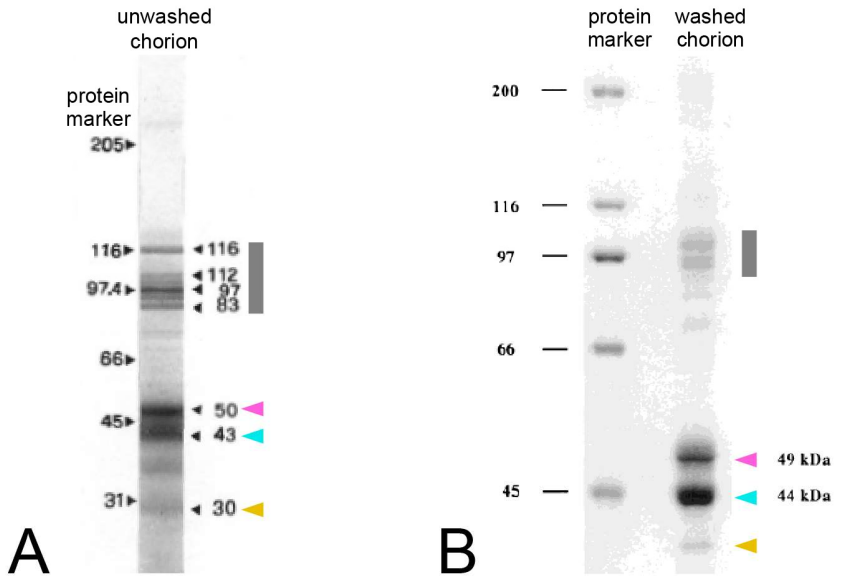

Figure 19: SDS-PAGE lanes of chorion obtained by methods of chorion isolation described in the literature. Molecular weights are given in kDa. **A**) From Bonsignorio, Perego et al. (1996). 5–15% gradient gel used. Protein marker standards are indicated by arrows at the left. **B**) From Mold, Kim et al. (2001). 7.5% gradient gel used

Moreover, washing during the preparation may remove proteins from the chorion. However, molecules serving a haptotactic guidance function are likely to be firmly tethered to the surface of the chorion to be able to generate a concentration gradient. Because the goal of my analysis of the chorion's protein composition is to identify such potential haptotactic signalling molecules, even extensive washing to achieve a clean chorion preparation should not lead to the loss of these molecules. In the following, I used the methods by Bonsignorio et al. (1996) and Mold et al. (2001) and compared supernatant and chorion samples with SDS-PAGE. To facilitate comparison, protein bands will be referred to by the color of the arrows in the figures.

Using the Bonsignorio method, I observe a pattern similar to that described by Bonsignorio et al. (Figure 20A). Two bands are very prominent in the chorion sample (Figure 20B, pink and cyan arrow), with the cyan band being also weakly visible in the supernatant sample. The yellow band is visible in both the supernatant and chorion sample, but enriched in the supernatant (Figure 20B, yellow arrow). I also detected a protein band between 100 and 135 kDa (green arrow) both in the supernatant and chorion sample, but enriched in the supernatant. Several weaker bands are visible at around 100 kDa (Figure 20B, green arrow, gray bar). These green and gray bands potentially correspond to the bands from 83 to 116 kDa in the Bonsignorio et al. report (Figure 20A, gray bar, empty green arrow), although a clear assignment is not possible.

The pink and cyan bands are most likely chorion-specific protein bands because they occur predominantly in the chorion sample, both in the Bonsignorio et al. report and my own experiments (Figure 20). I cannot exclude that the supernatant contains small amounts of chorion because grinding up the oocytes with a pestle may cause small fragments of chorion to become separated from the whole chorion. By contrast, the green and yellow bands may represent contamination from the oocyte because they are, although present in the chorion sample, enriched in the supernatant (Figure 20B).

In conclusion, the preparation method for isolated chorions by Bonsignorio et al. (1996) likely leads to considerable contamination of the chorion with oocyte components (Figure 20A–B, yellow arrow, green arrow).

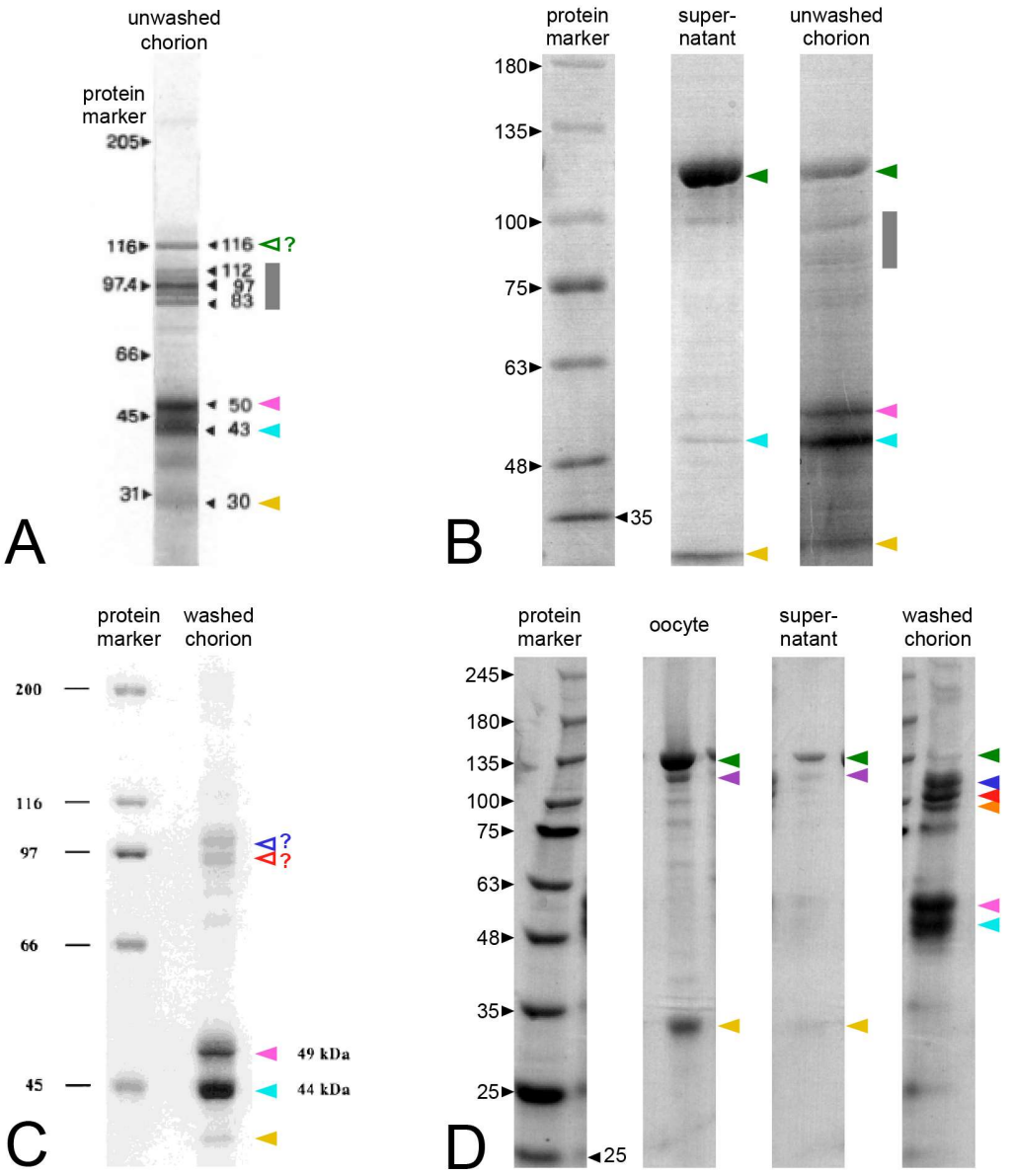

Figure 20: Comparison of chorion isolation methods described in the literature via SDS-PAGE of supernatant, and chorion samples. Supernatant contains components set free by the isolation process such as yolk, oocyte plasma membrane, and oocyte cytoplasm. Mw is given in kDa. **A**) From Bonsignorio et al. (1996). 5–15% gradient gel used. Protein marker standards are indicated by arrows at the left. **B**) My own preparation according to the method by Bonsignorio et al. (1996), using a 4–20% gradient gel. **C**) From Mold et al. (2001). 7.5% gradient gel used. **D**) My own preparation according to Mold et al. (2001), using a 4–20% gradient gel. In addition to supernatant, an oocyte sample was also used in this preparation for comparison.

Using the preparation method by Mold et al., I observe a similar pattern of the pink and cyan bands around 45 kDa (Figure 20C–D, pink and cyan arrow). The yellow and green bands are also detected, quite strong in the oocyte sample, weaker in the supernatant sample, and either absent or strongly reduced in the chorion sample (Figure 20D, yellow arrow and green arrow, respectively). Furthermore, several prominent bands can be observed around 100 kDa in the chorion sample (Figure 20D, blue, red, orange arrow). A band appears below the prominent green band in the oocyte and supernatant samples (Figure 20D, purple arrow), and seems to be absent in the chorion sample.

The pink, cyan, blue, orange, and red bands are likely chorion-specific protein bands (Figure 20D), due to their absence in the oocyte and supernatant samples. Potentially the blue and red bands correspond to the two weaker bands observable in the original Mold preparation (Figure 20C, empty blue and red arrow), since they are the two most prominent bands in that molecular weight range. For the green, yellow, and purple bands, their absence (yellow and purple) or great reduction (green) in the chorion sample suggests they are oocyte-specific protein bands (Figure 20D).

Taken together, the preparation according to Bonsingorio leads to considerable contamination and is therefore not suited for my purposes. The method by Mold presents an improvement in this regard, but is still not a sufficiently clean chorion preparation. Furthermore, the grinding during isolation employed by both methods damages the chorions mechanically.

To improve the preparation technique, I tested different methods of isolation and washing of chorions. For the chorion isolation, dissociated oocytes were triturated, instead of being homogenized, through a Pasteur pipet tapered to less than 0.5 mm diameter at the opening. For each washing step, chorions were agitated in a shaker before sedimenting via gravity, as opposed to the method by Mold, which only sediments chorions via gravity between exchanges of the washing solution. For the control, oocytes were only triturated, but not washed.

The protein band pattern that results from the above preparation (Figure 21A) is with one exception very similar to that observed with the Mold method (Figure 20D): the pink, cyan, blue, red, and orange bands are prominently visible in the chorion samples (both unwashed and washed) and absent in the supernatant, supporting the notion that these bands represent chorion-specific proteins (Figure 21A). However, the yellow band is clearly absent in the chorion samples (Figure 21A) in contrast to the Mold method (Figure 20C). The purple band might also be absent in the chorion samples; however, its M_w is similar to that of the relatively broad blue band, which makes this observation uncertain (Figure 21A). The green band, although present in both supernatant and chorion samples, is much weaker in the unwashed chorion, and is further weakened in the washed chorion, showing that its abundance is lowered through the washing steps (Figure 21A). I

interpret this to indicate that it either represents an oocyte-specific contamination or a chorion-adjacent protein that is not tethered firmly to the protein matrix of the chorion and can be removed by washing. In either case, it is unlikely to be a protein that serves as a haptotactic signalling molecule.

Taken together, the new chorion isolation method leads to less damaged chorions with less contamination from oocyte proteins (absence of yellow band) compared to the method described by Mold et al. (2001). This improved isolation method still involves destroying the entire oocyte to remove the chorion, thereby bringing it into direct contact with internal components of the oocyte. This contamination then necessitates extensive washing to remove it again.

To avoid such a contamination in the first place, I attempted to isolate chorions without damage of the oocyte. Oocytes from ovulatory female zebrafish were submerged in hyperosmotic PBS, which leads to shrinking of the oocyte itself and detachment of the plasma membrane from the chorion. This allows for removal of chorions using forceps.

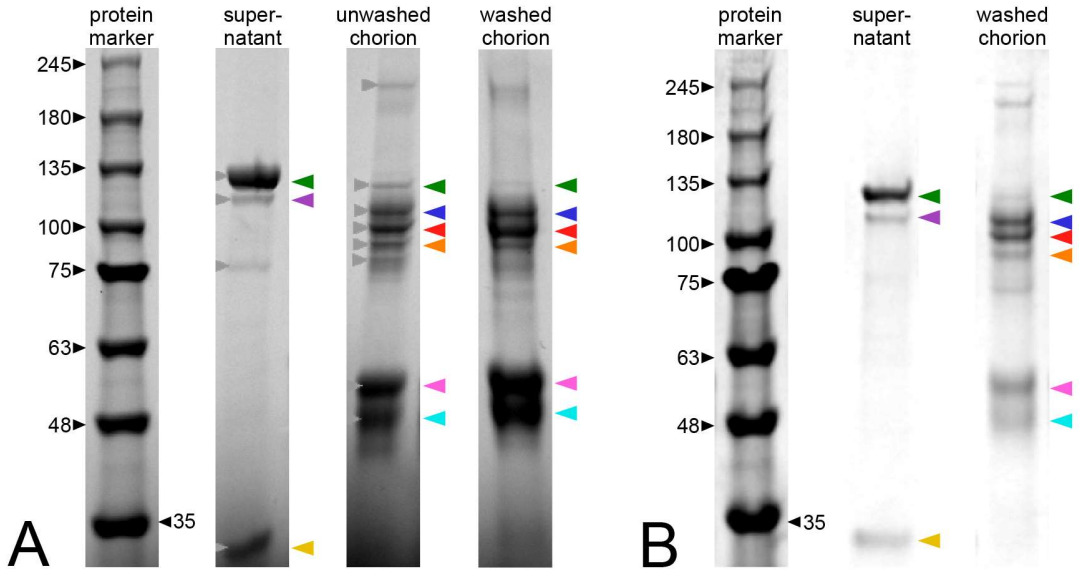

Figure 21: SDS-PAGE lanes of chorion and supernatant from different methods of chorion isolation. Supernatant contains components set free by the isolation process such as yolk, oocyte plasma membrane, and oocyte cytoplasm. Gels are 4–20% polyacrylamide gradient gels. Molecular weights are given in kDa. **A**) Oocytes were washed in PBS and triturated through a tapered-down pasteur pipet. **B**) Dissociated oocytes were suspended in hyperosmotic PBS and had their chorions mechanically removed using forceps.

When using this more gentle method of chorion isolation, the pattern of protein bands observed previously persisted for the most part (Figure 21B): In the chorion sample, the blue and red bands are most prominent, but the orange, pink, and cyan bands are clearly visible as well, and are absent in the supernatant.

The green, purple, and yellow bands occur again in the supernatant sample, with the yellow being clearly absent in the chorion sample (Figure 21B). Regarding the purple band, the situation is less straightforward (Figure 21A), due to the similar M_w of the blue and purple bands in the chorion sample. A very faint green band can also be detected in the chorion sample (Figure 21B). This band pattern is very similar to that obtained with the trituration method (Figure 21A). However, the isolation from mature oocytes using forceps enables chorion isolation without damaging the plasma membrane of the oocyte and, therefore, without releasing internal oocyte components.

Table 5 gives an overview of the average molecular mass for the characteristic bands detected in chorion and supernatant samples. The M_w values are somewhat higher than those reported by Bonsignorio et al. and Mold et al. (1996; 2001) (Figure 19). I attribute this to differences in gel preparation, or potentially technical errors: the M_W given in the Bonsignorio gel for one of the protein bands is 112 kDa, based on the protein marker weights however, it should be 101 kDa (Figure 19A).

Table 5: Average and standard deviations for molecular weights of the most common bands (as indicated by colored arrows in Figure 20B, D, Figure 21) in supernatant and chorion samples.

supernatant		**chorion**	
MW [kDa]	*s. d. [kDa]*	*MW [kDa]*	*s. d. [kDa]*
123	± 10	107	± 8
110	± 10	100	± 7
32	± 2	95	± 6
		53	± 3
		48	± 2

In conclusion, I was able to improve on the methods for chorion isolation, thereby reducing or removing contamination from the oocyte and reducing damage to the chorions themselves, although an entirely clean chorion preparation remains elusive.

3.4.3. Mass spectrometry of the zebrafish chorion

I chose the following approach to identify potential micropyle-specific proteins in the zebrafish chorion: three whole chorion samples (containing the micropyle area) were compared to three chorion samples with the micropyle area removed (Figure 22). Using mass spectrometry, proteins that occur only in micropyle-containing samples can be identified. Even if this differential approach might not yield an identification of micropyle-specific proteins, a list of proteins occurring in the chorion would still be a valuable resource for further analysis of potential sperm-chorion interactions.

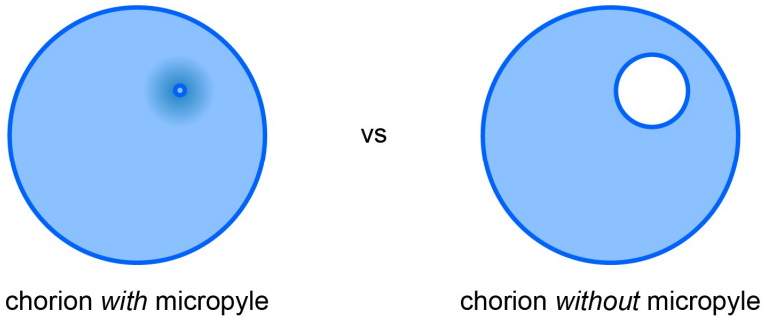

Figure 22: Schematic representation of chorion samples with (whole-chorion) and without micropyle area (micropyle-missing) to be compared by MS analysis. Micropylar area is shown with dark blue gradient.

For the MS measurements, chorions were isolated from oocytes, and stained with Coomassie Blue to facilitate identification of the micropyle. The micropyle area of chorions were removed using laser-capture microdissection. The collected samples were examined by SDS-PAGE and subjected to in-gel proteolytic digestion prior to MS measurement. Peptide sequences obtained by MS were used as queries to identify the corresponding proteins in the Uniprot database for zebrafish (The UniProt Consortium 2021).

3.4.3.1. High variability in identified proteins in chorion samples

Initially, chorions were isolated by trituration of oocytes from ovaries obtained through dissection. Since this procedure disrupts the oocytes, the chorions were subsequently subjected to multiple washing steps to remove oocyte material as far as possible (Bonsignorio et al. 1996). This method is hereafter referred to as method A. Three samples were prepared, each from a different fish, and each containing about 20 chorions. From the resulting protein hits, four different lists were generated (Appendix Table 4): lists contain all proteins found (i) in the whole-chorion samples (WC), (ii) in the micropyle-missing samples (MM), (iii) the

subset of proteins that are common to the three whole-chorion samples (WC_{subset}), and, finally, (iv) the subset of proteins common to the micropyle-missing samples (MM_{subset}). To determine proteins that occur only in the micropyle, I subtracted MM from WC_{subset}. What is the rationale behind this procedure? WC_{subset} is used to lower false positives from spurious protein hits due to contamination. MM is used to remove proteins not located to the micropyle. This subtractive procedure yielded four protein hits: two cytoplasmic polyadenylation element-binding proteins (CPEB1, CPEB1b), and two hits for vitellogenin 2 (vtg2, a yolk precursor protein). In other words, these proteins stem from contamination with the oocyte cytoplasm (CPEB1, CPEB1b) or yolk (vtg2). In fact, the majority of proteins identified in the chorion samples obtained by method A are contaminant proteins from the yolk or cytoplasm (e.g. vitellogenin, actin, tubulin). Of 279 proteins identified, 24 are clearly a result of contamination with yolk, and 143 proteins of contamination with cytoplasm (Appendix Figure 12, Appendix Table 6). Evidently, even the intensive washing used in method A was not sufficient to completely remove oocyte material. This high amount of contamination could mask the presence of chorion-specific proteins and as such, method A is unsuitable to reliably identify proteins specific to the excised micropylar area. (Figure 22).

Furthermore, the MS results using method A show a high variability: only 40% of protein hits found in the whole chorion preparation occur in all three samples (Figure 23). Ovaries contain oocytes of varying maturation stages (Wang and Ge 2004), but the exact distribution of stages depends on the phase of the ovulatory cycle (Hisaoka and Firlit 1962). Thus, the variability could result from the use of fish at different points of the ovulatory cycle. The large variability could yield false-positive and false-negative results for the differential approach, and also presents a problem for establishing a proteome for zebrafish chorion.

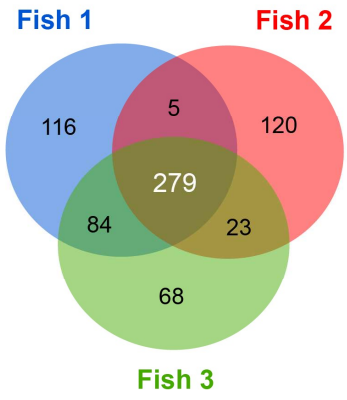

Figure 23: Inter-fish variability of protein hits for preparation method A, shown by Venn diagram. Three fish were analyzed, one whole-chorion sample per fish. Protein subsets are visualized by overlapping colors. Numbers refer to number of protein hits in the respective subset.

I next used the optimised preparation method for chorions (discussed in the previous section 3.4.2.; hereafter called method B). It is expected to yield a cleaner preparation. Mature oocytes were obtained by belly massage (Zhang et al. 2005; Westerfield 2007), subsequently submerged in hyperosmotic medium, and chorions were isolated via forceps. This preparation method was performed with whole chorion to determine inter-fish variability and the level of contamination by non-chorion proteins. It is expected that both will be substantially decreased compared to method A, and if so, a differential approach could be expected to be successful.

Furthermore, I included a blank control in the measurements to identify potential contamination from external sources: empty SDS-gel that was treated equally to the protein-containing SDS-gel in the preparation for MS. Again, three fish were used, but additionally, the chorion preparation for each fish was divided into three sub-samples subsequent to chorion isolation, leading to nine samples total. This was done to examine not only inter-fish but also intra-fish variability.

The total number of protein hits per sample was reduced using method B even before the blank test was subtracted, in all but one case (Figure 24, Appendix Table 5). An examination of the proteins found (Appendix Table 6) shows a similar amount of chorion-specific proteins (ZP2, ZP3, Mold et al. 2001; Liu, Wang, and Gong 2006) to preparation A. Therefore, I conclude that contaminations by yolk and cytoplasm are reduced.

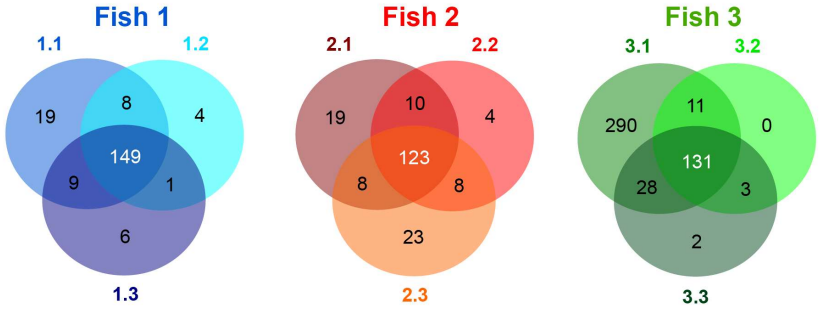

Figure 24: Intra-fish variability of protein hits for preparation method B, shown by Venn diagram. Three fish were analyzed, three whole-chorion samples per same fish. Protein subsets are visualized by overlapping colors. Numbers refer to number of protein hits in the respective sections, after subtraction of blank test.

With one exception, the amount of protein hits unique to a single sample within one fish is in the range of 0–14%. For example, when comparing the protein lists of the samples from fish 1, six of 165 protein hits (4%) present in sample 1.3 are unique to that sample (fish 1, Figure 24). The intra-fish variability is, therefore,

small. Sample 3.1 is a complete outlier, with 63% unique protein hits, equivalent to over ten-fold the standard deviation calculated from all other samples (s.d. = 5%). The sample is therefore likely contaminated with drastically more oocyte material than the other samples, and was omitted in subsequent comparisons.

Next, I investigated the inter-fish variability. Because the intra-fish variability is rather small, all protein hits from one fish can be summed together, and compared to the summed protein hits from other fish. Carrying out this comparison, we find that the inter-fish intersection is 71% for preparation method B (Figure 25B), whereas for preparation method A it was only 40% (Figure 23), representing a considerable improvement regarding the inter-fish variability. This is likely due to a reduction in contaminant proteins from yolk and cytoplasm, and the usage of chorions from a narrower range of oocyte maturation stages. However, the intersection between fish is still far from 100%. Belly massage is expected to only yield mature oocytes (Zhang et al. 2005; Westerfield 2007), but smaller differences between maturation stages due to fish being at different points of the ovulatory cycle (Hisaoka and Firlit 1962) cannot be excluded and may explain part of the remaining inter-fish variability.

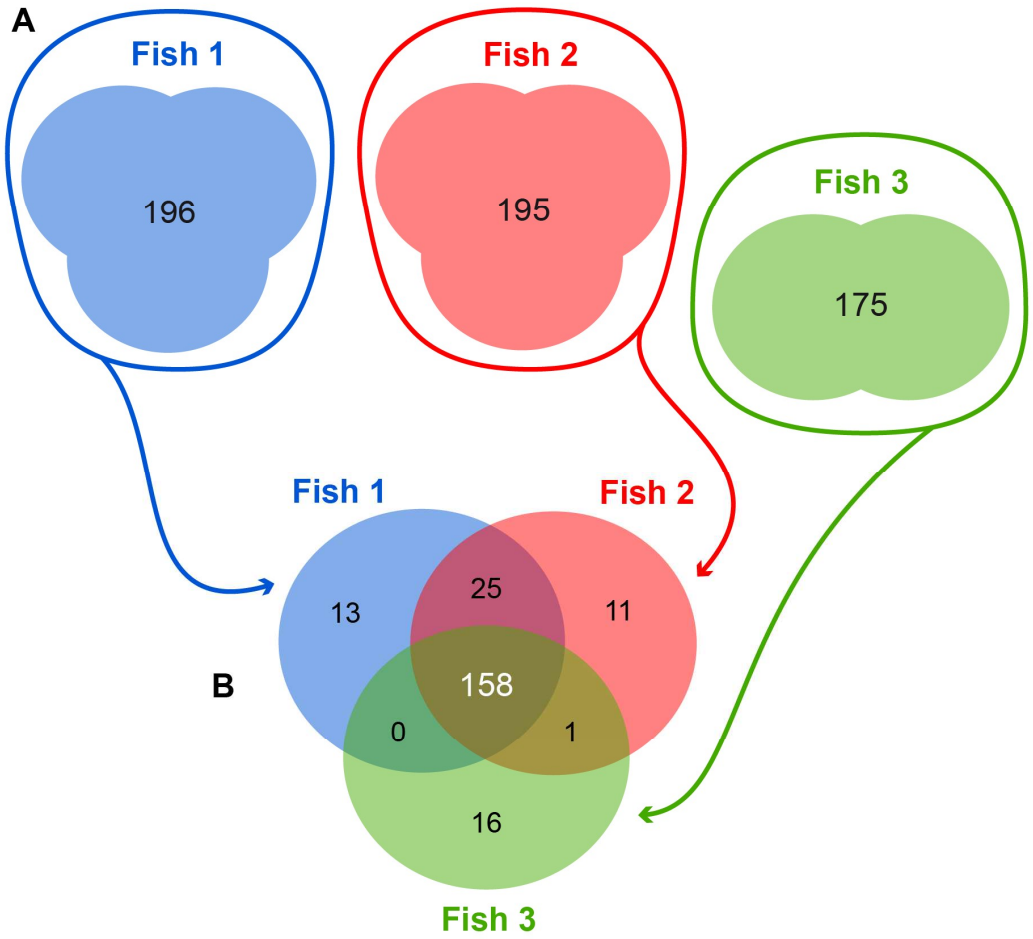

Figure 25: Inter-fish variability of protein hits for preparation method B, shown by Venn diagram. Protein subsets are visualized by overlapping colors. Numbers refer to number of protein hits in the respective sections, after subtraction of blank test. A) Intra-fish variability (as in Figure 24, sample 3.1 excluded). B) Inter-fish variability. Sum of all protein hits found in fish 1, 2, and 3 (A) are used to create the new Venn diagram.

Taken together, the variability in protein hits observed between chorion samples could be reduced by method B, but still constitutes a problem for any kind of differential screening. Furthermore, if a protein gradient would extend across a considerably larger area of the chorion surface than the area that was excised, no micropyle-specific proteins could have been identified by the differential approach. Thus, no further differential screening attempts were made. Nevertheless, the results obtained for whole chorions can be used to gain insight into the proteome of the zebrafish chorion.

3.4.3.2. Majority of proteins found in the zebrafish chorion are zona pellucida proteins

For subsequent discussion it is important to note that proteins/protein hits refers to the proteins identified by MS, *not* the detected peptides, which were used to identify proteins. Furthermore, several protein isofoms may be assigned to a single gene in the Uniprot database, and as such the proteins found represent an upper limit for the respective genes.

For analysis of the chorion proteome, only protein hits present in all samples of preparation method B were considered. Protein hits found in preparations using method A contained large numbers of proteins that obviously represent contaminants from the oocyte cytosol or membrane; they were not further considered (Appendix Figure 12, Appendix Table 6). The blank control for method B contained 72 hits (Appendix Table 7), which obviously cannot stem from the chorions, and were therefore subtracted. Due to the sensitive nature of the MS and the gel electophoresis not being performed in a clean room or hood the most likely explanation for these hits is a contamination by human proteins. In fact, most of these 72 hits are keratins, which might be expected as airborne contamination if no special precautions such as clean room are taken. Indeed in a random sample of three hits, the associated peptide sequences were found to be identical to those of human keratin sequences.

The proteins identified by MS fall into three categories or classes: proteins that are most likely chorion-specific, proteins that represent contaminations from various sources, in particular the oocyte, and proteins that are uncharacterized and whose function is unknown.

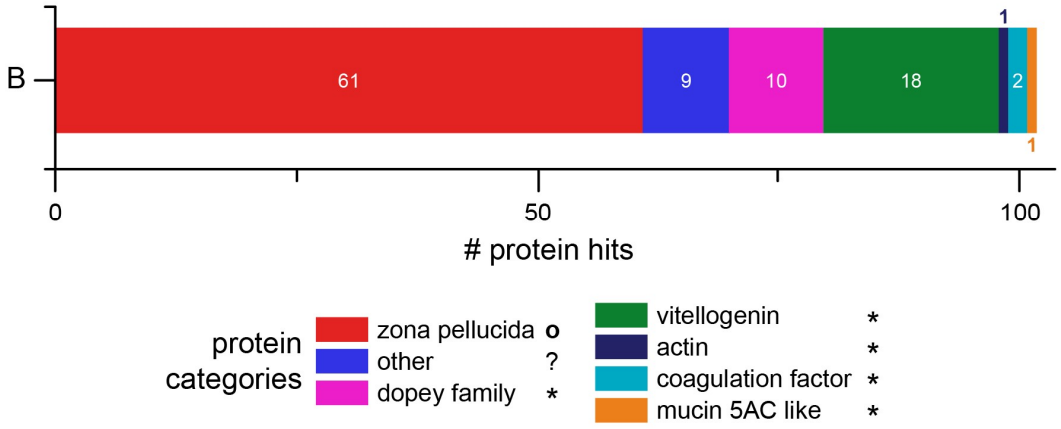

Figure 26: Categorization of proteins found in whole-chorion samples (method B). Categories according to legend, with the symbol after the category name denoting assignment: ? = potentially chorion-specific or chorion-associated protein; * = contaminant protein, originating from the oocyte, ovarian tissue, or an external source; **o** = chorion-specific protein.

More than half of the proteins identified (61 of 103) show high sequence similarity to mammalian zona pellucida (ZP) proteins (Figure 26, Appendix Table 6), and are indeed annotated as zona pellucida proteins in the Uniprot database (The UniProt Consortium 2021). These 61 proteins are associated with 23 different genes (due to the presence of several isoforms), which is a much larger number than the 3–4 genes reported for mouse and human, respectively (Spargo and Hope 2003; Wu et al. 2018). Note that the mammalian zona pellucida is the structural equivalent of the chorion of fishes, and thus the fish orthologs of mammalian ZP proteins are generally designated as zona pellucida proteins (Mold et al. 2001; Liu, Wang, and Gong 2006). Unfortunately, the nomenclature of ZP proteins is highly inconsistent between different publications, both because there are different naming conventions for different subfamilies and because the assignment of individul genes to particular subfamilies also is not consistent (Spargo and Hope 2003; Wu et al. 2018). To obtain an unambiguous assignment of the proteins identified in the MS analysis, I generated a phylogenetic tree with all identified ZP proteins, the complete repertoire of zebrafish ZP genes, and an extended list of reference genes from other species, which will be discussed below (see 3.4.3.3.).

Another major protein fraction (18 out of 103) belongs to the family of vitellogenins, which represent the main component of yolk proteins (Figure 26). I conclude that the chorion preparation still contains a sizeable amount of contaminating oocyte proteins, and shows that, although no visible damage to the oocyte membrane occurred during chorion preparation, it is difficult to obtain a reasonably pure chorion preparation.

Two hits for mucin 5AC-like proteins were found, which are mucus proteins. Mucus is an extracellular protective layer for epithelial surfaces (Dash et al. 2018), and oocytes squeezed out by belly massage can be expected to be covered with mucus. Several proteins of the dopey family are also found. Dopey proteins are involved in intracellular vesicle transport (Molière, Beer, and Wehman 2022), and as such are expected to be part of the oocyte. Coagulation factor protein is a member of the blood coagulation cascade, and blood can be a consequence of belly massage (Kendall 1921, 204) or may stem from decapitation of the fish prior to belly massage. Actin is a cytoskeletal protein, and therefore part of the oocyte. Proteins designated as 'other' are listed as 'uncharacterized' in the Uniprot database.

In conclusion, a proteome of the zebrafish chorion could be established. The majority of the proteins are homologs of ZP proteins. Many more different ZP proteins were found in the zebrafish chorion compared to the overall small size of the mammalian ZP family.

3.4.3.3. Phylogenetic analysis of ZP proteins identified by MS

As mentioned above, there exists no unified nomenclature for ZP proteins, and even the number of subfamilies is controversial (Wu et al. 2018). The latest attempt to generate a unified nomenclature (Wu et al. 2018) recognizes five subfamilies (Table 6).

Table 6: ZP protein subfamilies according to Wu et al. (2018). Human and zebrafish ZP proteins are given by their Uniprot names, and assigned to the respective subfamily according to Wu et al.
*Annotated in Uniprot as si:dkeyp-110a12.4.

Wu et al. subfamilies	*ZPA*	*ZPB*	*ZPC*	*ZPD*	*ZPAX*
Human ZP proteins	ZP2	ZP1, ZP4	ZP3	–	–
Zebrafish ZP proteins	–	ZP2	ZP3	ZPD*	ZPAX

However, (Wu et al. 2018) employed the neighbor-joining algorithm in their phylogenetic analysis to assign gene identities. Unfortunately, this algorithm is unsuitable for a complex phylogenetic analysis such as this one, as it is ill-suited to obtain global optima (Yang 1994). Therefore, I could not rely on the gene naming suggested in this paper. To achieve a robust assignment of the proteins identified in MS as ZP proteins I employed a maximum-likelihood algorithm (see Materials & Methods 2.2.1.) and additionally considerably increased the set of ZP reference proteins.

For use as reference sequences in the tree, I employed the repertoire of ZP proteins listed by Wu et al. (2018), including sequences that were not part of the final tree shown in the paper. Additionally, I searched the zebrafish Ref Seq RNA database with tblastn and all four human ZP as queries to ensure completeness of the zebrafish ZP repertoire. For a better understanding of the early evolution of the ZP gene repertoire, I performed the same search in two early-derived fish species, small spotted catshark and sea lamprey, which also possess high quality Ref Seq RNA databases. Because several RNA sequences are often associated with the same gene, in the next step I extracted unique hits for each gene locus, choosing the longest isoform. This reduced the number of candidates to about 60–70% (Table 7).

Table 7: The ZP repertoire of zebrafish and two early-derived fish.

species	# RNA seq candidates	# unique hits	# ZP genes
zebrafish	82	55	29
catshark	71	44	36
sea lamprey	110	66	55

To proceed, it is important to know that the characteristic ZP domain also occurs in several other proteins, which are unrelated to the chorion. To eliminate such proteins I performed phylogenetic analysis with all unique gene candidates from zebrafish, catshark and sea lamprey together with the ZP reference genes. In fact, up to half of the gene candidates found were located outside the ZP protein clade (Table 7). Annotation of these outside-lying zebrafish genes generally showed the presence of ZP domains. The occurrence of such ZP domain-containing genes in the search results suggests the search to be complete for actual ZP proteins. Furthermore, all genes in the clade containing the established ZP reference genes can be considered as validated ZP genes.

This leaves us with 29, 36, and 55 validated ZP genes for zebrafish, catshark and lamprey, respectively (Table 7), which were used together with the ZP genes listed by Wu et al. to reliably assign the zebrafish ZP proteins identified by MS. For construction of the phylogenetic tree, see Materials & Methods 2.2.1. .

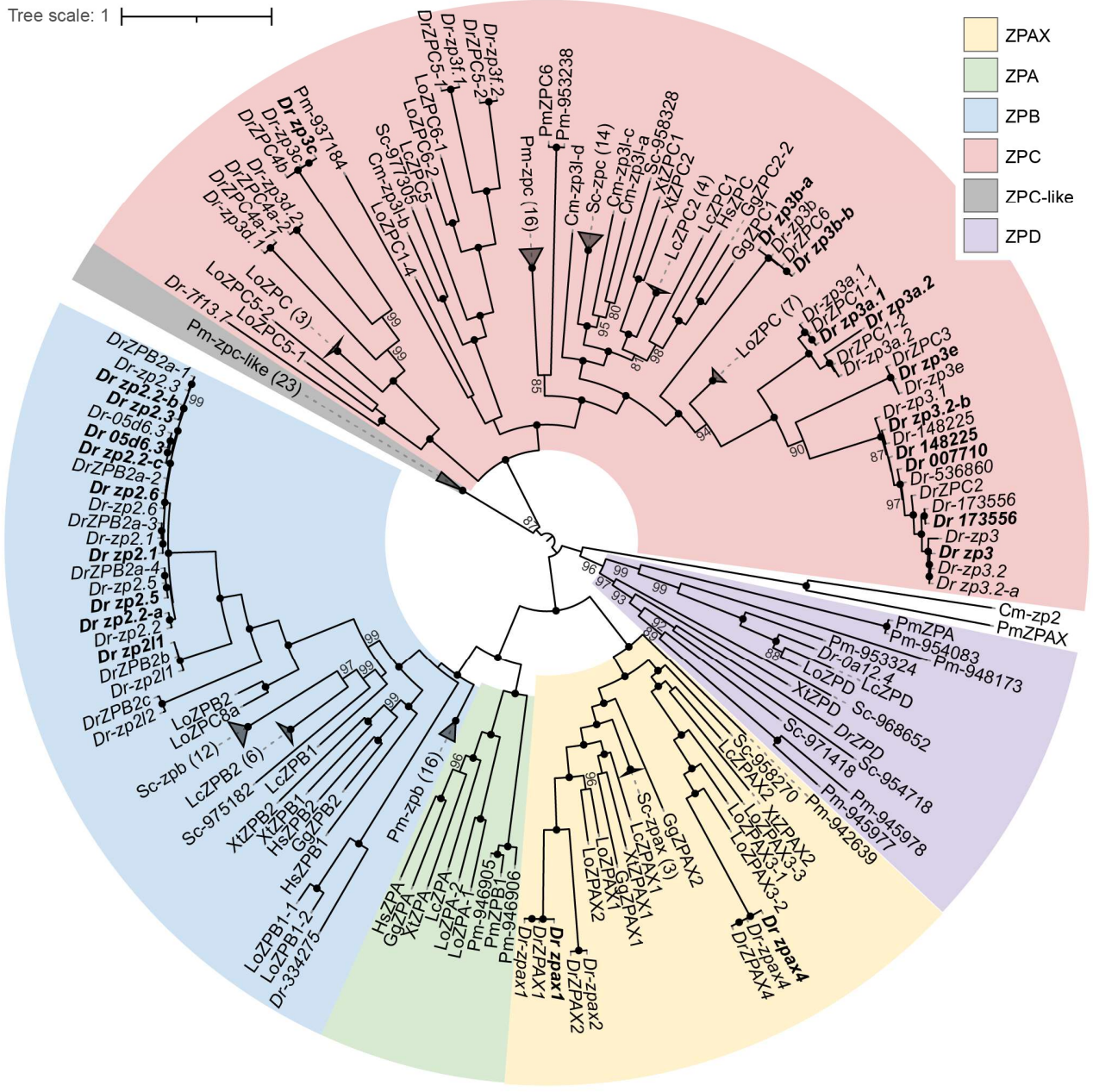

Figure 27: Phylogenetic tree of ZP proteins. Includes proteins listed in Wu et al. (2018), ZP proteins identified by MS of the zebrafish chorion (designated by *bold italic*), and reference proteins from zebrafish, lamprey, and catshark (designated by species abbreviation followed by hyphen). All zebrafish proteins are marked in *italic*. Branch support values are given in percent for values between 80 and 99%. Nodes marked with black dots have 100% branch support. For collapsed clades, number of genes is given in brackets. Scale bar value represents number of amino acid substitutions per position. Species abbreviation as follows:

Cm	Callorhinchus milli	elephant shark	Lo	Lepisosteus occulatus	spotted gar
Dr	Danio rerio	zebrafish	Pm	Petromyzon marinus	lamprey
Gg	Gallus gallus	chicken	Sc	Scyliorhinus canicula	catshark
Hs	Homo sapiens	human	Xt	Xenopus tropicalis	clawed frog
Lc	Latimeria chalumnae	coelacanth			

The phylogenetic analysis shows clear segregation into five subfamilies. The root node for each subfamily has maximal, and in one case near-maximal, branch support. The subfamilies correspond to ZPA, ZPB, ZPC, ZPD, and ZPAX, as defined by Wu et al. (2018). A large clade of exclusively lamprey ZP genes found in my gene searches presents as a clear sister clade to ZPC with very high branch support and was therefore named ZPC-like. Two genes, one from elephant shark and one from lamprey (Cm-zp2 and PmZPAX), lie completely outside the five subfamilies and may represent the remnants of a subfamily lost in bony vertebrates.

As mentioned, neighbor-joining as a method can be unreliable, and indeed several gene names proposed by Wu et al. appear to be wrong, based on their phylogenetic position (Figure 27). For example, three lamprey genes (PmZPA, PmZPB1, PmZPAX) are in fact ZPD, ZPA, and outside the 5 subfamilies, respectively.

All zebrafish genes (those identified by MS, from reference gene searches, and from Wu et al.) can be unambiguously assigned to four of the subfamilies (ZPB, ZPC, ZPD, ZPAX). There are two species-specific gene expansions, in ZPB and ZPC, each with maximal branch support at their root node (Figure 27, Figure 28). Similar, and even larger, species-specific gene expansions are found in catshark and lamprey (Figure 27). Since such gene expansions are not found in mammals, this results in much larger numbers of ZP genes in fish compared to e.g. human. Goudet et al. (2008) have proposed that species with external fertilization require higher numbers of ZP proteins than species with internal fertilization, where the oocyte environment is much more controlled.

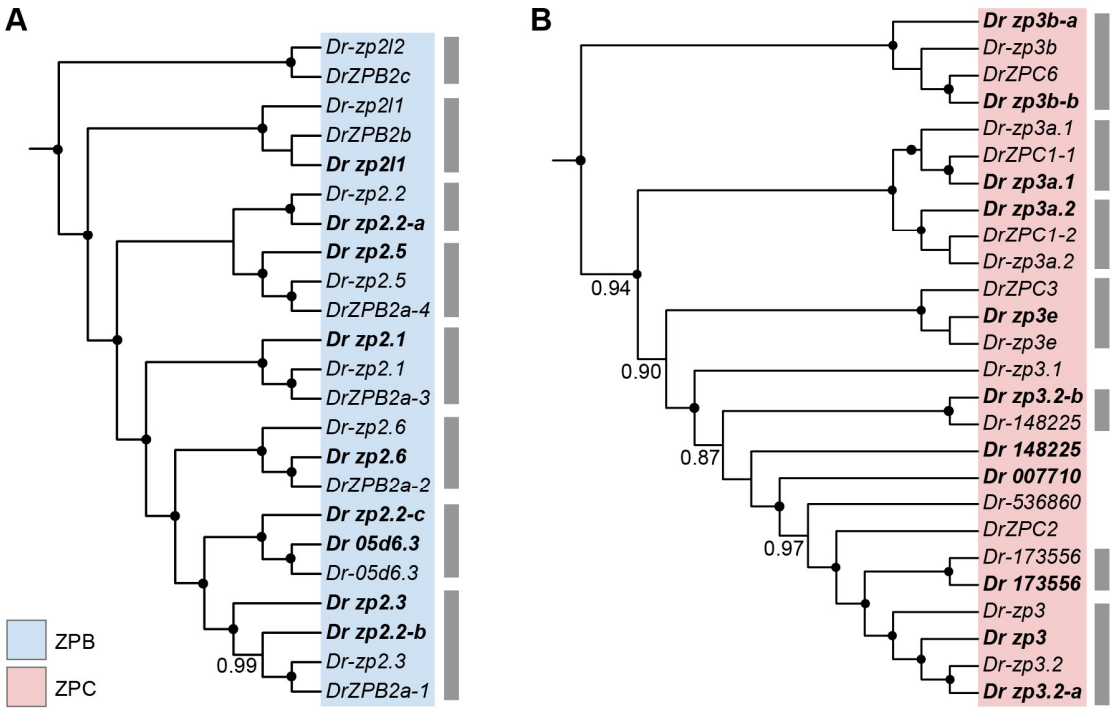

Figure 28: Cladogram of clades of zebrafish ZP proteins derived from tree in Figure 27. Includes proteins listed in Wu et al. (2018), ZP proteins identified by MS of the zebrafish chorion (designated by *bold italic*), and reference proteins from zebrafish (designated by species abbreviation followed by hyphen). Branch support values are given in percent for values between 80 and 99%. Nodes marked with black dots have 100% branch support. Gray bars to the right of the respective cladogram indicate which genes correspond to one another, since they stem from different sources (i.e. *Dr-zp2l1*, *Dr zp2l1*, and DrZPB2b refer to the same gene.)

Next, I used the phylogenetic tree (Figure 27) to compare the ZP proteins identified by MS with the reference ZP proteins. Chorions contained ZP proteins from 20 different genes, which is the large majority of the zebrafish ZP gene repertoire (29, see Table 7). For all 19 proteins with an informative gene name stated in Uniprot (such as zp2.3, etc.), the naming is consistent with their position in the phylogenetic tree (Figure 27, Table 8). Four proteins without an informative gene name (such as LOC100007710) could be assigned to ZPB (one protein) and ZPC (three proteins) subfamilies (Table 8).

Taken together, the phylogenetic analysis allowed an unambiguous assignment of all zebrafish ZP proteins identified by MS in the chorion samples.

Table 8: Nomenclature of zebrafish ZP proteins identified by MS, as assigned by phylogenic analysis (Figure 27). Note that zebrafish do not possess ZPA proteins, and the single ZPD protein was not found by MS. In brackets, the Uniprot gene name at the time the MS analysis was performed is given where relevant.

tree name	Uniprot gene name	assignment
subfamily ZPAX		
Dr zpax1	zpax1 (formerly si:dkeyp-50f7.2)	name confirmed
Dr zpax4	zpax4 (formerly si:dkey-19b23.11)	name confirmed
subfamily ZPB (synonym ZP2)		
Dr 05d6.3	si:zfos-1505d6.3	confirmed as ZPB
Dr zp2.1	zp2.1	name confirmed
Dr zp2.2-a	zp2.2	name confirmed
Dr zp2.2-b	zp2.2	name confirmed
Dr zp2.2-c	zp2.2	name confirmed
Dr zp2.3	zp2.3	name confirmed
Dr zp2.5	zp2.5	name confirmed
Dr zp2.6	zp2.6	name confirmed
Dr zp2l1	zp2l1	name confirmed
subfamily ZPC (synonym ZP3)		
Dr 007710	LOC100007710	confirmed as ZPC
Dr 148225	LOC100148225	confirmed as ZPC
Dr 173556	zgc:173556	confirmed as ZPC
Dr zp3	zp3	name confirmed
Dr zp3.2-a	zp3.2	name confirmed
Dr zp3.2-b	zp3.2 (formerly zgc:173556)	name confirmed
Dr zp3a.1	zp3a.1	name confirmed
Dr zp3a.2	zp3a.2	name confirmed
Dr zp3b-a	zp3b	name confirmed
Dr zp3b-b	zp3b	name confirmed
Dr zp3c	zp3c	name confirmed
Dr zp3e	zp3e (formerly zgc:171779)	name confirmed

3.5. Zebrafish sperm display a variety of swimming patterns

Sperm need to adapt their motility during their life cycle as they are immotile while in the testis but start to swim upon spawning or ejaculation. This process is referred to as activation of sperm. Mechanisms for activation are diverse, in zebrafish it is the hypoosmotic shock upon spawning. Activation results in the basal motility which can last from several seconds up to multiple days depending on the species.

The basal motility can be modulated by chemoattractants released from the oocyte (guidance cues) and mechanical or chemical cues present on the oocyte surface. Such modulation occurs for example in sea urchin sperm, which use the chemoattractant molecule resact to perform chemotaxis, (Ward et al. 1985). While it is still unknown whether zebrafish sperm use chemoattractants as a means to locating the oocytes, previous work has shown that internal calcium levels regulate swimming behavior (Fechner et al. 2015) and thus internal calcium might work as second messenger in motility regulation. Fechner et al. (2015) employed a light-induced increase of internal calcium by photolysis of caged compounds and observed that zebrafish sperm begin to swim in tight drilling circles upon calcium increase. This change in swimming behavior might reflect a behavior that occurs during spawning or during navigation toward the oocyte. However, it is unknown whether such a calcium increase indeed does occur during these processes, and if it does occur, it might well be smaller than that produced by uncaging calcium. Consequently, the magnitude of the change in swimming behavior might be less pronounced during spawning and/or navigation.

To observe potential changes in motility during navigation, it is essential to establish the baseline swimming behavior of zebrafish sperm after activation, but in the absence of potential guidance stimuli. This baseline behavior has not been examined in detail yet.

Here, I studied the basal swimming behavior of zebrafish sperm after activation of motility by hypoosmotic shock. Sperm were obtained as described (Materials & Methods 2.7.1.) and suspended in isoosmotic ES. Immediately before recording, the sperm suspension was mixed with system water (1:30) in custom-built motility chambers (Figure 3) and transferred to the microscope. The time delay from activation to the start of the measurements was generally less than 5 seconds. Video was taken for 32 s (800 frames), i.e. during the main swimming phase. Video recording was done using darkfield imaging which gives the best contrast.

I observed several different swimming patterns in zebrafish sperm upon activation with water (Figure 29). These patterns can be assigned qualitatively to three groups: largely straight paths, paths with constant curvature where the degree of curvature is variable between paths, and paths with changing curvature. Occasionally, sperm swim on narrow circles (constant curvature), reminiscent of the drilling motion observed by Fechner et al. (2015). Taken together, this demonstrates a high variability of basal swimming behavior of zebrafish sperm.

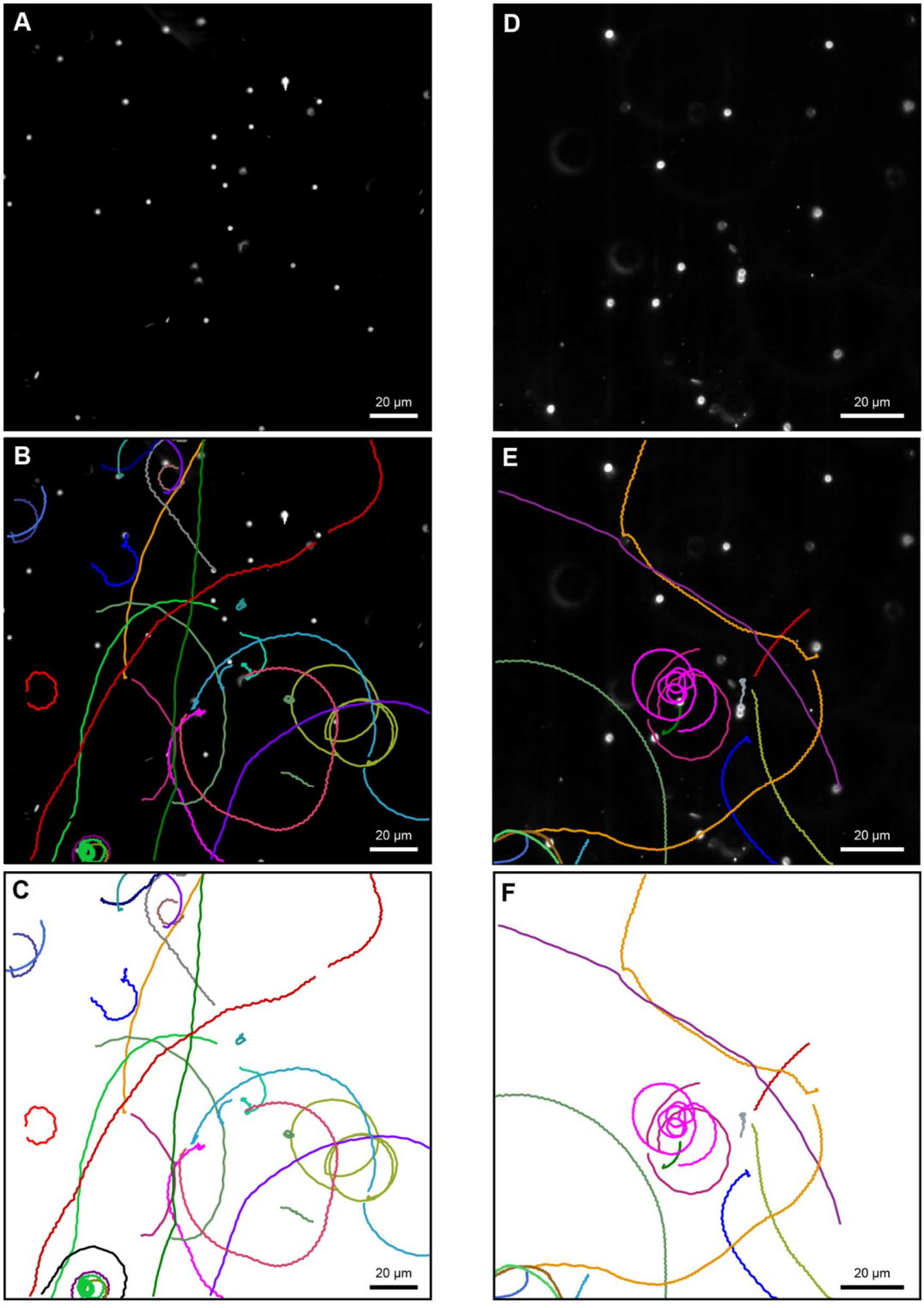

Figure 29: 2D swimming paths of zebrafish sperm activated with water and imaged at 25 frames per second. A, D) Darkfield images of sperm. **B, E**) Darkfield images of sperm overlaid with tracked swimming

paths. Individual paths are color-coded. Small gaps in the tracks (red track in **B**, orange track in **E**) are due to interference with other particles. **C, F**) Tracked swimming paths of sperm from panels **B**) and **E**), shown here without darkfield. Color-coding same as in **B, E**.

For a quantitative analysis of the sperm trajectories, three parameters were evaluated to characterize the swimming patterns: point-to-point velocity (**V**elocity **C**urvi**L**inear, VCL), velocity determined on a locally smoothened path (**V**elocity **A**verage-**P**ath, VAP), and overall velocity from starting point to maximally distant point (**V**elocity **S**traight **L**ine, VSL). The definitions are illustrated in Figure 30. Furthermore, two derived parameters of sperm motility were calculated: the linearity (LIN) and steadiness (STE) of a sperm cell's path. LIN is calculated by dividing VSL by VAP, its maximal possible value is LIN = 1, i.e. a straight line, Lin = 0 equals strong curvature. STE is calculated by dividing VAP by VCL and describes the amount of wobble the sperm head exhibits. STE = 1 equals the absence of wobble, i.e. maximal steadiness. The smaller the STE value the higher the wobble.

For all three velocity parameters, the respective histograms depict a broad range of velocities, from 2 to > 40 μm/s (Figure 30), confirming the qualitative result of high variability between sperm, see Figure 8. The VCL distribution (Figure 30A) is broader than that of VAP (Figure 30B) and VSL (Figure 30C), with a full width at half maximum (FWHM) of 8 bins, compared to 2 bins for VAP and VSL. This is expected, since both VAP and VSL cannot exceed VCL, but can be smaller, thus the whole distribution of VAP and VSL will be compressed compared to VCL. In particular, in the VSL distribution a considerable number of sperm have a velocity < 1 μm/s, resulting from sperm swimming tighter circles and thus not reaching far beyond their starting point (Figure 30C).

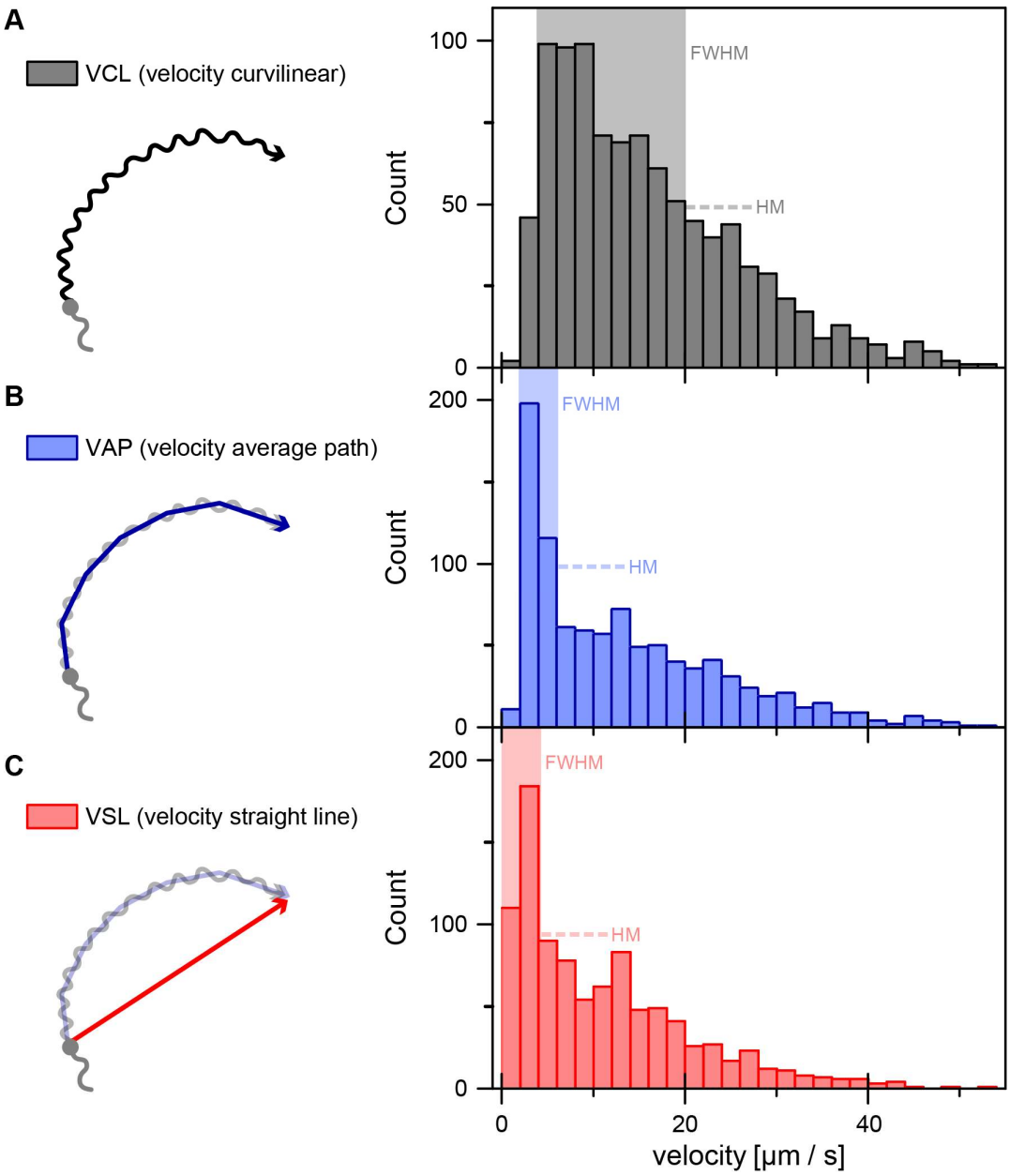

Figure 30: Frequency distribution of different swimming velocities of zebrafish sperm. A–C) On the left, schematics showing the sperm in gray and the velocity parameters color-coded as indicated, with the respective underlying parameters shown at reduced opacity. On the right, the respective histogram showing the distribution. Bin width is set to two µm/s. HM, half maximum; FWHM, full width at half maximum, indicated by light color overlay on the respective bins. **A**) Velocity curvilinear: point-to-point velocity of the sperm, calculated frame by frame. It indicates how quickly a sperm moves along its actual path, including any side-to-side movements. **B**) Velocity average path: point-to-point velocity of the sperm, calculated over a sliding average of 6 frames. It indicates how quickly a sperm moves along its trajectory, with side-to-side

movements smoothed out. **C**) Velocity straight line: Velocity calculated using the first point of the average path (calculated as given in B) and the farthest away point that is reached during the window of measurement (Wilson-Leedy and Ingermann 2007).

For LIN and STE, the range of values is also broad (0–1 for LIN, and 0.1–1.1 for STE), but skewed toward higher values compared to the velocity parameters (Figure 31). For LIN the interval 0.9 to 0.95 shows highest abundance, indicating a great number of sperm whose swimming paths show little curvature (Figure 31A). In total, half of all sperm exhibit swimming paths with a LIN greater than 0.8 (Figure 31A). For STE, the interval with highest abundance is 0.95–1.0, and half of all sperm show STE values larger than 0.85 (Figure 31B), indicating that many sperm swim with little extraneous head movements.

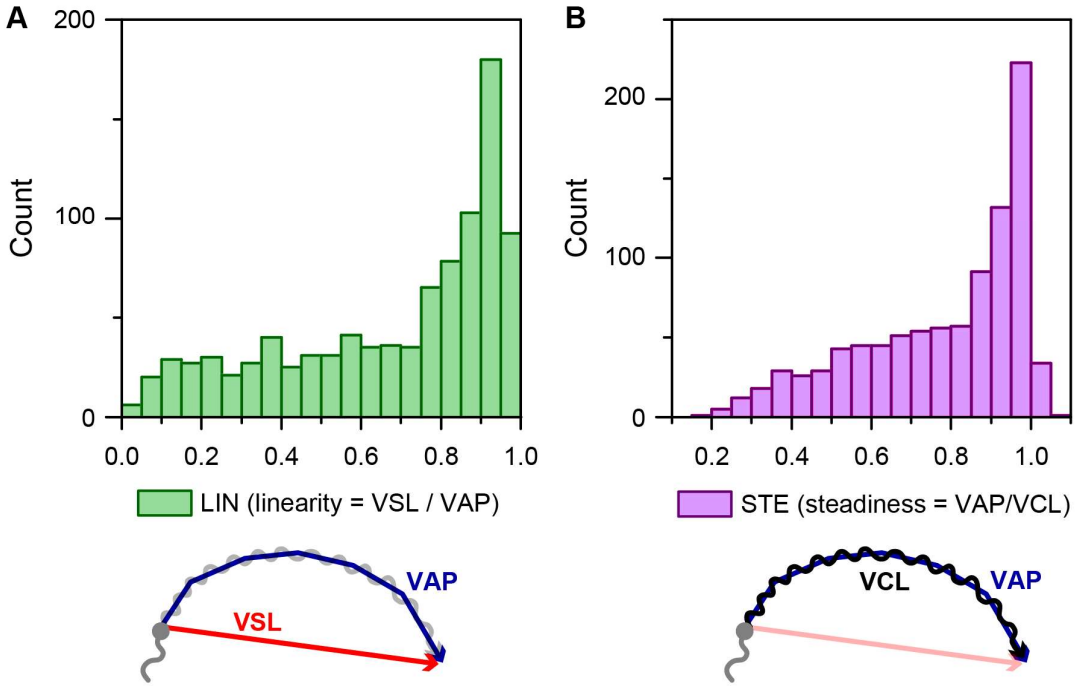

Figure 31: Frequency distributions for derived parameters of sperm motility. Bin width is set to 0.05. Color code according to legend. **A**) Linearity: derived from VSL and VAP, this measures the curvature of a sperm's swimming path. Higher values indicate higher linearity and less curvature. **B**) Steadiness: derived from VAP and VCL, this measures the wobble/side-to-side movement of a sperm's head along its swimming path. Higher values indicate a steadier path; lower values indicate a higher degree of wobble.

In conclusion, zebrafish sperm display great variation in their swimming behavior in the absence of stimuli, manifesting in a wide range of curvatures and velocities. This means one needs to measure large populations of sperm to detect changes in swimming behavior in response to stimuli that are significant. This

makes the method, as employed, unsuitable as bioassay to test a large range of potential guidance stimuli. Therefore, I next turned to investigation of intracellular ionic levels of the sperm cells as potential indicators of guidance responses.

3.6. Fluorescence imaging reveals ionic changes within zebrafish sperm upon activation by hypoosmotic shock

Intracellular changes in ion concentrations are an integral part of many signaling cascades, such as the one responsible for sperm guidance in sea urchin (Seifert et al. 2015). Calcium and pH are of particular interest, because both play an important role in the sperm signaling cascade of several species (sea urchin, mouse, and human, Wachten, Jikeli, and Kaupp 2017). Calcium controls the flagellar beat and can induce motility changes.

In sperm from sea urchin, mice, and humans, these ion changes and the signalling components, e.g., the CatSper ion channels, are localized to the flagellum (Nomura and Vacquier 2006; Seifert et al. 2015; Chung et al. 2014; Miller et al. 2015; 2018). By contrast, in zebrafish, ion channels that have been identified so far are localized to the sperm head—a HCN1-like channel, which conducts protons, and CNGK, a potassium channel, which is controlled by pH (Wobig et al. 2020; Fechner et al. 2015). Little is known about the ionic changes involved in the motility of zebrafish sperm: Release of calcium from caged calcium by light in the cytoplasm changes the swimming behavior (Fechner et al. 2015)—however, extracellular calcium is not necessary for activation and motility (Wilson-Leedy, Kanuga, and Ingermann 2009).

Therefore, I looked for ion changes in both head and flagellum of zebrafish sperm upon activation (initiation of motility) and swimming in the absence of external stimuli using fluorescence imaging. These measurements constitute the necessary basis against which to compare sperm's reactions to potential chemotactic or haptotactic stimuli.

3.6.1. Optimization of dye loading

In previous experiments performed in our group, zebrafish sperm were loaded on ice for 2–3 h with 10 μM of the calcium-sensitive dye Cal520 (Fechner 2012; Fechner et al. 2015). Both the long loading time and relatively high dye concentration might stress the sperm cells. Moreover, in the meantime, an improved version of this dye with higher signal-to-noise ratio and better cell retention, called Calbryte520, became available. I optimized the dye-loading procedure for Calbryte520 with regard to loading time, temperature, and dye concentration.

The first issue was that of loading temperature: Previous experience in our lab and others suggested that lower temperatures are beneficial for sperm viability (Hagedorn et al. 2009). However, the dye is used in the acetoxy-methyl-ester form, which relies on cytoplasmic esterases to cleave the ester once the dye has entered the cell (Tsien 1981). Lower temperatures slow esterase activity and, thereby, the effective loading speed.

Therefore, I performed preliminary tests on the effect of storage at higher temperatures on viability, using the percentage of motile sperm as an indicator of overall viability (Figure 32). A high variance in motility can be observed. Nevertheless, storage temperatures around room temperature (18°C, 22°C) lead, on average, to higher percentages of motile sperm than storage at 0°C, both with and without dye loading. Thus, the experiments hint that storage at room temperature enhance rather than reduce motility. Therefore, all subsequent experiments to optimize the dye loading were performed at room temperature.

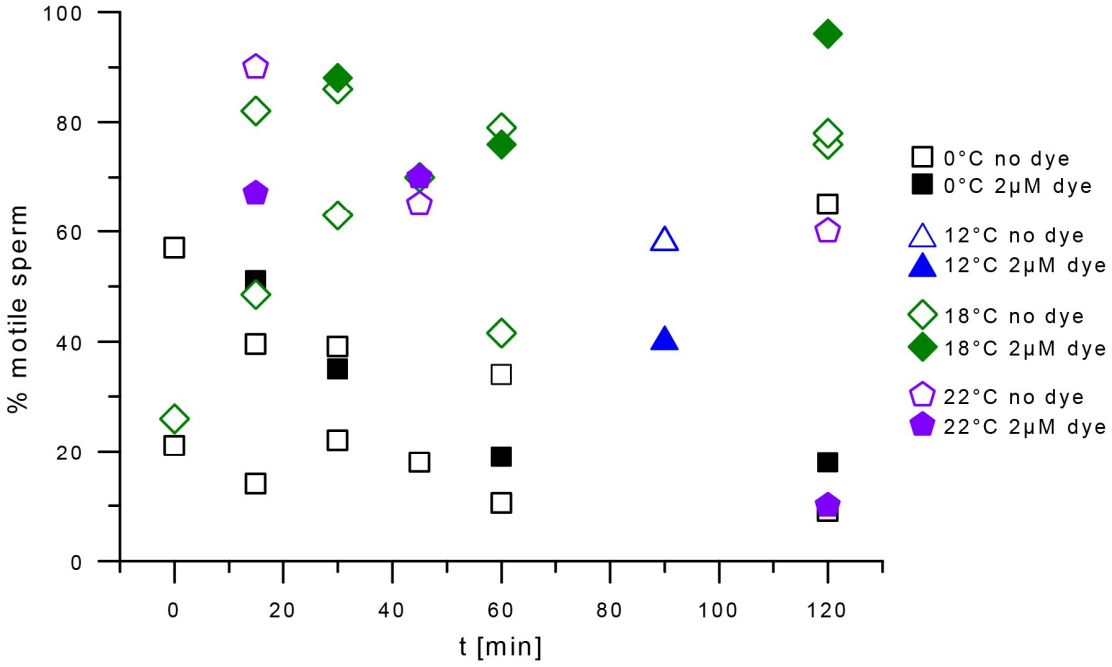

Figure 32: Percentage of motile sperm in a sample over time, in relation to different storage temperatures and presence or absence of Calbryte520 dye. Storage temperatures are color-coded as indicated, filled symbols indicate presence of dye.

Next, the effect of dye concentration was analyzed. The amount of dye taken up was determined by its fluorescence under saturating calcium concentrations. This was achieved by adding ionomycin, a calcium ionophore, which incorporates into the plasma membrane, enabling calcium transport across the membrane. The extracellular calcium concentration is high, leading to a large increase of intracellular calcium upon

addition of ionomycin, and a corresponding increase in fluorescence. Preliminary experiments with cultured CHO cells (Appendix Figure 13) indicate that dye concentrations in the nanomolar range are sufficient to detect ionomycin-generated calcium signals. Therefore, I examined three concentrations from 200 nM to 1 µM (Figure 33A). All three concentrations resulted in roughly the same change in fluorescence intensity over time (calculated as F/F_0, for details see Methods 2.9.7.). Consequently, a concentration of 200 nM suffices for loading. Higher dye concentrations can impair cell viability and may also affect calcium homeostasis, therefore, lower dye concentrations are beneficial.

Finally, different dye loading times from 15 to 90 min (increasing in 15 min increments) were tested (Figure 33B). While the loading time of 15 min gave the largest change in F/F_0 10 and 15 min after ionomycin addition, the signal was very noisy, presumably due to relatively low dye concentration achieved at this short loading time. Therefore 15 min loading time was not considered further, even though a short loading time would put less stress on the cells. F/F_0 signals after ionomycin addition were very similar for 75 and 90 min loading times, and clearly larger and less noisy over the entire 15 min after ionomycin addition compared to 30, 45, and 60 min loading time. Therefore, a loading time of 75–90 min was chosen for subsequent experiments.

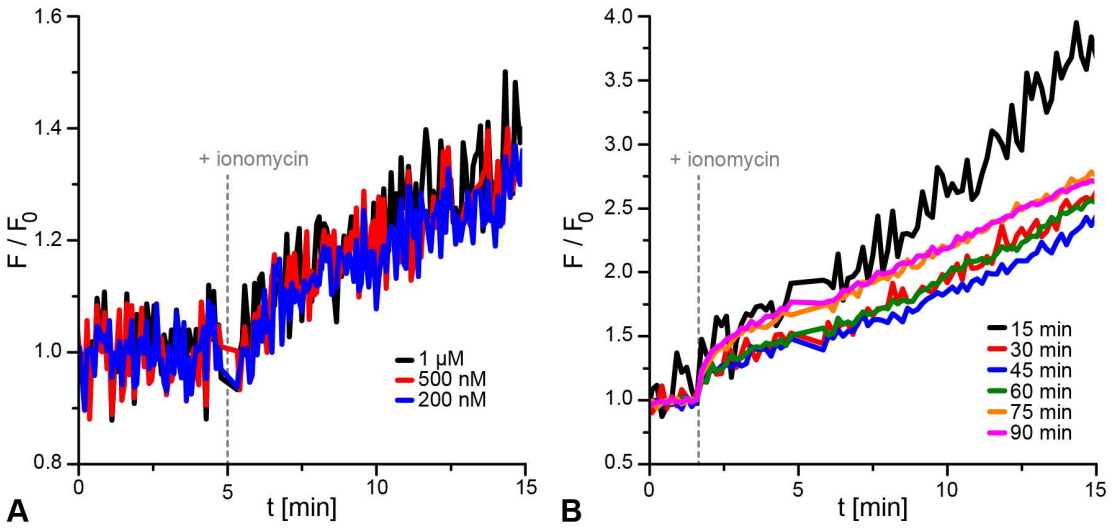

Figure 33: Time course of fluorescence changes in zebrafish sperm loaded with Calbryte520 in response to addition of ionomycin. A) Comparison of F/F_0 signals using different dye concentrations during loading. **B**) Comparison of the effect of different loading times on the F/F_0 signal. Note that noise decreases with increasing loading time, i.e. increasing dye concentration.

3.6.2. Changes in Calcium and pH in sperm head upon activation

With the dye-loading procedure established, I first examined changes in calcium and pH in the head of zebrafish sperm. Two different methods were used: stopped-flow and single-cell imaging. Stopped-flow allows rapid mixing of two solutions (sperm and stimulus) and subsequent fluorescence measurement in a small cuvette. This method measures the fluorescence of a large cell population. Because the fluorescence of the sperm head is so much stronger than that of the flagellum, in the stopped-flow device, the fluorescence signal stems primarily from the sperm head. The single-cell imaging under a fluorescence microscope uses video recording of single cells that are superfused with a solution. The superfusing solution can be switched, allowing addition of stimulus. This imaging technique allows to differentiate between fluorescence from the sperm head and flagellum.

Experiments to study sperm activation with calcium-sensitive dyes were performed with both techniques, i.e., in the stopped-flow apparatus and with single-cell imaging. Experiments with pH-sensitive dyes were performed with single-cell imaging only.

3.6.2.1. Calcium increases in the sperm head upon activation

Zebrafish sperm were loaded with Calbryte520 and subjected to hypoosmotic shock via system water (water prepared for use in the zebrafish facility, see 2.3.1.) to induce activation.

A fluorescence increase was observed in the sperm head upon contact with system water, both in the stopped-flow and single-cell imaging experiments (Figure 34). This indicates an increase of intracellular calcium in the sperm head upon activation. In the stopped-flow device (Figure 34A), the increase in F/F_0 remains just below 10% upon mixing with system water, and the signal is very noisy. The large noise precludes an analysis on the fast timescale theoretically possible with the 2 ms sampling rate of the experiment. The fluorescence increase approaches a plateau over the measurement duration of 40 s. In the single cell imaging experiment (Figure 34B), F/F_0 changes are much larger, reaching to a five-fold increase in some cases. However, the time course of the increase is similar: A plateau is reached after about 50 s. Note that the single cell imaging experiments represent only the subset of analyzable sperm cells: Sperm that move vigorously or tear loose during the experiment could not be analyzed.

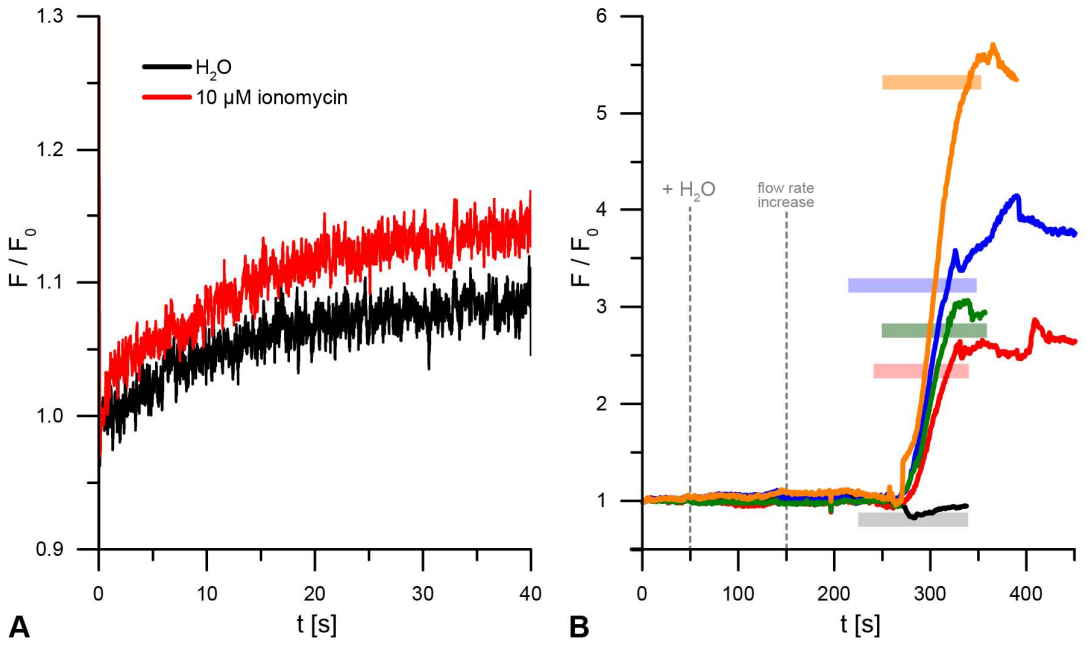

Figure 34: Fluorescence changes in zebrafish sperm loaded with Calbryte520. A) Population measurement of sperm in stopped-flow set-up. Black and red traces represent fluorescence signals recorded from immotile sperm in ES mixed 1:1 with system water or ionomycin in ES, respectively. **B**) Single cell imaging experiment in superfusion set-up. Colored lines show representative sperm cells. Sperm sometimes detach from the surface, resulting in shorter traces. Dashed gray lines indicate changes to superfusion. +H2O means a switch from ES to system water at the inflow, the solution change in the superfusion chamber itself occurs with a latency. The increase in flow rate is induced by added pressure on the superfusing syringe (for detailed experimental set-up, see Methods 2.9.6.). Colored bars indicate duration of flagellar movement.

The drastically higher F/F_0 in the single-cell measurements (Figure 34B) compared to the population measurements (Figure 34A) are difficult to explain. A partial reason could be the inherently large variability of the sperm cell responses. Not every single sperm cell undergoes a fluorescence increase (just like not every single sperm cell reacts with motility upon contact with system water). Some sperm show either no fluorescence change or even a fluorescence decrease (see e.g. black trace in Figure 34B). On average, 6% of sperm show no fluorescence increase, and 15% even show a clear decrease in fluorescence (Appendix Figure 14). Since in the population measurement all these responses contribute to the mean value, the increase of the overall fluorescence will be correspondingly smaller. However, this is expected to be a minor influence, since the clear majority of sperm (Appendix Figure 14) do respond with an increase, with Figure 34B representing the spectrum of those responses. For other possible reasons see 3.6.2.2.

The duration of sperm motility in the single-cell imaging experiments is about 100 s (colored bars in Figure 34B). This duration is a bit longer than the 60–80 s reported by (Wilson-Leedy, Kanuga, and Ingermann 2009), presumably because the exchange of isoosmolar solution with system water in the superfusion setup is not instant (see 2.9.6.), resulting in some mixing and consequently in a less severe hypoosmotic shock. Smaller hypoosmotic shocks enable sperm to swim for longer (Wilson-Leedy, Kanuga, and Ingermann 2009).

The onset of motility sometimes precedes the calcium increase in the sperm head (colored bars in Figure 34B), but I also observe concurrent effects or even delayed onset of motility compared to the calcium increase. In principle, the temporal relationship between onset of motility and ionic changes in the sperm could give insights into a potential causal order. If the calcium increase can follow the motility increase, the sperm might use other signals (e.g. pH) to induce motility. However, the single-cell imaging set-up as used is not well-suited to examine this question. Ideally, one would image fluorescence and darkfield simultaneously, because darkfield imaging allows a more robust detection of sperm than is possible with just the fluorescence signal.

3.6.2.2. Calcium response depends on strength of hypoosmotic shock

A hypoosmotic shock can activate zebrafish sperm, and the duration of motility is inversely related to the strength of the hypoosmotic shock, as long as the shock reaches a certain threshold necessary for activation (Wilson-Leedy, Kanuga, and Ingermann 2009). In my experiments, I have used a half-maximal shock in the stopped-flow device: zebrafish sperm in ES (about 300 mOsm) are mixed with system water (about 10 mOsm) at 1:1, which results in a reduction of osmolarity, i.e. hypoosmotic shock, of about 145 mOsm. Single cell imaging meanwhile allowed for near-maximal shock via the replacement of ES with system water, a shock of about 290 mOsm. Both are strong enough to induce activation within the sperm.

This range of motility-inducing hypoosmotic shocks allows to investigate whether the strength of the calcium response is a function of the strength of the hypoosmotic shock. I tested various mixing ratios of sperm in ES, loaded with Calbryte520, and system water in the stopped-flow apparatus. The mixing ratios were 1:1, 1:2, 1:3, 1:4, and 1:5 of sperm to system water, which corresponds to a hypoosmotic shock of roughly 145, 200, 220, 230, and 240 mOsm, respectively. Note that the fluorescence signal becomes increasingly noisy with higher mixing ratios (Figure 35, Appendix Figure 15), presumably because the final volume in the observation cuvette of the stopped-flow device remains unchanged but the number of sperm cells—that are loaded with fluorescent dye and can thus contribute to the calcium signal—decreases.

With increasing hypoosmotic shock, F/F_0 also increases (Figure 35), albeit not in a linear fashion. The F/F_0 increase between mixing ratios 1:2 and 1:3 is slightly larger than that between mixing ratios 1:1 and 1:2, even though the difference in hypoosmotic shock is 55 mOsm for the latter and only 20 mOsm for the former. Moreover, a further 20 mOsm increase between mixing ratios 1:3 and 1:5 does not result in any additional increase in F/F_0 (Appendix Figure 15). Therefore, the saturation of the response at the mixing ratio of 1:3 cannot be explained as an artifact of progressively smaller increases of the hypoosmotic shock with increasing mixing ratios. Thus, the F/F_0 increase saturates at the mixing ratio of 1:3, equal to a hypoosmotic shock of about 220 mOsm (Figure 35).

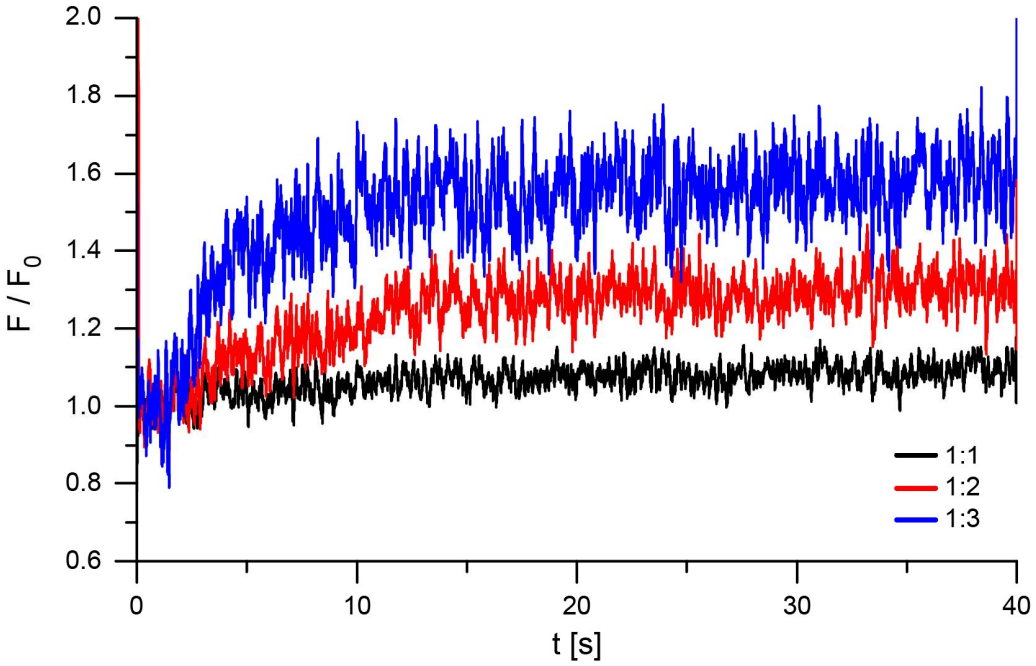

Figure 35: Fluorescence changes in zebrafish sperm loaded with Calbryte520, measured in a population measurement in the stopped-flow set-up. Immotile sperm in ES are mixed at ratios of 1:1, 1:2, or 1:3 with system water. Results for mixing ratios 1:4 and 1:5 are undistinguishable from those obtained for 1:3 and are shown separately for better discernability (Appendix Figure 15).

As noted in 5.2.1., the population measurements showed a far smaller F/F_0 signal than the single cell measurements. The dependence of the calcium response on the strength of the hypoosmotic shock likely contributes to this difference in observed F/F_0 changes, because the population measurements used a much smaller hypoosmotic shock to activate the sperm (145 mOsm vs. 290 mOsm for the single cell imaging experiments).

3.6.2.3. Internal calcium increase upon activation does not require extracellular calcium

Previous studies showed that zebrafish sperm can be activated in calcium-free solution (Wilson-Leedy, Kanuga, and Ingermann 2009). However, I observe a noticeable increase of intracellular calcium in the sperm head upon activation. To examine the source of this calcium increase, I activated Calbryte520-loaded sperm with calcium-free system water (containing 5 mM EGTA). Any calcium increase remaining under these conditions is expected to result from release of internal calcium stores.

Superfusion of zebrafish sperm with calcium-free system water results in a calcium increase (Figure 36) that is similar to that observed upon superfusion with plain system water, which contains 76 µM calcium (see Methods) (see section 3.6.2.1, Figure 34B). The majority of cells show an increase in fluorescence and, thereby, calcium. The fluorescence change also reaches a plateau (Figure 36, black and blue traces), unless the sperm is detached from the glas support before the signal plateau is reached (Figure 36, red and orange traces). Thus, external calcium is not required for either the activation of zebrafish sperm or the accompanying increase of calcium in the sperm's head.

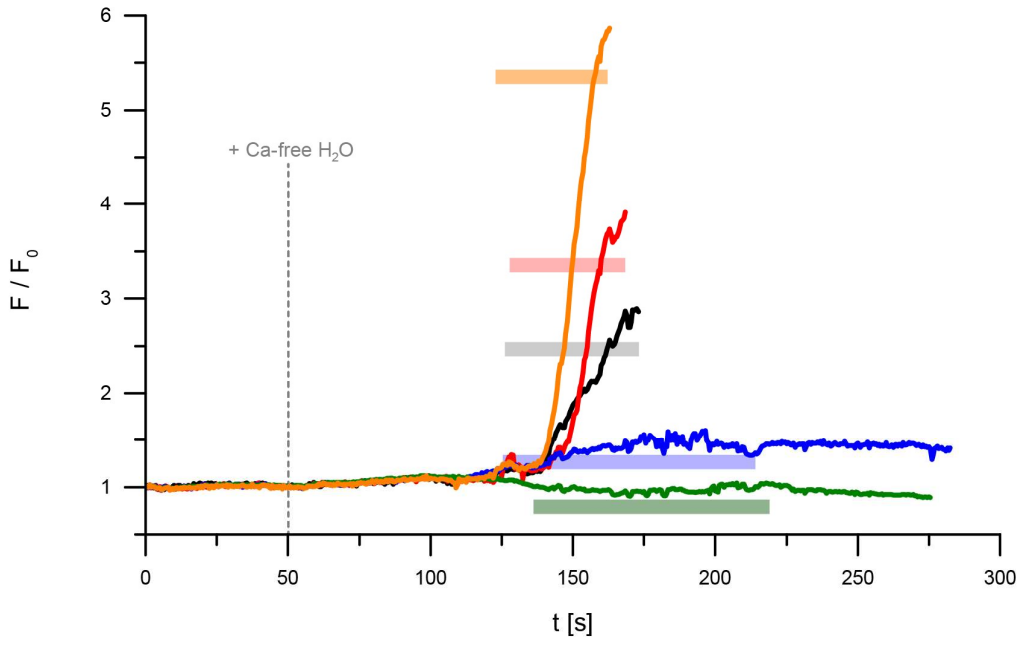

Figure 36: Fluorescence changes in zebrafish sperm loaded with Calbryte520. Colored lines show representative sperm cells that are activated with calcium-free system water (5 mM EGTA) in a single cell imaging experiment. Sperm sometimes detach from the surface, resulting in shorter traces. Dashed gray line indicates switch from ES to system water at the inflow, the solution change in the superfusion chamber itself occurs with a latency. Colored bars indicate duration of flagellar movement.

In addition, I attempted to determine the intracellular calcium concentration of zebrafish sperm at rest, since it is an unknown parameter in the physiology of zebrafish sperm. I chose the pseudo-null-point method (described for measurement of internal pH by Eisner et al. 1989; Chow, Hedley, and Tannock 1996). Ionomycin was added to sperm under various concentrations of extracellular calcium. Because ionomycin shuttles calcium across cell membranes according to the calcium concentration gradient, it should lead to a fluorescence decrease if the external calcium concentration is lower than the internal, and a fluorescence increase if the external calcium concentration is higher. However, in single-cell imaging experiments, even in calcium-free solution, some sperm showed a fluorescence increase upon addition of ionomycin. It is conceivable that such increase would result from release from internal calcium stores, but in such a case I cannot rely on the results of the experiment. Therefore, I was unable to make use of this method to determine resting cytosolic calcium concentration of the sperm.

3.6.2.4. Sperm head acidifies upon activation

For pH measurements, zebrafish sperm were loaded with either pHrodo Red or BCECF. These two dyes exhibit opposite responses to pH changes: pHrodo Red fluorescence increases upon acidification while BCECF fluorescence decreases.

Sperm loaded with pHrodo Red showed an increase in fluorescence upon superfusion with system water (Figure 37A), whereas sperm loaded with BCECF showed a decrease in fluorescence (Figure 37B). Both results indicate that the sperm head acidifies. This is consistent with experiments performed previously in our group (Reinhard Seifert & Thomas Berger, unpublished data), where a fluorescence increase occurred when similar experiments were made with pHrodo Red-loaded zebrafish sperm in the stopped-flow device.

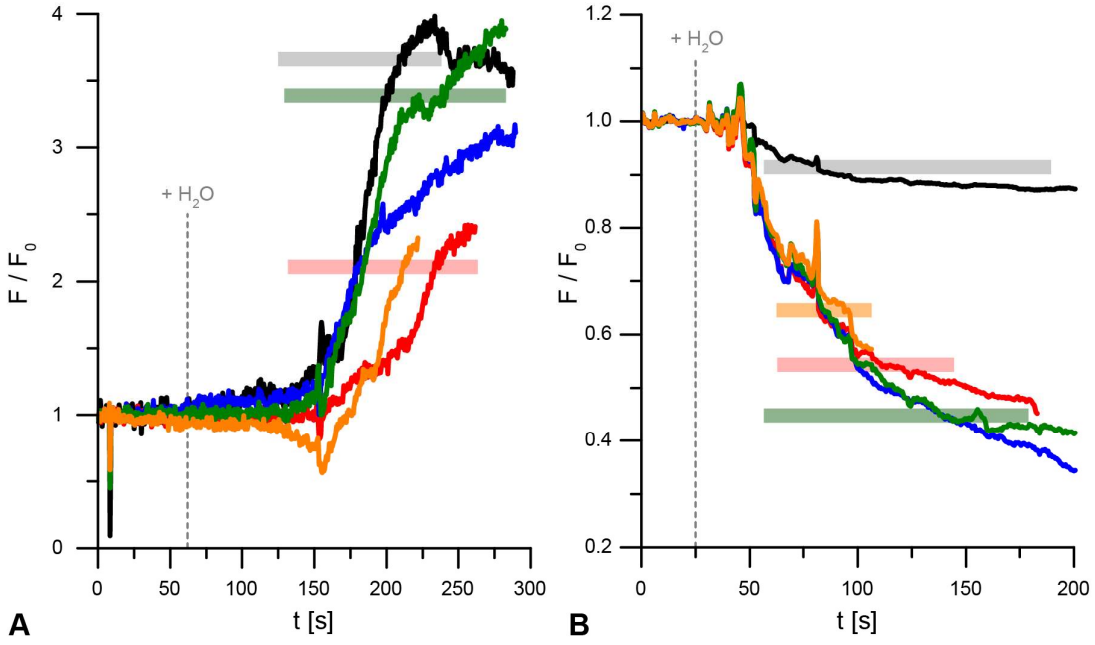

Figure 37: Fluorescence changes in zebrafish sperm upon superfusion with system water. Colored lines show representative sperm cells. Sperm sometimes detach from the surface, resulting in shorter traces. Dashed gray line indicates switch from ES to system water at the inflow, the solution change in the superfusion chamber itself occurs with a latency. Colored bars indicate duration of flagellar movement (the flagella are not visible in all cases). **A**) Sperm loaded with pHrodo Red. **B**) Sperm loaded with BCECF.

The fluorescence changes in pHrodo Red- and BCECF-loaded sperm only sometimes saturate, although in all cases the slope of the traces decreases over time, suggesting beginning saturation (Figure 37). This differs from the results for calcium, but may also simply be due to the shorter observation time in this set of experiments.

The temporal relation between onset of motility and pH change appears variable, in some sperm motility appears to precede the pH change (e.g. Figure 37A), in other sperm it follows the pH change (Figure 37B). As was discussed in detail for the calcium increase in the sperm head (3.6.2.1.), the single-cell imaging set-up as used is not well-suited to examine temporal and therefore possibly causal relationships.

3.7 Flagella of zebrafish sperm show brightly fluorescent spots upon activation

I then turned my attention from the head of zebrafish sperm to the flagella. Although the heads display much brighter fluorescence during single cell imaging, dye-loaded flagella can also be detected, and their fluorescence analyzed.

The fluorescence along the flagellum is homogenous after dye-loading. Upon superfusion with system water intensely fluorescent spots appear in flagella loaded with Calbryte520 (Figure 38).

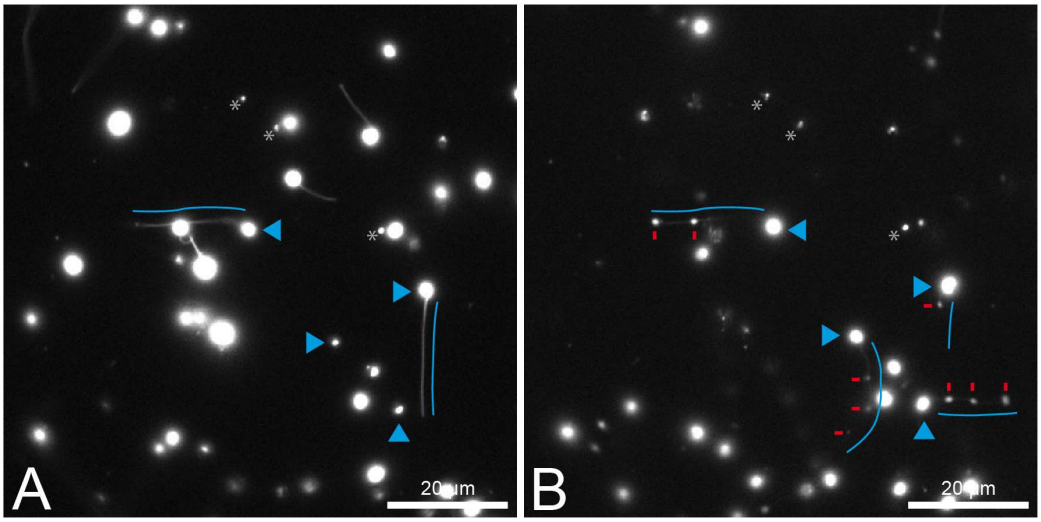

Figure 38: Appearance of bright spots in flagella of zebrafish sperm loaded with Calbryte520 upon activation with system water. Sperm heads are indicated by cyan arrowheads, their flagella are pointed out by thin cyan lines. Light gray asterisks denote artifacts not associated with sperm cells. **A**) Resting state of zebrafish sperm adhered to glass during superfusion with ES. The apparent size of the sperm heads varies due to focus and fluorescence intensity. **B**) Same field of view after activation of sperm with system water. Several sperm have moved, but analysing the video over time allows unambiguous tracking of many sperm. Red dashes indicate the appearance of small brightly fluorescing spots in several flagella.

These bright spots occur both in immotile flagella and in rapidly beating flagella. The appearance of the bright spots also coincides with the fluorescence increase within the head of Calbryte520-loaded sperm that accompanies activation. The spots show a distinct spatial pattern: In most cases, a spot is localized at what appears to be the tip of the flagellum, although no simultaneous darkfield recording was possible to verify this. Two to four additional spots are localized along the length of the flagellum. These spots appear

somewhat regularly spaced, and are of roughly similar size (Figure 38). After activation, most to all observable flagella exhibit such bright spots. Before activation, such bright spots are never observed.

For many sperm, the bright spots appear to move closer to the sperm head toward the end of the motility period (Figure 39). This does not appear to be a migration of the bright spots along the flagellum, because no flagellum segments are ever visible beyond the farthest bright spot. Nor can it be explained with bending of the flagellum—which would also bring the bright spots closer to the sperm head (Figure 39). Sáez-Espinosa (2022) report that zebrafish sperm flagella are coiled up after activation. Such a process of coiling up would explain the apparent shortening of the flagella observed here.

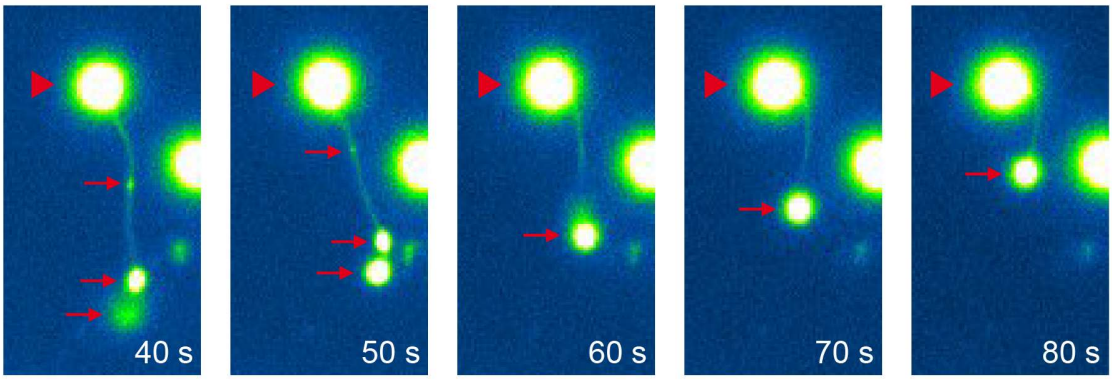

Figure 39: Close-ups of a sperm with motile flagellum containing three bright spots. Sperm were loaded with Calbryte520. Time points are given from the onset of motility; motility stops at 90–100 seconds. False color is used to improve visibility of flagellum. The sperm head is denoted by a red arrowhead, the bright spots in the flagellum are denoted by red arrows.

The appearance of these bright spots suggests local increases in the concentration of intracellular calcium or the dye along the flagellum upon activation. To investigate this observation further, I analyzed the fluorescence changes along the flagellum.

3.7.1. Fluorescence decreases in the in-between flagellum segments

Fluorescence was tracked separately in the bright spots and the segments in-between of the flagellum (Figure 40A, C). The bright spots constitute an increase in fluorescence. In the segments between spots, the fluorescence actually decreases (Figure 40B, D). The fluorescence increase in the bright spots is more pronounced than the decrease of the in-between segments. However, taking into account the larger length of

in-between segments (Figure 40A, C), the fluorescence increase in the bright spot segments may match the summed-up decrease of in-between segments.

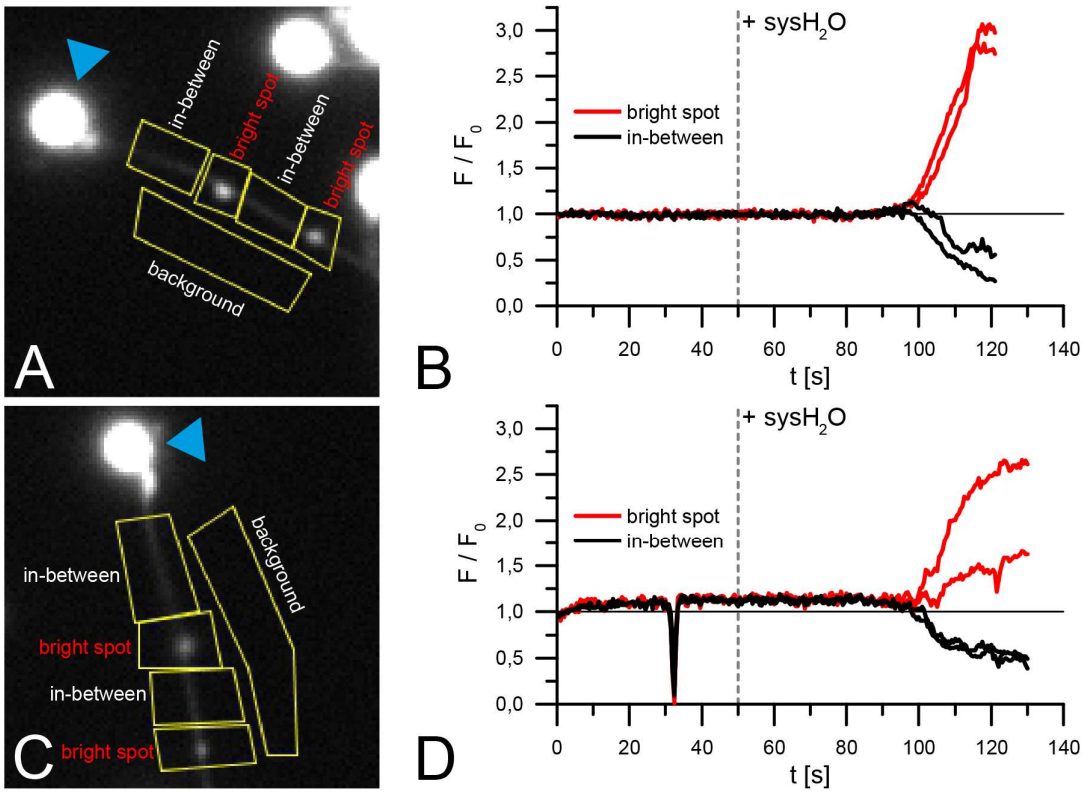

Figure 40: Fluorescence changes in exemplary zebrafish sperm flagella upon activation. Zebrafish sperm are loaded with Calbryte520. Sperm heads are denoted with cyan arrowheads. **A, C**) Bright spots and in-between segments of the flagellum are tracked with separate ROIs (yellow boxes in **A** and **C**). **B, D**) Fluorescence changes over time are quantified for all segments. Background is subtracted for each time point and fluorescence is normalized to initial fluorescence (F_0) of the respective segment. The sudden decrease at 32 s in **D**) is an artifact due to another sperm moving through the background ROI. Dashed gray line indicates switch from ES to system water at the inflow, the solution change in the superfusion chamber itself occurs with a latency. Red traces are from ROIs containing bright spots, black traces are from in-between flagellar segments.

These results could indicate a local redistribution of the calcium concentration along the flagellum. However, it is also possible that the dye molecules themselves undergo a redistribution along the flagellum, which would lead to the same observation of local increases and decreases in fluorescence. Measurements using a ratiometric calcium dye instead of Calbryte520 could clarify this issue. Changes in its fluorescence

ratio would only occur for changes in the calcium concentration, and not changes in the dye concentration. But due to technical limitations of the experimental set-up, this was not possible.

Because it was uncertain at this stage whether the appearance of these bright spots upon activation indeed reflects a change in local calcium concentration, or instead might represent a peculiar dye artifact, I tested the response of various other fluorescent dyes to activation.

3.7.2. Bright spots occur with several different fluorescent dyes

Zebrafish sperm were loaded with one of the following dyes: Calbryte520 and -590 (calcium-sensitive), pHrodo, BCECF, and SNARF-1 (pH-sensitive) or ANG-2, (sodium-sensitive), and observed under superfusion with system water.

The fluorescence of Calbryte520 and -590, and ANG-2 increases when the concentration of their respective binding ion increases. For the pH-sensitive dyes, opposite effects are observed: when the pH decreases, BCECF and SNARF-1 fluorescence also decreases, whereas pHrodo Red fluorescence increases (Boens et al. 2006; Wieder, Hang, and Fox 1993; Arppe et al. 2014).

If the bright spots indicate local changes in the calcium concentration, one would expect that these spots occur with another calcium-sensitive dye as well, although redistribution of dye molecules remains a potential explanation. If the other calcium-sensitive dyes do not show bright spots upon activation, it might suggest that the spots represent an artifact specific to Calbryte520. If ANG-2 and the pH-sensitive dyes also produce bright spots upon activation, it could be a clue that the redistribution of dye molecules is quite common and not specific to the Calbryte calcium-sensitive dyes. Nevertheless, a concomitant change in calcium, sodium, and pH cannot be excluded yet. However, the opposing fluorescence change behaviors of the pH-sensitive dyes can decide this question if bright spots occur. A localized pH change would be expected to result in a spot-like fluorescence increase with one dye and a corresponding localized decrease with the other dye.

Bright spots occur in all examined fluorescent dyes upon activation (Figure 41). For each dye most to all visible flagella show three to five bright spots per flagellum. Additionally, all examined dyes show similar fluorescence changes as Calbryte520 with regard to the bright spots and in-between segments of the flagellum: Fluorescence increases in the bright spots and it decreases homogenously in the in-between segments (Figure 42). A spot-like local decrease of fluorescence ('dark spots') was never observed.

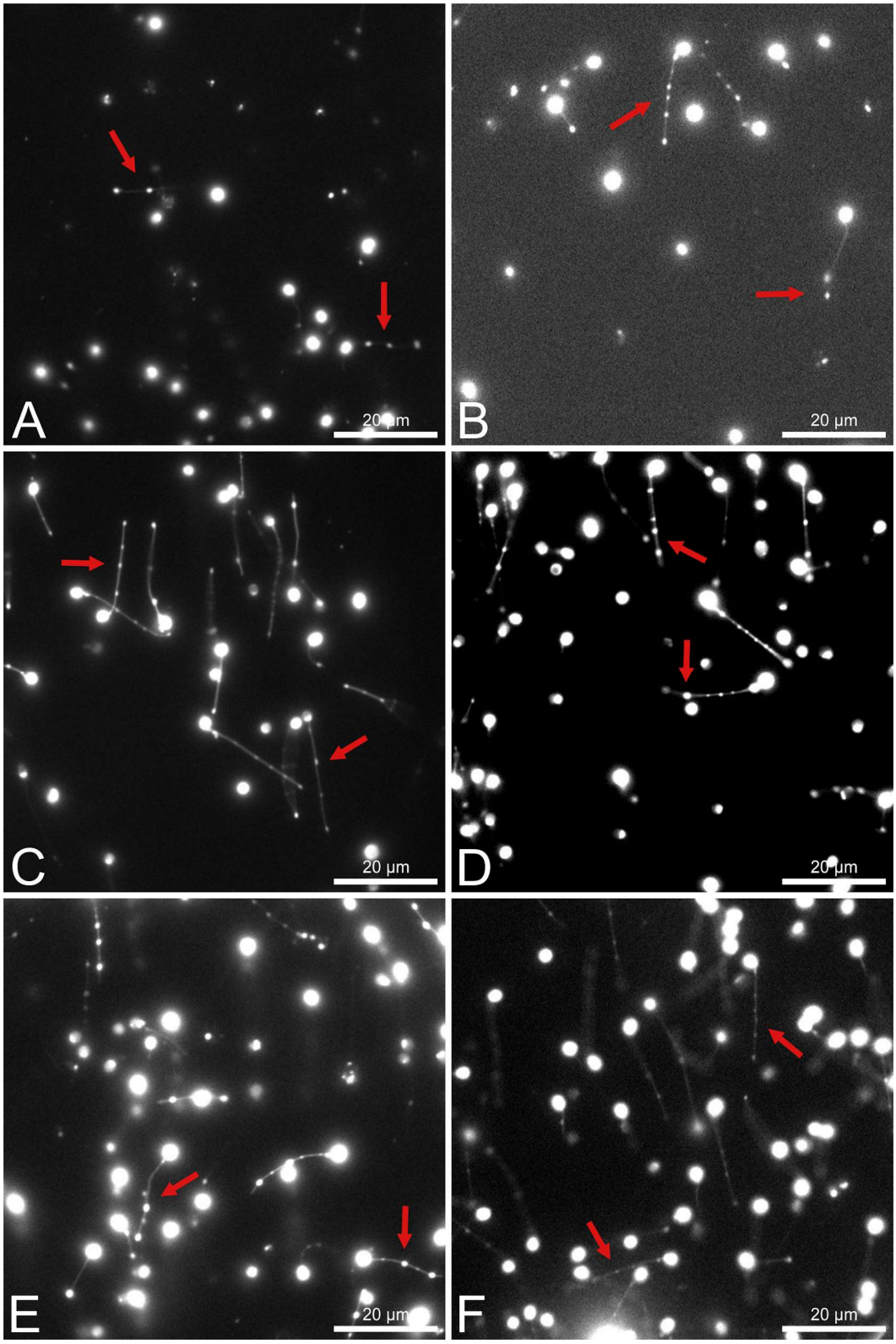

Figure 41: Activated zebrafish sperm loaded with different fluorescent dyes. Arrows highlight some of the flagella where bright spots have appeared upon activation. **A**) Calbryte520, calcium-sensitive. **B**)

Calbryte590, calcium-sensitive. **C**) ANG-2, sodium-sensitive. **D**) pHrodo Red, pH-sensitive. **E**) BCECF, pH-sensitive. **F**) SNARF-1, pH-sensitive.

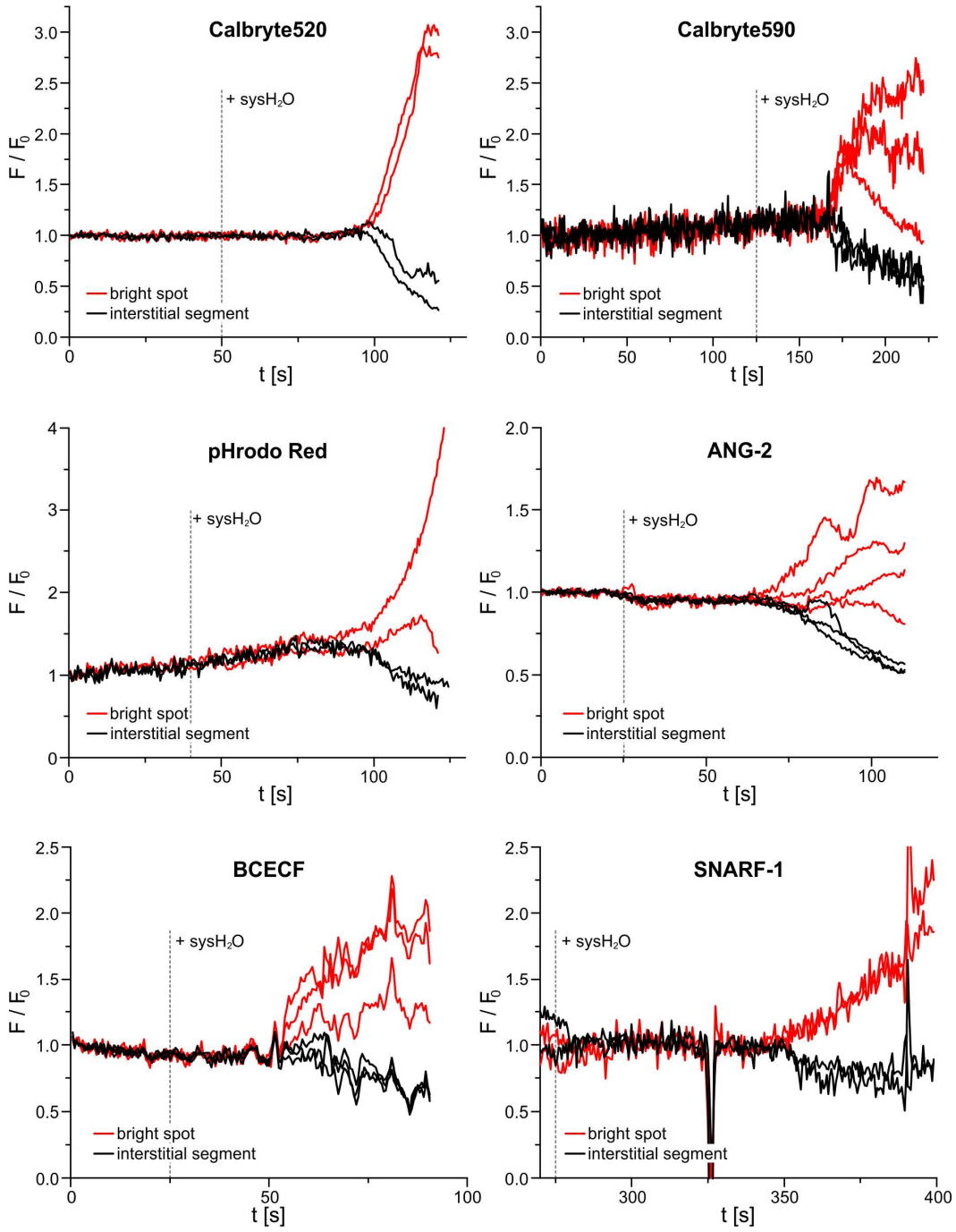

Figure 42: Fluorescence changes in zebrafish sperm flagella upon activation. Bright spots and in-between segments of the flagellum are tracked with separate ROIs as in Figure 40. Fluorescence changes over time are quantified for all segments. Background is subtracted for each time point and fluorescence is normalized to initial fluorescence (F_0) of the respective segment. Dashed gray line indicates switch from ES

to system water at the inflow, the solution change in the superfusion chamber itself occurs with a latency. Red traces are from ROIs containing bright spots, black traces are from in-between flagellar segments. Zebrafish sperm were loaded with six different dyes: **A**) Calbryte520, calcium-sensitive. **B**) Calbryte590, calcium-sensitive. **C**) ANG-2, sodium-sensitive. **D**) pHrodo Red, pH-sensitive. **E**) BCECF, pH-sensitive. **F**) SNARF-1, pH-sensitive.

For most dyes the size and arrangement of bright spots is uniform: the bright spots within one flagellum are of similar size, and a bright spot occupies the end of the flagellum. BCECF is an exception: Here, smaller spots are interspersed between larger ones (Figure 41E), and sometimes the visible tip of the flagellum is not occupied by a bright spot (Figure 41E). This could potentially be because BCECF is a much brighter dye than the others and thereby increases the visibility of the tail end of the flagellum under fluorescence. Rarely such a tail end beyond the most distal bright spot can also be observed in sperm loaded with pHrodo Red (Figure 41D).

It would have been interesting to analyse the fluorescence changes for the two pH-sensitive dyes with opposing dependance on pH (pHrodo and BCECF) simultaneously to check for co-localisation of their respective bright spots. Unfortunately this was not possible because the experimental set-up did not allow for simultaneous excitation and emission measurement of those two dyes. However, it is important to note that none of the pH-sensitive dyes display a spot-like fluorescence *decrease* (dark spots), the decrease in the in-between segments is always homogenous along the flagellum. If the fluorescence change were indicative of real physiological change within the flagellum, either pHrodo Red or BCECF and SNARF-1 ought to display such dark spots.

This similar occurrence of bright spots in the flagella in all three pH-sensitive dyes (Figure 41D–F) strongly suggests they are a result of a redistribution of dye molecules, rather than a sign of local changes in pH. Accordingly, the bright spots occurring with Calbryte520, -590, and ANG-2 (Figure 41A–C) are also likely not due to local changes in calcium or sodium concentration but due to a redistribution of the dye.

From previous experiments (see section 3.6.2.4.), it is known that zebrafish sperm acidify upon activation. Furthermore, activation itself is brought on by a substantial hypoosmotic shock (a drop from ca. 300 mOsm to 5–10 mOsm under physiological conditions). Both of these changes might have an effect on the dye distribution.

3.7.3. Acidification is not responsible for appearance of bright spots

To test whether the activation-induced acidification of zebrafish sperm might be responsible for the appearance of bright spots, I superfused zebrafish sperm loaded with either BCECF or pHrodo Red with

propionic acid to lower the intracellular pH without activation of the sperm. As control, the sperm subsequently were superfused with system water to test whether the sperm could activate (be motile) normally following the acidification and whether bright spots would appear.

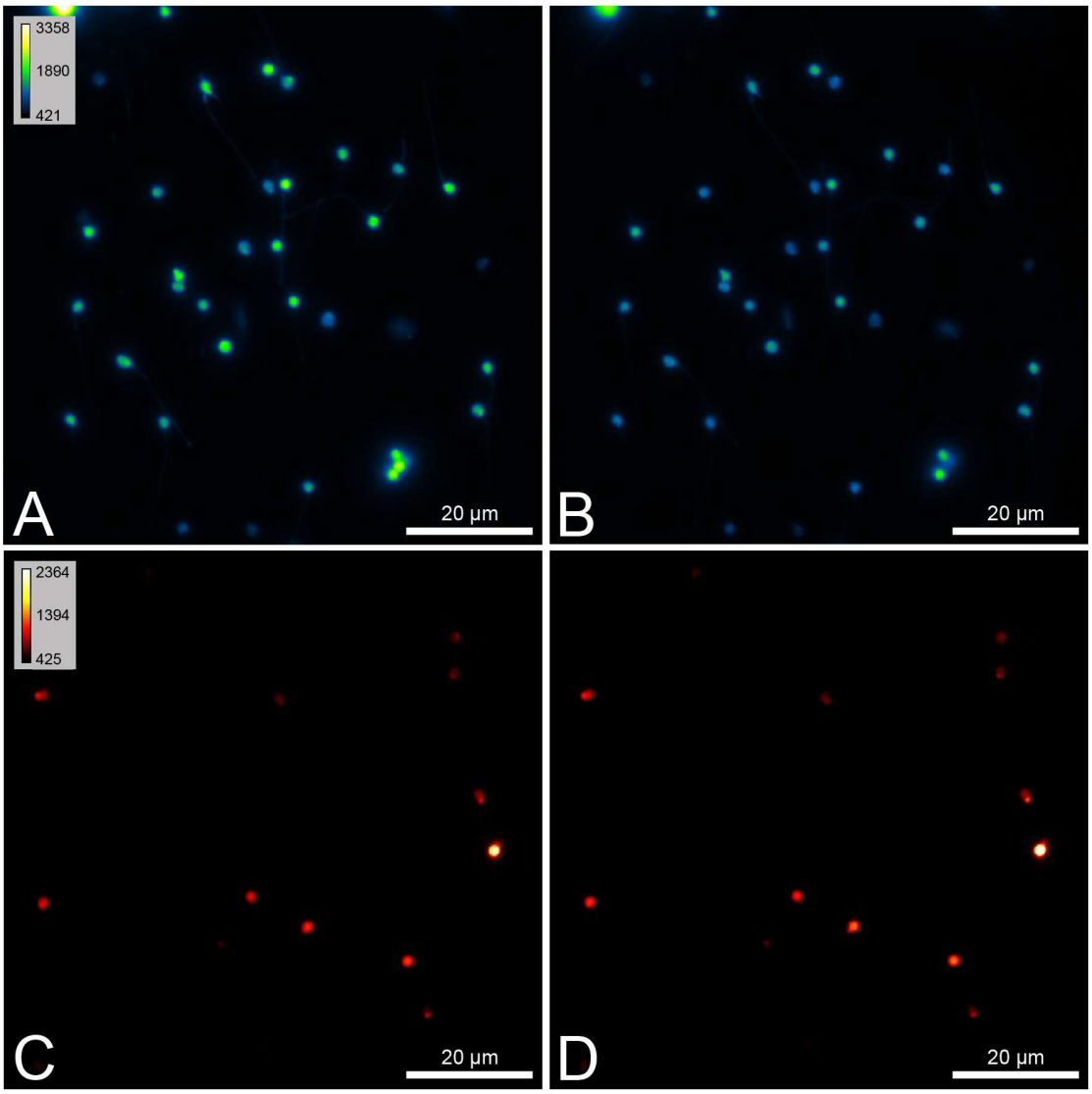

Figure 43: Fluorescence change in zebrafish sperm loaded with the pH indicator dyes BCECF (A, B) or pHrodo Red (C, D) in response to superfusion with propionic acid. A, C) Control, sperm superfused with ES. **B, D**) Same field of view, after superfusion of sperm with propionic acid. Note the decrease in fluorescence intensity between **A**) and **B**), and the increase in fluorescence intensity between **C**) and **D**).

For both BCECF- and pHrodo Red-loaded sperm, superfusion with 45 mM propionic acid led to the expected decrease in pH (visualized by a fluorescence increase of pHrodo Red and a decrease of BCECF fluorescence, Figure 43). However, this acidification did not lead to the appearance of bright spots (Figure 44B). To examine, whether the absence of bright spots might be due to some damage of the sperm due to propionic acid treatment, the sperm were washed after acidification with ES to remove the propionic acid and subsequently superfused with system water. The sperm activated normally, and the bright spots appeared as before (Figure 44C). Consequently, the acidification of sperm upon activation is not the cause of the bright spots.

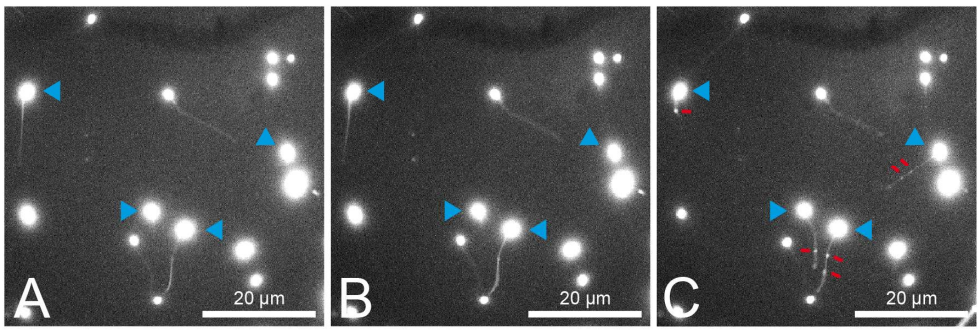

Figure 44: Zebrafish sperm loaded with pHrodo Red and superfused with propionic acid before being activated. All panels show the same field of view. Sperm heads are indicated by cyan arrowheads. **A**) Resting state of zebrafish sperm during superfusion with ES. **B**) After addition of 45 mM of propionic acid, causing acidification. **C**) Activation of sperm with system water. Bright spots are indicated by red dashes.

In some experiments with BCECF-loaded sperm, bright spots appeared in a small fraction of total number of flagella after removal of propionic acid and switch to ES but before superfusion with system water (Figure 45C). The number of spots per flagellum was similar to that appearing after activation with system water. Such spots never appeared before and during the propionic acid treatment. The switch from ES containing 45 mM propionic acid (390 mOsm) to standard ES (300 mOsm) is equal to a decrease in osmolarity of ca. 90 mOsm, which represents a small hypoosmotic shock, albeit from a higher starting point than zebrafish sperm would experience under physiological conditions (from 300 down to 5–10 mOsm). The 90 mOsm decrease after removal of propionic acid does not lead to initiation of motility of the sperm, but it does (rarely) generate some bright spots (Figure 45C). This observation decouples the appearance of bright spots from the initiation of motility.

Thus it is possible that the hypoosmotic shock itself and possibly some early downstream consequences but not the final initiation of motility causes the bright spots. Because bright spots after propionic acid

removal (small hypoosmotic shock) do not appear as consistent and as frequent as bright spots after activation with system water (large hypoosmotic shock), the frequency of bright spots might be correlated with the strength of the hypoosmotic shock. This hypothesis was tested next.

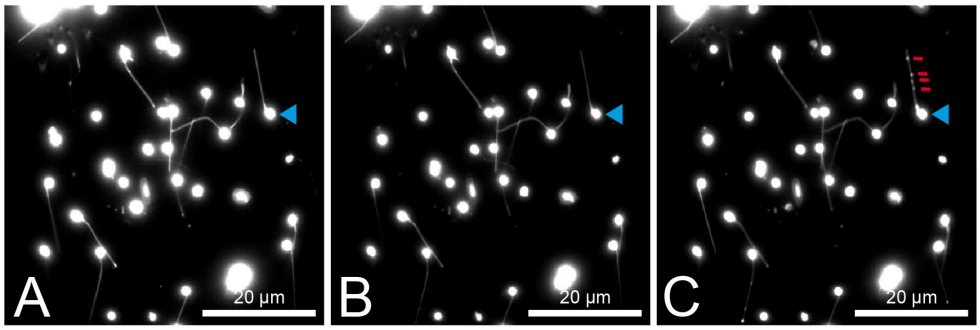

Figure 45: Zebrafish sperm loaded with BCECF and superfused with propionic acid. Cyan arrowhead indicates relevant sperm head. **A**) Resting state of zebrafish sperm during superfusion with ES. **B**) Addition of 45 mM of propionic acid, causing acidification and an increase in osmolarity of ca. 90 mOsm. Note the decrease in fluorescence intensity, and the absence of bright spots in the flagella. **C**) Removal of propionic acid, which returns the osmolarity to ca. 300 mOsm. Red dashes indicate bright spots in a flagellum appearing without activation of the sperm. Note that most flagella do not show bright spots, in stark contrast to the high frequency observed after activation (see Figure 41E).

3.7.4. Strength of hypoosmotic shock has no influence on appearance of bright spots in the range necessary for activation

Under physiological conditions, the hypoosmotic shock that zebrafish sperm are exposed to is quite strong (from ca. 300 mOsm to 5–10 mOsm). It has been reported that sperm can be activated with smaller hypoosmotic shocks (Wilson-Leedy, Kanuga, and Ingermann 2009); therefore, I investigated the dependence of bright spots on the strength of the hypoosmotic shock.

I superfused zebrafish sperm loaded with Calbryte520 with system water diluted with ES at different ratios (1:1, 1:2, 1:3, 1:4 ES to system water), corresponding to a hypoosmotic shock, i.e., a decrease in osmolarity, by about 150, 200, 220, and 230 mOsm, respectively. In all cases, activation of sperm is observed.

At all levels of hypoosmotic shock tested, bright spots appeared in the flagella (Figure 46). The pattern of bright spots within the flagella, their frequency per flagellum and the frequency of flagella with bright spots was undistinguishable between the different osmolarities.

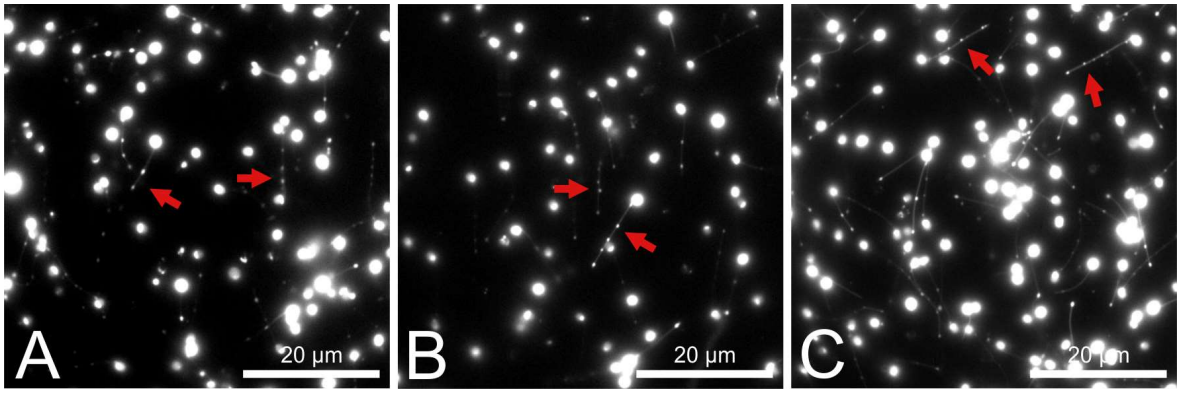

Figure 46: Appearance of bright spots in zebrafish sperm flagella upon activation with different osmolarities. Bright spots occur for all levels of hypoosmotic shock. Zebrafish sperm are loaded with Calbryte520. **A**) Pure system water, final osmolarity 5–10 mOsm. **B**) 1:3 ES to system water, final osmolarity ca. 80 mOsm. **C**) 1:1 ES to system water, final osmolarity ca. 150 mOsm.

Thus, in the range examined (150 to 230 mOsm hypoosmotic shock), neither the appearance of the bright spots nor their frequency (per flagellum, and percentage of flagella with bright spots) is correlated to the strength of the hypoosmotic shock. However, the weaker hypoosmotic shock of 90 mOsm, insufficient for sperm activation, described in section 3.7.3. resulted in a much smaller percentage of flagella with bright spots (the frequency of bright spots per flagellum appeared unchanged). It is therefore conceivable that the hypoosmotic shock itself causes bright spots independent of sperm activation, and that this process saturates somewhere between 90 and 150 mOsm.

On one hand, the formation of bright spots in dye-loaded flagella upon activation presents a technical problem, because it complicates or prevents the detection of changes in calcium concentration or pH_i in zebrafish flagella. On the other hand, the dye accumulation into bright spots presumably mimics physiological accumulation of flagellar components upon activation and as such presents an excellent starting point to investigate the underlying structural changes.

3.8. Neither calcium nor pH appear to signal the presence of oocytes to zebrafish sperm

Finally, I analyzed the calcium and pH response in the head of zebrafish sperm to potential chemoattractants and compared it to the response during normal activation to investigate whether chemotaxis contributes to the sperm's guidance.

If zebrafish oocytes release chemoattractants during spawning, those molecules should be contained in the surrounding water. To produce such oocyte-conditioned water, mature zebrafish oocytes were left in

system water for a few minutes to mimic the process of spawning. The oocyte density was set to about 150 oocytes/ml. Oocyte-conditioned water was prepared in advance and frozen until use to enable the collection of enough volume. Sperm were superfused with this oocyte-conditioned water or with system water serving as control. Sperm were loaded with either Calbryte520 for calcium measurements (4 independent experiments) or pHrodo Red dye for pH determination (3 independent experiments). For each experiment 2–3 videos were obtained per condition.

Activation with oocyte-conditioned water leads to fluorescence increases similar to those observed with system water in earlier experiments (see section 5.2.1) and similar to the current control with system water, both for Calbryte520- (Figure 47) and pHrodo Red-loaded sperm (Figure 48). Thus, under the conditions examined, the rise in intracellular calcium and the acidification that accompany activation are not noticeably affected by oocyte-conditioned water compared to the control with system water.

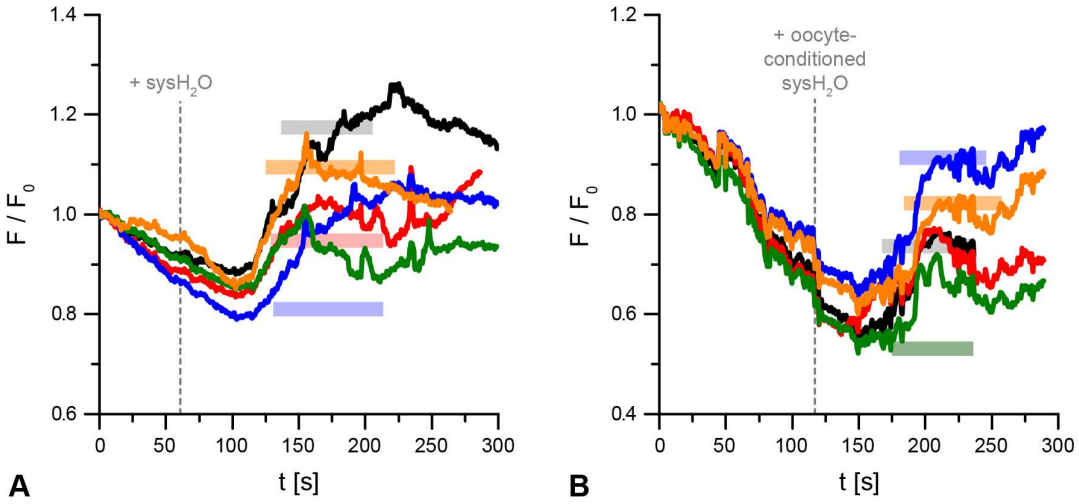

Figure 47: Fluorescence changes in representative single zebrafish sperm cells loaded with Calbryte520 upon superfusion with system water (A) or oocyte-conditioned water (B). Dashed gray line indicates switch from ES to system water or oocyte-conditioned water at the inflow, not yet in the superfusion chamber itself. Colored bars indicate duration of sperm movement, where identifiable.

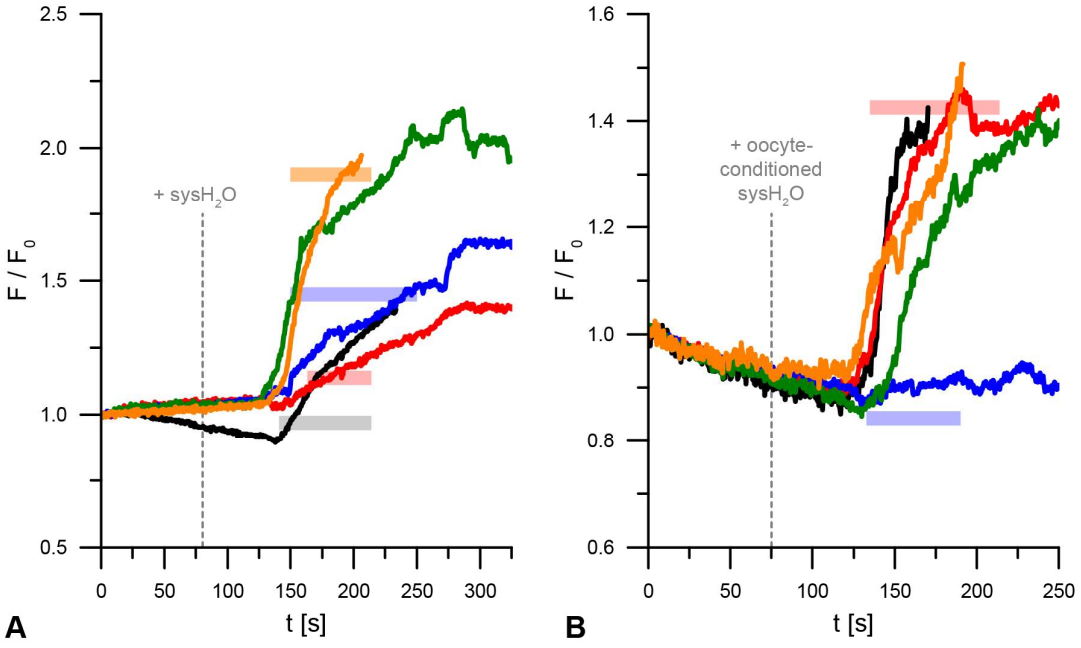

Figure 48: Fluorescence changes in representative single zebrafish sperm cells loaded with pHrodo Red upon superfusion with system water (A) or oocyte-conditioned water (B). Dashed gray line indicates switch from ES to system water or oocyte-conditioned water at the inflow, not yet in the superfusion chamber itself. Colored bars indicate duration of visible sperm movement, where identifiable.

It should be noted that fast transient changes in intracellular calcium concentration or pH might potentially still occur but the limited temporal resolution of the experiments prohibits identification of them (videos were recorded at 2 Hz frame rate). Furthermore, small differences in the fluorescence responses would not be detectable due to the inherent variability of measurements with single cells. Moreover, one has to consider the chemical and physical stability of a potential chemoattractant. The oocyte-conditioned water had to be collected over a longer time period to obtain sufficient amounts, so it had to be kept frozen before the assay was performed. It must be noted that freezing can damage proteins (Arsiccio et al. 2020). Thus, if the potential chemoattractant were a protein, this procedure may hamper its detection. A lack of chemical stability could include e.g. sensitivity to oxidation for low molecular weight compounds; for radical reactions this would be exacerbated by frozen storage. Because the nature of the potential chemoattractants is unknown, it is unclear to what extent such processes may have influenced the negative results reported here. At the very least, the results obtained do not suggest that oocyte-derived factors signal the presence of the oocyte to sperm by calcium or pH changes.

4. Discussion

In all sexually reproducing species, the sperm cell has to become motile (activation) and has to find the immotile oocyte in order to fuse with the plasma membrane of the oocyte, thereby allowing fertilization to occur. In some species, such as sea urchin, human, and mouse (Nowicka-Bauer and Szymczak-Cendlak 2021), these processes are well examined. The underlying molecular mechanisms differ greatly among species. Owing to the environmental differences where oocyte and sperm meet—sea urchin are external fertilizers in a marine environment, whereas mammals are internal fertilizers in an oviduct environment—this is to be expected. Yet even between human and mouse large differences exist (Figure 1) (Wachten, Jikeli, and Kaupp 2017; Kaupp and Strünker 2017). Nevertheless, all three species share the acrosome reaction (Mengerink and Vacquier 2001) as a mechanism to allow sperm passing the egg envelope, despite the vastly different circumstances under which fertilization takes place. However, the acrosome reaction is not universal, and many species such as fish and insects have no acrosome; they rely on the micropyle, an opening in the egg envelope that provides access to the plasma membrane of the oocyte (Amanze and Iyengar 1990).

Although zebrafish is an established vertebrate model system for humans, little is known in this species about fertilization in general and the interaction between sperm and oocyte, sperm and micropyle, and the underlying molecular mechanisms in particular. Upon release into fresh water, zebrafish sperm are activated via hypoosmotic shock, swim for about one minute, and then cease swimming (Wilson-Leedy, Kanuga, and Ingermann 2009; Ingermann et al. 2011). Zebrafish oocytes, after exposure to fresh water, close the micropyle after about one minute. Thus, the timeframe during which fertilization can occur is very short compared to other species, such as sea urchin (several hours, Tyler 1953) or humans (several days, Mansour et al. 1995). Notwithstanding, fertilization is very efficient (over 90% of spawned oocytes are fertilized, Gonzales Jr 2012).

Although some signaling components are shared between sperm of zebrafish and sea urchin, their function is profoundly different: The zebrafish CNGK channel is not activated by cyclic nucleotides but by alkalization (Fechner et al. 2015). Recently, it has also been discovered that zebrafish sperm possess a HCN-like channel that, unlike other HCN family members, does not function as a relatively non-selective cation channel, but as a highly selective proton channel (Wobig et al. 2020).

Many questions remain unsolved. What happens during activation of zebrafish sperm? Do they employ chemotaxis or haptotaxis to locate the oocyte and/or the micropyle? Do zebrafish sperm possess further proteins that in other species are known components of sperm signaling cascades, such as CatSper or sAC?

Here, I elucidate some aspects of these questions. I have examined the basic swimming patterns and ionic changes of zebrafish sperm after initiation of motility as a prerequisite to examine potential changes after stimulation by oocyte-derived factors. I have searched for potential indications of pathfinding mechanisms in zebrafish sperm, examining both sperm and oocytes. I have performed phylogenetic analysis to examine the presence of CatSper and sAC in zebrafish and to understand the evolution of these molecules in vertebrates. Finally, I will discuss an unexpected observation that, despite being caused by an artifact, reveals a novel element of sperm morphology.

4.1. Ionic changes during zebrafish sperm activation and contact with oocyte-conditioned water

Generally, ionic changes play a crucial role in the initiation of motility (Lishko et al. 2012; Wang, McGoldrick, and Chung 2021). In particular, an increase of cytosolic calcium is an essential component. In human and sea urchin, calcium enters the cell from the outside (Thomas and Meizel 1988; Seifert et al. 2015). I showed that zebrafish also exhibit a cytosolic calcium increase during initiation of motility and that this calcium is released from internal stores. This is in accordance with an earlier observation that zebrafish sperm swim normally in calcium-free water (Wilson-Leedy, Kanuga, and Ingermann 2009).

Changes in intracellular pH also play an important role. Mammalian sperm alkalize upon both activation and later capacitation (Hamamah and Gatti 1998). Similarly, sea urchin sperm alkalize as part of activation (Hamamah and Gatti 1998). In contrast, my studies show that zebrafish sperm experience a *decrease* in internal pH once they are activated; the cells acidify. This observation is consistent with Wobig et al. (2020).

To conclude, the ionic changes accompanying activation of zebrafish sperm suggest a different mechanism for the initiation of motility than that in other species, extending the known variability of sperm activation mechanisms even further.

Once sperm have become motile, they are capable of swimming without contact to any guidance factor or mechanism, such as chemoattractants or fluid flow. I have shown that in zebrafish this unstimulated swimming behavior (sperm have only been subjected to hypoosmotic shock to induce motility) displays a broad range of movement patterns, with a preponderance of sperm trajectories with higher linearity, i.e. lower curvature. However, occasionally, a high-curvature "drilling" motion also occurs. Consistent with my observations, a certain variability in sperm trajectories is visible in unstimulated swimming in the study by Fechner et al. (2015), although no incidences of "drilling" motion were reported for unstimulated swimming. The focus of that study lay on the large increases in curvature elicited by two subsequent instances of internal

uncaging of calcium (stimulated swimming). However, a non-negligible number of sperm kept swimming on unchanged trajectories, both after the first and second uncaging of calcium (Fechner et al. 2015). Thus, a great variability in swimming patterns is a consistent feature of both unstimulated and stimulated swimming of zebrafish sperm.

The molecular mechanisms generating such variability remain unknown. A potential biological function for variable swimming patterns could be that they increase the spatial range accessible to sperm, which would increase the probability of successful fertilization. Sperm are not deposited on stationary oocytes in zebrafish, but both are released simultaneously by adjacently swimming fish (Zempo et al. 2021).

So far, no chemoattractant has been found that zebrafish sperm could employ to locate the oocyte. I hypothesised that a chemoattractant may be released by the oocyte and therefore would be present in the supernatant of an oocyte suspension. However, in my initial experiments, I found no effect of oocyte supernatant on ionic changes in zebrafish sperm. Those would be expected, because chemotaxis would result in a change in motility and we know that motility and ionic changes are associated, both from Fechner et al. (2015) and the results presented here. This could indicate that zebrafish sperm do not use chemotaxis, but there are other explanations for the lack of reaction. Perhaps the chemoattractant is unstable and/or its concentration was insufficient under my assay conditions. While I did not measure swimming behavior in this assay, it should be noted that the technical implementation of such measurements can make a big difference in detected behavior. For example, in the sea urchin *Strongylocentrotus purpuratus*, it is very difficult to detect chemotaxis in two-dimensional swimming experiments (Ramírez-Gómez et al. 2020), whereas it is easy in the sea urchin *Arbacia punctulata* (Ward et al. 1985), despite both species having very similar signaling pathways (Solzin et al. 2004).

In conclusion, it is possible that zebrafish do not employ chemotaxis; however, further studies are needed to answer this question fully.

In the case of species where the oocyte possesses a micropyle, locating the oocyte itself is only part of the pathfinding obstacle for the sperm cells. They must also locate the micropyle itself for fertilization to occur. One mechanism to aid in this is haptotaxis: the orientation along a chemoattractant gradient tethered to a surface. The sperm of pacific herring have been shown to use haptotaxis (Yanagimachi et al. 2013; 2017). In other types of cells, haptotaxis has been studied for a long time (Carter 1967; Ricoult, Kennedy, and Juncker 2015); for example it is employed by dendritic cells (Schwarz and Sixt 2016). In some species, sperm also display a tendency to swim along surfaces, a process named thigmotaxis, which does not rely on any direct protein interactions (Cosson, Huitorel, and Gagnon 2003; Denissenko et al. 2012; Ishimoto 2017).

I attempted to identify potential haptotactic chemoattractants by mass spectrometric analysis of the chorion. Because haptotaxis involves cell–surface interaction, the sperm must interact with chorion components while it swims along the surface of the egg envelope. Consequently, the active component should be distributed in a spatial gradient. I found no clear differentially expressed protein candidates that might be used for haptotaxis. However, I detected a large number of zona pellucida (ZP) proteins. In other species such as mouse and human, certain ZP proteins are involved in sperm–oocyte interactions, specifically the acrosome reaction (Wassarman and Litscher 2018; Gupta 2021). Although zebrafish sperm do not possess an acrosome, it is conceivable that ZP proteins nonetheless fulfill a function of sperm–oocyte interaction, e.g., ensuring that sperm remain in contact with the chorion while swimming. Such tethering would already increase the likelihood of a sperm cell encountering the micropyle, because its movements are restricted to a two-dimensional surface instead of freely moving in three dimensions.

To unambiguously identify the ZP proteins detected in zebrafish chorion it is necessary to perform a phylogenetic analysis using ZP proteins from other species as reference. A complication in identification of reference ZP proteins is their bewildering nomenclature across species. Several attempts have been made to suggest a unified nomenclature (Spargo and Hope 2003; Goudet et al. 2008; Wu et al. 2018). Here I have used the most recent one (Wu et al. 2018) and compared those with the Uniprot assignments obtained for the peptides identified in MS analysis. In my phylogenetic analysis, I could confirm all Uniprot assignments; furthermore all subfamily assignments of zebrafish ZP proteins by Mold et al. (2001; 2009) and Wu et al. (2018) could be reproduced. Moreover, I could assign several previously unspecified ZP proteins to a ZP subfamily.

In mammals, ZP2 is the protein that binds to acrosome-reacted sperm, while ZP3 (in humans also ZP1 and ZP4) binds to acrosome-intact sperm, prior to the acrosome reaction (Wassarman and Litscher 2018; Gupta 2021). Zebrafish lack an acrosome and might, therefore, be expected to use an ortholog of mammalian ZP2 for sperm–egg envelope interaction. However, they do not possess such an ortholog (Table 9). It is possible that ZPD and ZPAX, the two ZP subfamilies absent in mammals, have a similar role to ZP2 in mammals. Moreover, even zebrafish ZP2 and ZP3 (orthologous to ZP1 and ZP3 in mammals, respectively, see Table 9) cannot be excluded as candidates for sperm–egg envelope interaction, because the function of phylogenetic orthologs need not be conserved. An example for functional plasticity is the mammalian ZP1, which takes part in sperm–egg envelope interaction in human, but not in mouse (Table 9).

Table 9: Zebrafish possesses two additional ZP subfamilies compared to mammals.

green overlay = binds to capacitated / acrosome-intact sperm

blue overlay = binds to acrosome-reacted sperm

subfamilies (Wu et al. 2018)	ZPA	ZPB	ZPC	ZPD	ZPAX
Human	ZP2	ZP1, ZP4	ZP3	–	–
Mouse	ZP2	ZP1	ZP3	–	–
Zebrafish	–	ZP2	ZP3	ZPD	ZPAX

In comparison to human (four ZP proteins), zebrafish possess a large family of ZP proteins (29 ZP proteins). I showed expression of the majority of ZP genes (20 genes) in the zebrafish chorion. This is consistent with the hypothesis that external fertilizers with a more unpredictable environment for fertilization compared to internal fertilizers have a higher number of ZP proteins (Goudet et al. 2008; Wu et al. 2018).

In conclusion, both haptotaxis and thigmotaxis are conceivable for zebrafish sperm, albeit current experiments did not directly address this question. Further investigations will be required to obtain more definite answers. One set of experiments could test whether the sperm–chorion interaction can be reduced by competition with soluble ZP protein fragments, resulting in a lowered fertilization rate. For these experiments one could choose the regions in the zebrafish ZP proteins that are orthologous to the regions in mammalian ZP proteins that have been shown to interact with sperm (Avella, Xiong, and Dean 2013; Avella, Baibakov, and Dean 2014). Another possible experiment would be to solubilize the chorion and use the extract to stimulate sperm, while studying their swimming behavior and internal ion changes. A change in either aspect would indicate an interaction between sperm and components of the chorion. Subsequently, one could fractionate the chorion extract and repeat this bioassay to identify the specific sperm-interacting components.

4.2. Frequent gene loss events shape the evolution of CatSper and sAC in aquatic vertebrates

The CatSper channel was first discovered as a testis-specific channel that is homologous to voltage-gated calcium channels (Ren et al. 2001). Indeed, CatSper is a calcium channel that is activated by a combination of alkalization and voltage (Cai and Clapham 2012; Brenker et al. 2012; Seifert et al. 2015) and in some species additionally modulated, e.g. by progesterone in human (Strünker et al. 2011; Lishko, Botchkina, and Kirichok 2011). It is expressed specifically in sperm cells, and localized to the plasma membrane of the principal piece

of the sperm flagellum (Lishko et al. 2012). Upon activation, it leads to a calcium influx, which in turn triggers a motility response in sperm (Seifert et al. 2015)(Seifert et al. 2015)Seifert et al. 2015).

The CatSper channel itself consists of four different alpha-subunits (CatSper1–4) that form a hetero-tetramer, making up the channel pore (Qi et al. 2007). In addition, five auxiliary proteins have been found: CatSperB, D, G, and E are transmembrane proteins (Liu et al. 2007; Wang et al. 2009; Chung et al. 2011; 2017) while CatSperZ is a small soluble protein (Chung et al. 2017). The auxiliary transmembrane proteins possess large extracellular domains that form a "pavilion-like" structure above the channel pore, and are linked via short stems to the transmembrane domains that stabilize the pore itself (Lin et al. 2021). Stem domains do not interact with each other allowing free access of ions in-between the stems to the channel pore (Lin et al. 2021). All nine subunits are required for mammalian CatSper to function, thus the entire CatSper channel complex is required for fertility (Qi et al. 2007; Liu et al. 2007; Wang et al. 2009; Chung et al. 2011; 2017).

The evolutionary origin of CatSper dates back to even before the common ancestor of animals and fungi (both ophistokonts), because it was also found in a unicellular protist species, *Thecamonas trahens*, from the sister clade to ophistokonts (Cai and Clapham 2012). In *Thecamonas trahens*, also four principal CatSper subunits are present, placing the original gene duplication events that led to the four principal CatSper genes over one billion years ago (origin of ophistokonts, Dohrmann and Wörheide 2017).

Within the animal kingdom (Metazoa) both vertebrate and invertebrate species possess CatSper, but at the same time, it has also been lost frequently. CatSper was thought to be lost in bony fish (Teleostei), amphibians, and birds (Cai and Clapham 2008). In contrast, Romero and Nishigaki (2019b) reported in a preliminary analysis the presence of CatSper in three species of ray-finned fishes. Moreover, pharmacological evidence has suggested the presence of functional CatSper in Atlantic salmon, *Salmo salar* (Lissabet et al. 2020). However, all previous conclusions were made based on a very limited number of species examined. Recently, many more genomes became available, enabling a more thorough test of such assumptions. Indeed, my analysis of CatSper presence in several hundred species of aquatic vertebrates detected a much more fine-grained pattern of gene losses (Figure 7).

While many fish species, both Teleostei and earlier-derived species, have retained a complete or almost-complete inventory of CatSper genes (Figure 7, Appendix Table 2), many other species and higher order taxonomic groups have lost it. For example, herring possess at least eight of the nine CatSper genes (Rafati et al. 2020). But zebrafish, in the same cohort as herring (Otomorpha), have lost all these CatSper genes. The ninth gene CatSperZ was not analysed, as it is short, rapidly evolving (Chung et al. 2017), and thus near impossible to obtain a robust phylogeny of this gene over large evolutionary distances.

Synteny analysis for all CatSper channel subunits between zebrafish and the closely related goldfish (same order, Cypriniformes) corroborated the absence in zebrafish, thus excluding potential sequencing problems as possible cause for missing these sequences in zebrafish. Interestingly, none of the genes neighboring goldfish CatSper3 occur in the genomic neighborhood of herring CatSper3 (Rafati et al. 2020), suggesting massive rearrangements specific to either Cypriniformes or Clupeiformes (the order of which herring is a member). Because Rafati et al. (2020) found considerable synteny of the genes neighboring herring CatSper3 even with much more distantly related species (e. g. human), it is likely that the bulk of rearrangements have occurred within Cypriniformes.

To pinpoint the evolutionary level of the gene loss, CatSper presence and absence was examined at the level of species, genus, family, and order in Cypriniformes. The loss of the CatSper channel must have occurred in the most recent common ancestor of Danionidae (including zebrafish), Xenocyprididae and Leuciscidae, since the earlier-derived Cyprinidae (including goldfish) have retained the CatSper channel. The auxiliary CatSper genes are lost in a similar but not identical pattern to the CatSper channel genes. In some cases auxiliary CatSper subunits but not the principal channel subunits are retained, suggesting a possible neofunctionalization of the auxiliary CatSper subunits that would protect them from being lost.

Incidentally, the clear divide in CatSper presence between Cyprinidae (present) and Danionidae (absent) corroborates Stout et al. (2016) who re-classified zebrafish (formerly considered Cyprinidae) to their own family Danionidae.

What could the loss of CatSper in zebrafish mean for sperm motility? I showed that zebrafish sperm activation is accompanied by a calcium increase in the sperm head. Fechner et al. (2015) could show that artificial calcium increase strongly modulates the swimming pattern of already activated zebrafish sperm. However, external calcium is not required for initiation of motility in zebrafish sperm (Figure 36) (Wilson-Leedy, Kanuga, and Ingermann 2009), and the rise in internal calcium that accompanies activation is also independent of extracellular calcium (Figure 36). Thus zebrafish may not require a calcium channel in the plasma membrane dedicated to sperm motility. Therefore, the observed calcium increase may be caused by the release from *intracellular* calcium stores, i.e., either mitochondria and/or the redundant nuclear envelope (Ho and Suarez 2003). Candidates for intracellular calcium channels include two members of the TRP superfamily, PKD2 (synonym TRPP2) and TRPV1, which are not only found in the plasma membrane, but also in the membrane of endoplasmic reticulum (Koulen et al. 2002; Hagenacker, Ledwig, and Büsselberg 2008). In insects, the PKD2 channel triggers sperm motility responses (Gao, Ruden, and Lu 2003; Köttgen et al. 2011) and in zebrafish, the PKD2 channel has been shown to be involved in intra-ciliary calcium signaling (Yuan et al. 2015). A pharmacological study by Chen et al. (2020) showed that several different calcium

channel blockers, including ruthenium red, reduced zebrafish sperm motility and fertilization rates, albeit at high concentrations well above the IC_{50} values reported for the blockers. Nevertheless, the effect of ruthenium red was not observed in a zebrafish TRPV1 knockout (Chen et al. 2020), suggesting TRPV1 as candidate channel mediating the release of calcium from intracellular stores during sperm activation. Interestingly, basal sperm motility and fertilization rate in the TRPV1 knockout are indistinguishable from wild-type, suggesting compensatory recruitment of another calcium channel in the knockout.

In contrast to CatSper, other ion channels in the sperm signaling cascade of sea urchin and mammals are present in zebrafish sperm, but both their localization and their function differ considerably. The HCN-like and the CNGK channel are localized to the plasma membrane of the head of zebrafish sperm (Fechner et al. 2015; Wobig et al. 2020), not to the flagellar plasma membrane as in other species (Lishko et al. 2012).

Secondly, the HCN-like channel present in zebrafish is very proton-selective, but does not carry sodium or potassium ions as its sea urchin and mammalian homologues do (Wobig et al. 2020). I showed acidification of sperm accompanying activation, consistent with observations by Wobig et al. (2020), and suggesting the involvement of HCN-like channels in the activation process. The CNGK channel of zebrafish is activated by alkalization, not by cyclic nucleotides (Fechner et al. 2015). In these cases, changes in proton concentration are either a trigger or the result of channel action, indicating that protons rather than cyclic nucleotides serve as intracellular messengers in zebrafish sperm, albeit at different steps of the sperm signaling cascade. The mechanism for alkalization required to activate CNGK is unknown so far, but the closing of CNGK could be mediated by activation of the HCN-like channel and subsequent acidification (Wobig et al. 2020).

sAC (gene name *adcy10*) is the predominant adenylyl cyclase in the sperm tail (Buffone et al. 2014) out of the ten *adcy* genes known. sAC is the only soluble form, all others (*adcy1–9*) are transmembrane proteins. sAC generates cAMP, which seems to be important for both mammalian and many non-mammalian sperm. But its specific function in the respective signaling pathways is different (Figure 1). For example in sea urchin, cAMP is required for full activation of the HCN channel (Körschen et al. 2021). Mammalian sperm do not posses an HCN channel; however, cAMP is still required for capacitation and hyperactivation. The primary source for this cAMP is sAC, and its absence due to mutation or deliberate knockout results in male infertility (Esposito et al. 2004; Akbari et al. 2019). The absence of sAC has no other detectable phenotype in mice and humans (Esposito et al. 2004; Akbari et al. 2019), suggesting that sAC's main or even only function is in sperm. Thus, sAC is considered essential for sperm motility, just like CatSper. Because zebrafish do not possess CatSper, this poses the question whether they lack sAC too.

I performed phylogenetic analysis in aquatic vertebrates for sAC using the same methods as for my examination of CatSper genes. I found a fine-grained pattern of gene loss for sAC, analogous to my examination of CatSper, with similar evolutionary time points for gene loss events. For example, jawless fish lack both sAC and CatSper, while cartilaginous fish possess both. However, loss of sAC is more widespread than loss of CatSper (Figure 49). Although earlier-derived clades tend to either possess both sAC and CatSper or lack both, especially in Neoteleostei the difference in retention of sAC and CatSper becomes sharply obvious. No species in Neoteleostei has retained sAC, but several earlier-derived Neoteleostei species have retained CatSper. Note that within the Percomorpha clade, the largest clade within Neoteleostei, all species have lost both sAC and CatSper.

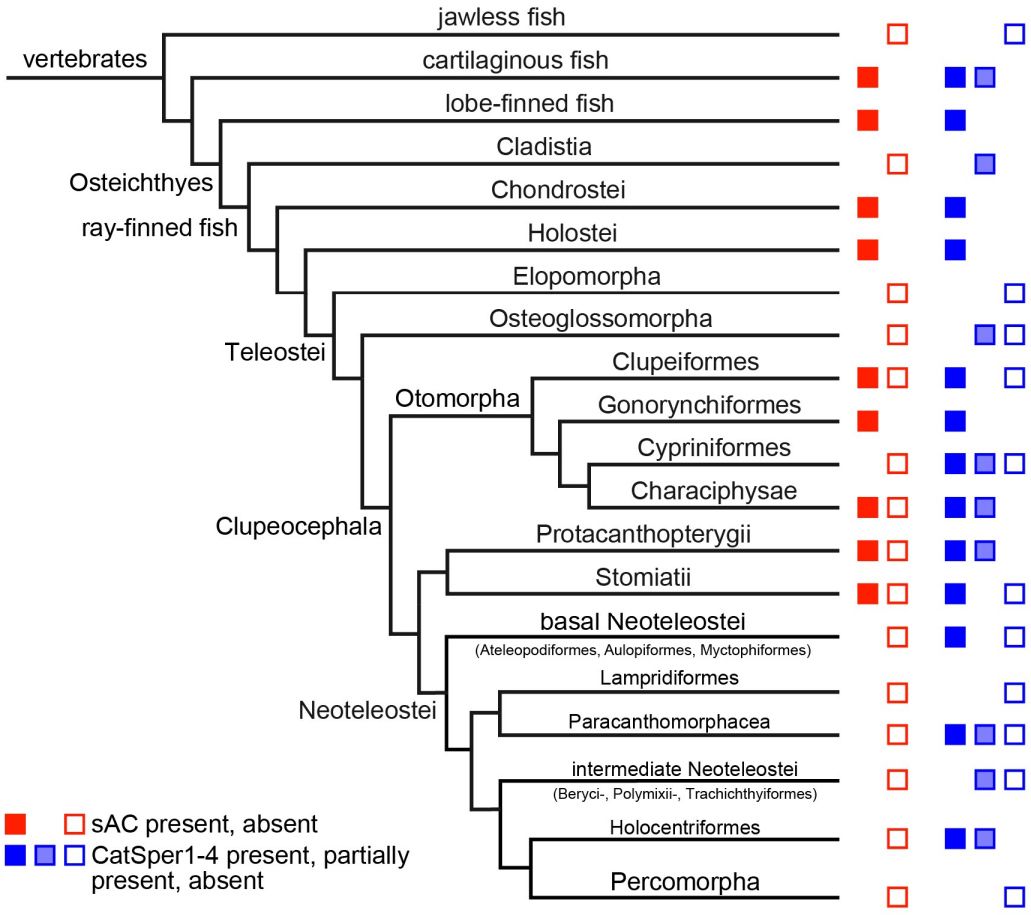

Figure 49: Cladogram of aquatic vertebrates according to Betancur (2013), showing presence and absence of sAC and CatSpers1–4. Color code according to legend. Filled-in squares, species in a given clade possess sAC or CatSper1–4. Empty squares, species in a given clade lack sAC or CatSper1–4. Pale blue square, species in a given clade possess some but not all of CatSper1–4. Auxiliary CatSpers are not depicted here because absence of the pore-forming subunits would already result in a non-functional channel.

In species that have lost sAC but retained CatSper, this could be a hint that they have evolved different cascades that lead to CatSper's activation. One possibility would be that species lacking sAC compensate for its absence by using one of the nine membranous adenylyl cyclases as replacement for cAMP generation (Esposito et al. 2004). It is even possible that sperm with CatSper but without sAC might not require cAMP as a signaling molecule.

sAC can be activated either by bicarbonate or alkaline pH (Rahman, Buck, and Levin 2013; Körschen et al. 2021). The former has been shown in mammals and a cyanobacterium (Chen et al. 2000; Kleinboelting et al. 2014), whereas alkaline activation was observed in a sea urchin and a salmon species (Rahman, Buck, and Levin 2013; Körschen et al. 2021). Activation by bicarbonate has been linked to a motif conserved in mammals and a cyanobacterium, K95/R176 (numbering refers to the human sequence, Körschen et al. 2021). Thus it might be expected that this motif is absent in species that use alkaline activation. Indeed, the species with alkaline activation do not exhibit the full K95/R176 motif, but retain only the K95 (sea urchin) or the R176 (salmon) (Körschen et al. 2021), replacing the respective other amino acid with asparagine (K95/N176 respectively N95/R176). However, there are counterexamples, such as dogfish, which has a N95/R176 motiv, but does respond to bicarbonate (Tresguerres et al. 2010). My phylogenetic studies for presence and absence of sAC allowed me to investigate the K/R polymorphism in a wide range of fish species (jawless, cartilaginous, ray-finned, and lobe-finned bony fish). In all but lobe-finned fish—coelacanth and lungfish, which retain K95/R176—K95 was replaced by another amino acid, in most cases N95. In contrast, R176 remained highly conserved. This detailed overview offers a basis for targeted functional studies to elucidate a potential causal relationship between polymorphism and bicarbonate vs. alkaline sensitivity. In such studies it will be imperative to clearly separate the bicarbonate influence from a pH increase introduced by the bicarbonate (see also Tresguerres et al. 2010).

In summary, zebrafish sperm lack two characteristic proteins of known sperm signaling cascades (sAC and CatSper). While they possess homologs of two other signaling proteins (CNGK and HCN-like channels), these function radically differently, and also are located in the sperm head, not in the flagellum (Fechner et al. 2015; Wobig et al. 2020). Thus it is likely that the overall mechanisms of sperm motility and potential pathfinding in zebrafish are profoundly different compared to those that possess the CatSper and sAC genes.

On the whole, a vast variety of sperm signaling cascades appears to exist, consistent with the hypothesis that rapid evolution of sperm signaling cascades could contribute to speciation (Swanson and Vacquier 2002; Carlisle and Swanson 2021).

4.3. A staining artifact reveals a novel structural element in the flagellum

The basic architecture of most sperm cells is simple, consisting of the head, the midpiece, and the flagellum (Figure 50), even if these elements can be very variable in their details (Pitnick, Hosken, and Birkhead 2008, 70–71; Alvarez 2017; Fitzpatrick, Kahrl, and Snook 2022). The sperm head houses the nucleus and the acrosome, in species which possess it (Kierszenbaum, Rivkin, and Tres 2007). The head is the most voluminous compartment of the sperm. The midpiece varies in size across species and contains mitochondria, which provide energy for the sperm (Pitnick, Hosken, and Birkhead 2008, 189). The flagellum contains a microtubuli core (axoneme): sliding of microtubuli relative to each other by means of dynein motor proteins results in bending of the flagellum and ultimately movement of the sperm cell (Pitnick, Hosken, and Birkhead 2008, 86; Lindemann and Lesich 2016).

The plasma membrane of the sperm cell contains sensing and signaling proteins such as receptors, channels, and transporters. These are often enriched or even restricted to a particular compartment of the cell. For example, in sea urchin, CatSper and other channels such as CNGK are found exclusively in the flagellum (Bönigk et al. 2009; Seifert et al. 2015). However, in zebrafish, CNGK and other channels such as HCN-like are localized to the head instead (Fechner et al. 2015; Wobig et al. 2020).

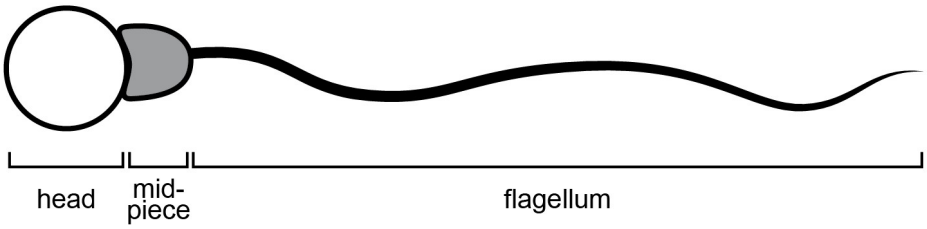

Figure 50: Schematic representation of basic sperm morphology.

In fluorescent imaging, the sperm head is usually far more visible than the flagellum because of its much greater volume, but it is possible to visualize flagella as well. I observed a remarkably consistent fluorescent signal in the flagellum of zebrafish sperm: two to several sharply localized and strong increases in fluorescence along the flagellar length (hereafter called bright spots for brevity). These bright spots appear upon activation of sperm motility, and occur with all fluorescent dyes examined. Bright spots are not caused by the acidification that accompanies sperm activation, and occur independent of the strength of the hypoosmotic shock. It cannot be examined whether the hypoosmotic shock itself is causal, because it is not possible to activate zebrafish sperm without it. Because the bright spots could be observed with pHrodo *and*

BCECF, pH-sensitive dyes that display opposite fluorescence changes to the same pH change, they cannot represent actual ionic changes, i.e. they constitute a remarkably consistent artifact.

Because bright spots appear with activation, they seem to be the consequence of structural changes in the flagellum that happen upon activation. This hypothesis is strengthened by the observation that the fluorescence along in-between flagellum pieces decreases concurrently with the appearance of the bright spots themselves. The magnitude of the fluorescence decrease is equivalent to the increase in the bright spots, suggesting transport of dye molecules towards the bright spots. Thus the bright spots should reflect a structural change in repeating segments of the flagellum that is caused by activation.

Zebrafish sperm indeed possess localized morphological features along the flagellum. Zhang et al. (2014) and Sáez-Espinosa et al. (2022) demonstrated that zebrafish sperm possess cytoplasmic vesicles along the flagellum, whose function is unknown. Several vesicles were reported per flagellum, which is similar to the frequency observed for bright spots. These cytoplasmic vesicles do exist already before activation (Zhang et al. 2014; Sáez-Espinosa et al. 2022), but might change during activation, which is plausible because zebrafish sperm undergo considerable morphological changes after activation, e.g. the nucleus deforms and the plasma membrane is damaged (Sáez-Espinosa et al. 2022).

I hypothesize that these vesicles correspond to the bright spots. If they inflate with cytoplasm during activation, they might soak up more dye molecules. However, this would only work for the AM-ester form of dyes, which is expected to be cleaved by generic esterases after loading. The hydrolyzed forms are polar and cannot diffuse across plasma membranes. Thus, transporters would be needed to facilitate this kind of dye transport. Organic anion transporters (OATs), a subgroup of the SLC22 superfamily, and ATP-binding cassette (ABC) transporters have been shown to transport a variety of compounds (Lage 2003; Nigam et al. 2015). Zebrafish possess members of both families, with high expression of OATs in testis (Mihaljevic et al. 2016). If the dye is brought into the vesicles via such transporters after the sperm undergoes hypoosmotic shock, perhaps the vesicles serve as an ion store to ameliorate the swelling of the flagellum due to the hypoosmotic shock.

My results suggest a potential function for thus far only structurally described entities (cytoplasmic vesicles, Zhang et al. 2014; Sáez-Espinosa et al. 2022). While it is much too early for definitive statements, my work shows a direction to examine a possible function for these vesicles. The next step would be to convert the fluorescence signal into an EM-visible stain (Lübke 1993; Meißlitzer-Ruppitsch et al. 2008) to examine whether the bright spots and the cytoplasmic vesicles are the same. If so, the presence and activity of organic anion transporters in the flagellum can be examined as a subsequent step.

5. Appendix

Appendix Table 1: Comparison of the number of fish genomes examined for presence of CatSper or sAC to the total number of fish species in the respective groups. Numbers for the latter were obtained from Fishbase.org and Catalogueoflife.org, accessed February 2021 (Froese, Pauly, and Editors 2020; Roskov et al. 2021).

group	# of examined genomes CatSper	# of examined genomes sAC	total # of species
jawless fish	3	5	129
cartilaginous fish	8	13	1282
lobe-finned fish	1	2	8
early-diverging ray-finned fish (Chondrostei, Cladistia, Holostei, Elepomorpha, Osteoglossomorpha)	9	29	2288
Otomorpha	38	72	10619
salmon-related fish (Protacanthopterygii + Stomiatii)	14	29	832
basal Neoteleostei (Ateleopodiformes, Aulopiformes, Myctophiformes)	3	593	523
Lampridiformes + Paracanthomorphacea	35		683
intermediate Neoteleostei (Beryci-, Holocentri-, Polymixii-, Trachichthyiformes)	13		274
Percomorpha	146		17301

Appendix Table 2: Overview of presence and absence of CatSper genes (A1–4, B, D, G, E) in all examined fish species. External Excel file.

Appendix Table 3: Overview of presence and absence of sAC genes in all examined fish species. External Excel file.

Appendix Table 4: Protein lists for preparation A, with accession numbers and description from the Uniprot database. Four lists, two for whole-chorion samples (WC, WC_{subset}) and two for micropyle-missing samples (MM, MM_{subset}). WC_{subset} denotes the subset of proteins that are common to the all three whole-chorion samples, MM_{subset} denotes the subset of proteins that are common to the all three micropyle-missing samples. External Excel file.

Appendix Table 5: Protein hit counts in MS data of preparation A (whole ovaries, chorions obtained via trituration) and preparation B (mature oocytes, chorions removed via forceps). Individual fish are numbered separately for each method, the designation .x indicates technical replicates. Starred (*) samples are micropyle-missing samples, all others are whole-chorion samples.

method	**sample**	**# protein hits**	
		full	*– blank test*
method A	fish 1	484	n.a.
	fish 2	427	n.a.
	fish 3	454	n.a.
	fish 1 *	270	n.a.
	fish 2 *	373	n.a.
	fish 3 *	295	n.a.
method B	fish 1.1	228	185
	fish 1.2	204	162
	fish 1.3	191	165
	fish 2.1	188	160
	fish 2.2	165	145
	fish 2.3	205	162
	fish 3.1	503	460
	fish 3.2	154	145
	fish 3.3	193	164

Appendix Table 6: Categorization of the common proteins of preparation A, and those common to preparation B. Accession numbers and descriptions from the Uniprot database are shown. Third column shows the category (zona pellucida, actin, etc.). External Excel file.

Appendix Table 7: Protein hits found in blank test of preparation B. Accession numbers and descriptions from the Uniprot database are shown. External Excel file.

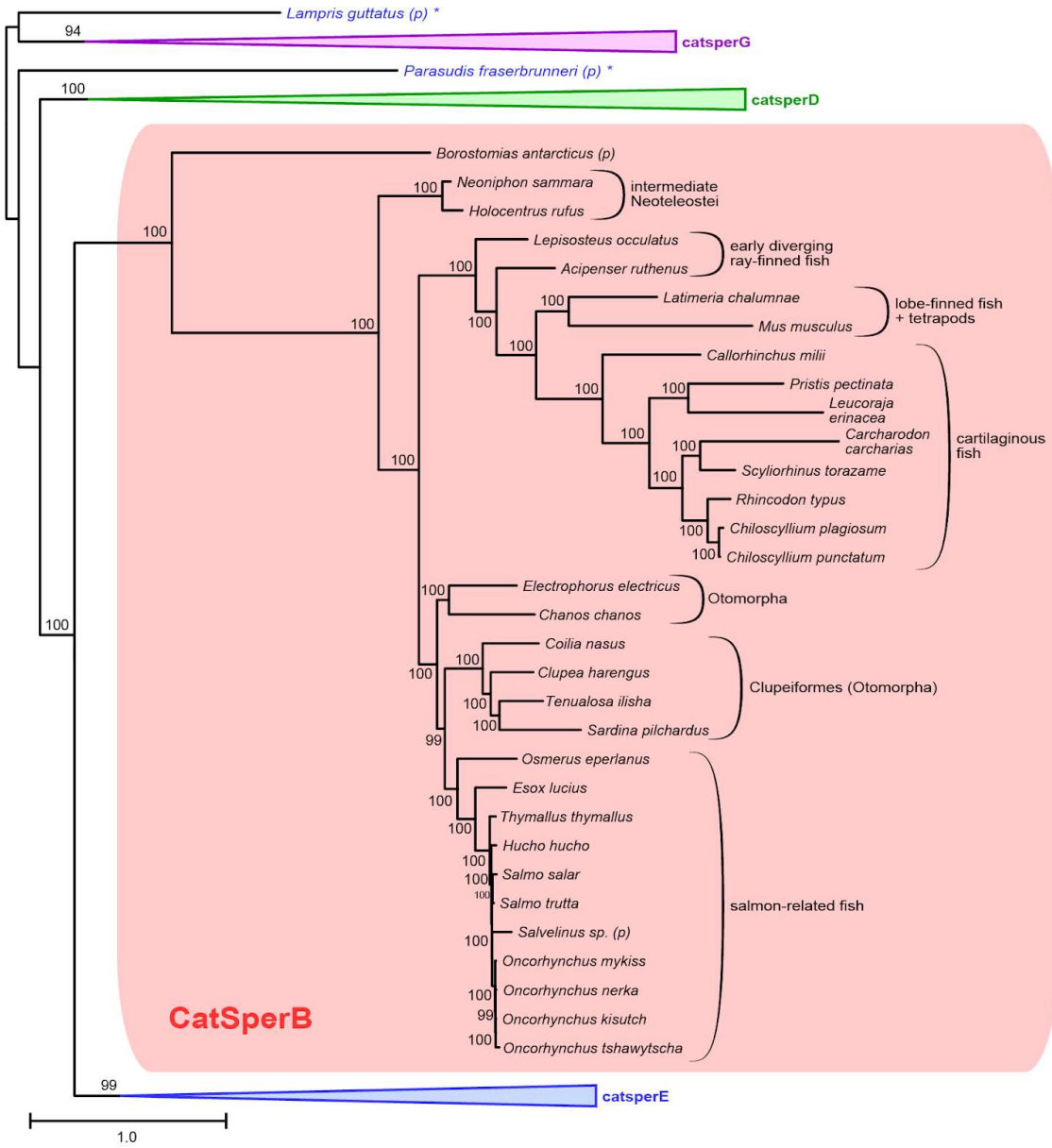

Appendix Figure 1: Phylogenic tree of new-found CatSperB genes and known CatSperB genes (such as *Mus musculus, Lepisosteus occulatus*), with the other associated CatSper genes as outgroup. Branch support values are given in %, if above 80%, at their respective node. Scale bar value (1.0) denotes the replacement rate of amino acids on every position of the sequences. Genes marked (f) are fragments (< 200 amino acids); genes marked (p) are pseudogenes. Genes marked with * were annotated as CatSperE.

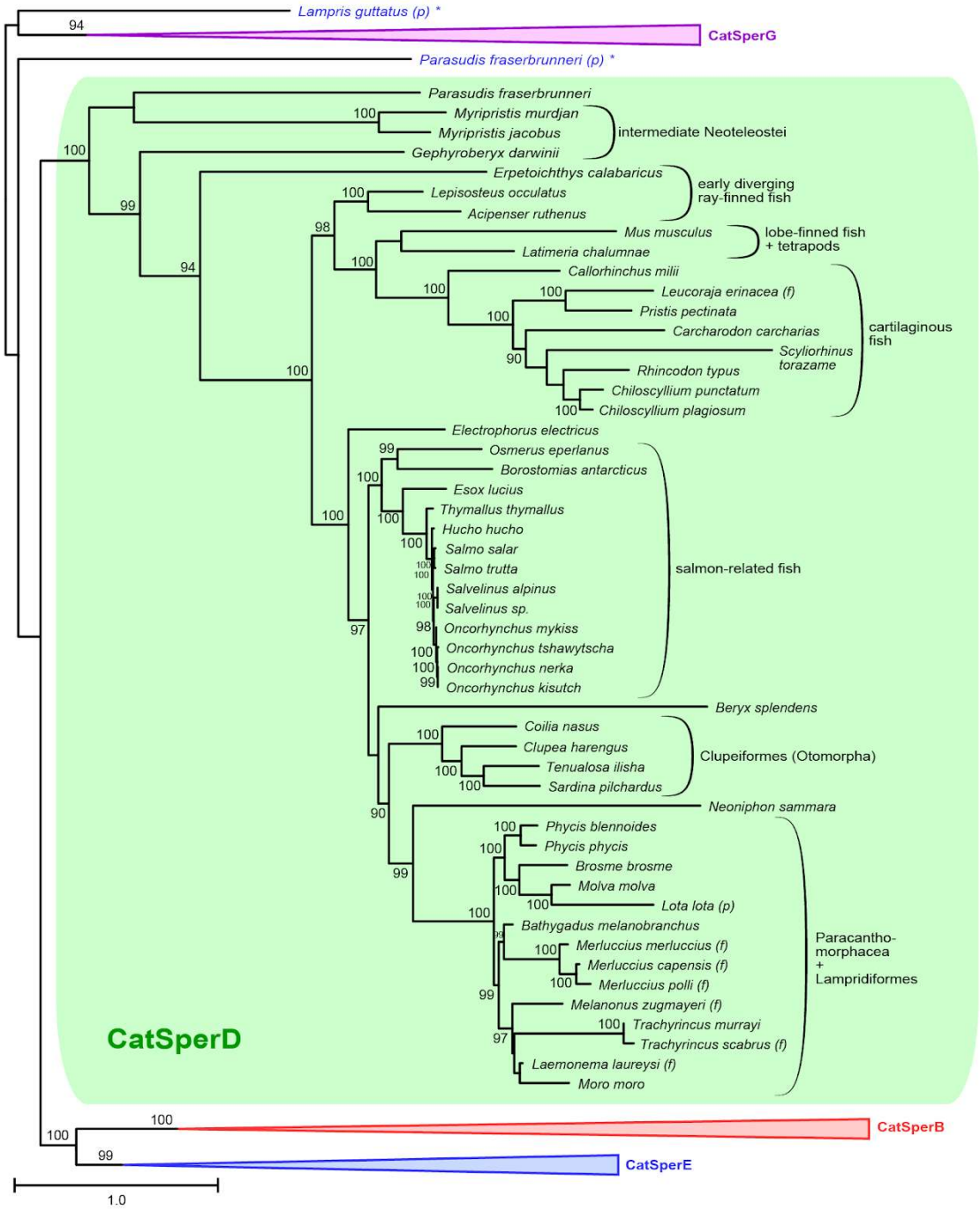

Appendix Figure 2: Phylogenic tree of new-found CatSperD genes and known CatSperD genes (such as *Mus musculus, Lepisosteus occulatus*), with the other associated CatSper genes as outgroup. Branch support values are given in %, if above 80%, at their respective node. Scale bar value (1.0) denotes the replacement rate of amino acids on every position of the sequences. Genes marked (f) are fragments (< 200 amino acids); genes marked (p) are pseudogenes. Genes marked with * were annotated as CatSperE.

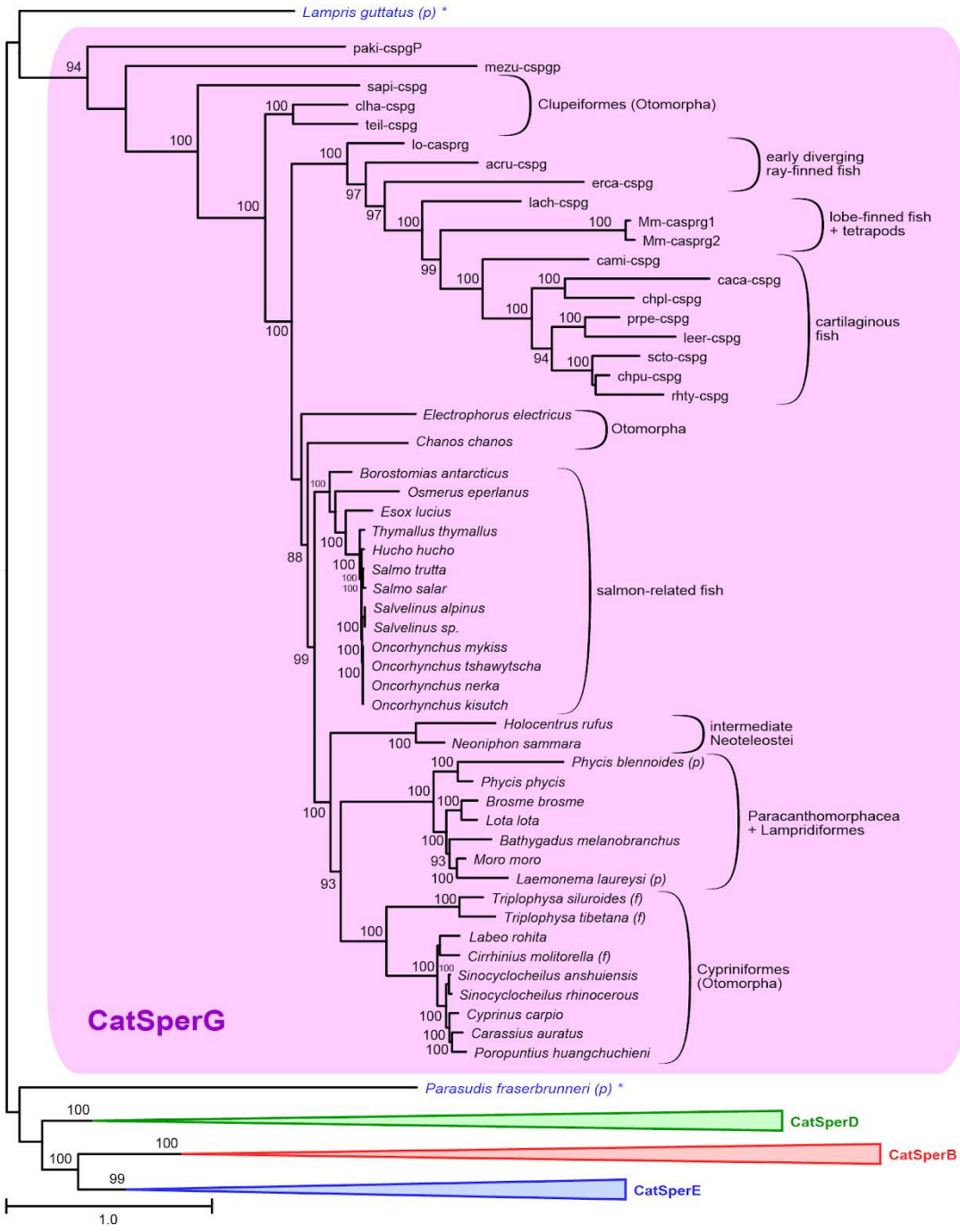

Appendix Figure 3: Phylogenic tree of new-found CatSperG genes and known CatSperG genes (such as *Mus musculus, Lepisosteus occulatus*), with the other associated CatSper genes as outgroup. Branch support values are given in %, if above 80%, at their respective node. Scale bar value (1.0) denotes the replacement rate of amino acids on every position of the sequences. Genes marked (f) are fragments (< 200 amino acids); genes marked (p) are pseudogenes. Genes marked with * were annotated as CatSperE.

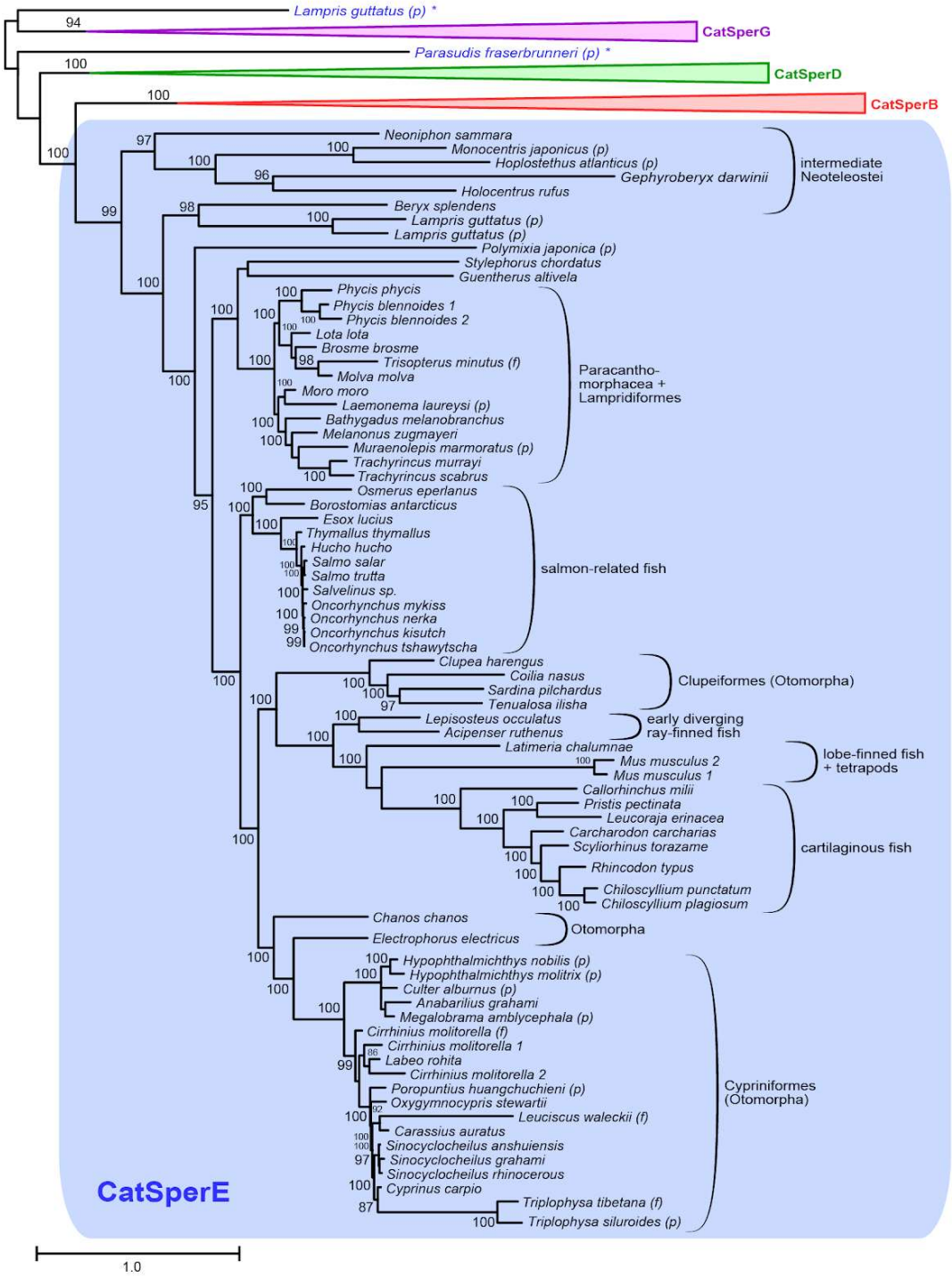

Appendix Figure 4: Phylogenic tree of new-found CatSperE genes and known CatSperE genes (such as *Mus musculus, Lepisosteus occulatus*), with the other associated CatSper genes as outgroup. Branch support values are given in %, if above 80%, at their respective node. Scale bar value (1.0) denotes the replacement rate of amino acids on every position of the sequences. Genes marked (f) are fragments (< 200 amino acids); genes marked (p) are pseudogenes. Genes marked with * were annotated as CatSperE.

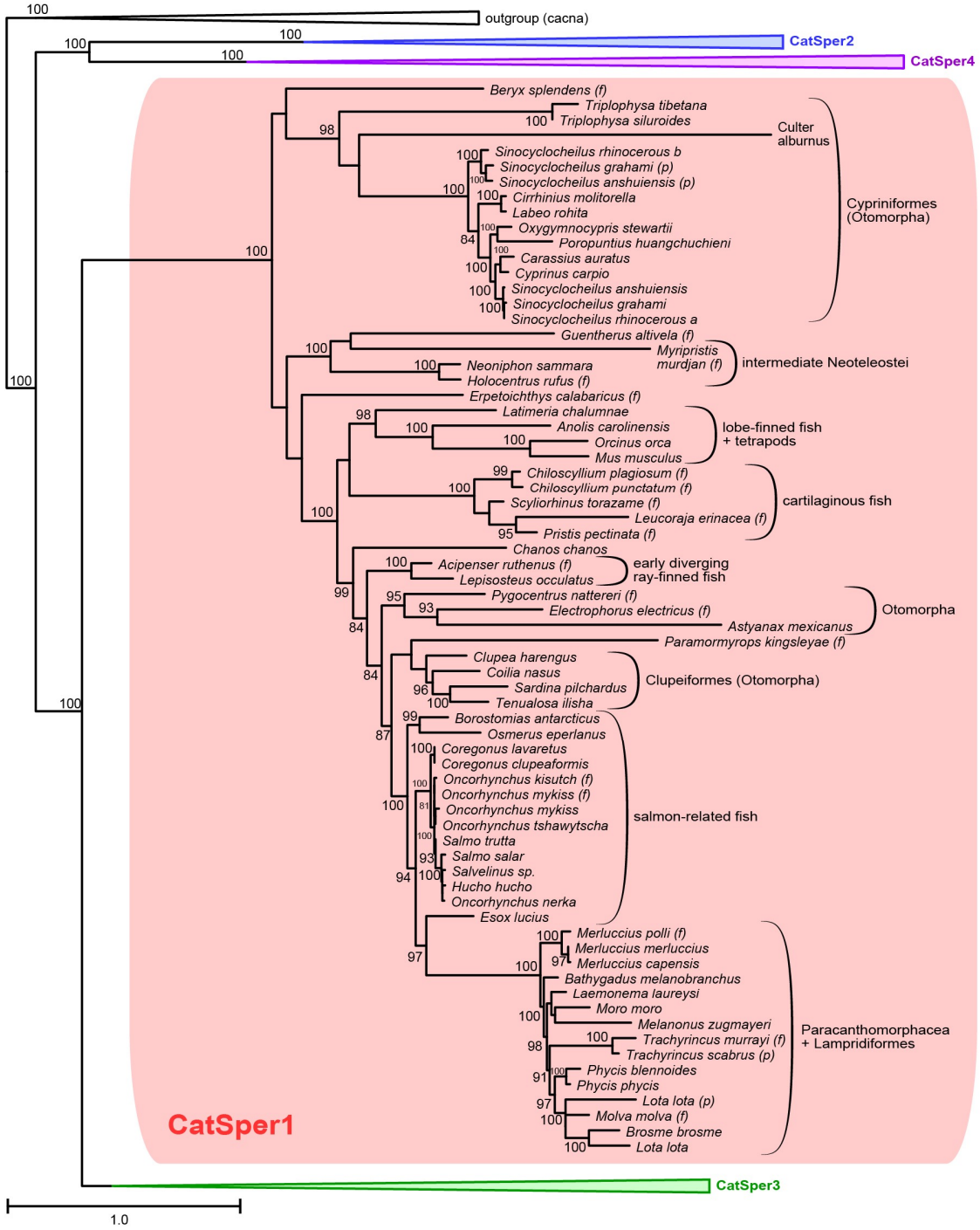

Appendix Figure 5: Phylogenic tree of new-found CatSper1 genes and known CatSper1 genes (such as *Mus musculus, Lepisosteus occulatus*), with cacna/Cav genes as outgroup, and CatSper2-4 (collapsed). Branch support values are given in %, if above 80%, at their respective node. Scale bar value (1.0) denotes the replacement rate of amino acids on every position of the sequences. Genes marked (f) are fragments (< 200 amino acids); genes marked (p) are pseudogenes.

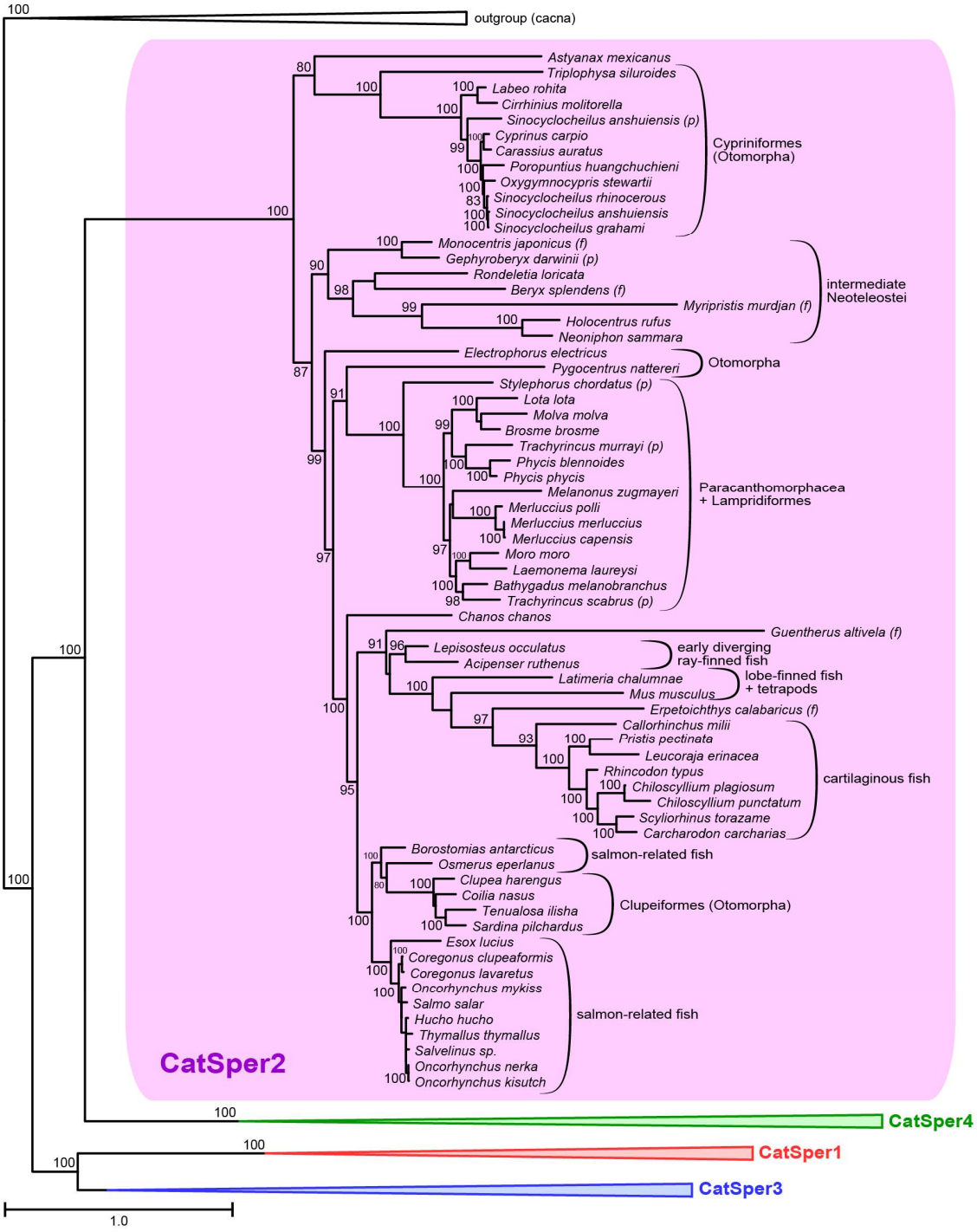

Appendix Figure 6: Phylogenic tree of new-found CatSper2 genes and known CatSper2 genes (such as *Mus musculus*, *Lepisosteus occulatus*), with cacna/Ca_V genes as outgroup, and CatSper1,3-4 (collapsed). Branch support values are given in %, if above 80%, at their respective node. Scale bar value (1.0) denotes the replacement rate of amino acids on every position of the sequences. Genes marked (f) are fragments (< 200 amino acids); genes marked (p) are pseudogenes.

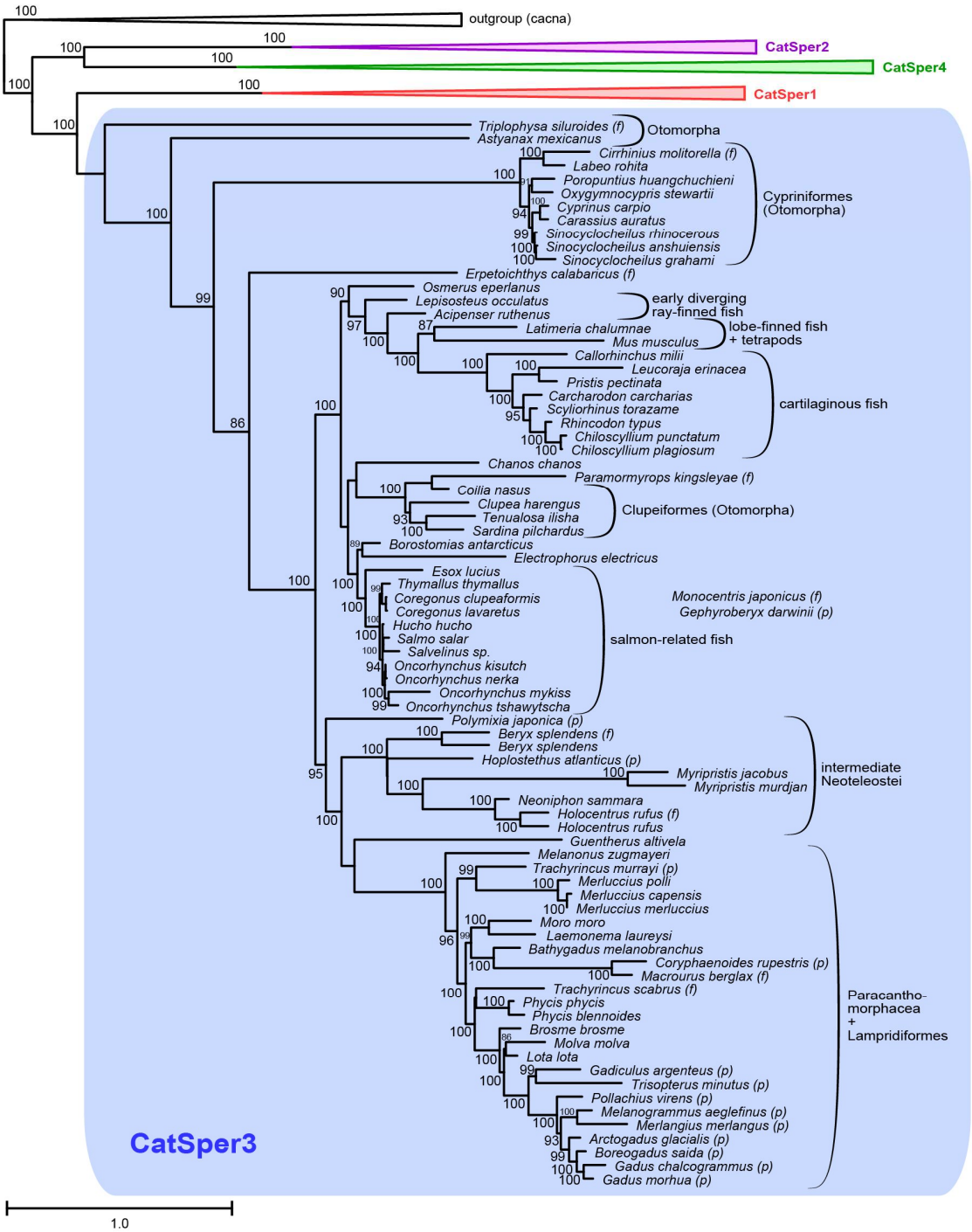

Appendix Figure 7: Phylogenic tree of new-found CatSper3 genes and known CatSper3 genes (such as *Mus musculus*, *Lepisosteus occulatus*), with cacna/Ca_V genes as outgroup, and CatSper1-2,4 (collapsed). Branch support values are given in %, if above 80%, at their respective node. Scale bar value (1.0) denotes the replacement rate of amino acids on every position of the sequences. Genes marked (f) are fragments (< 200 amino acids); genes marked (p) are pseudogenes.

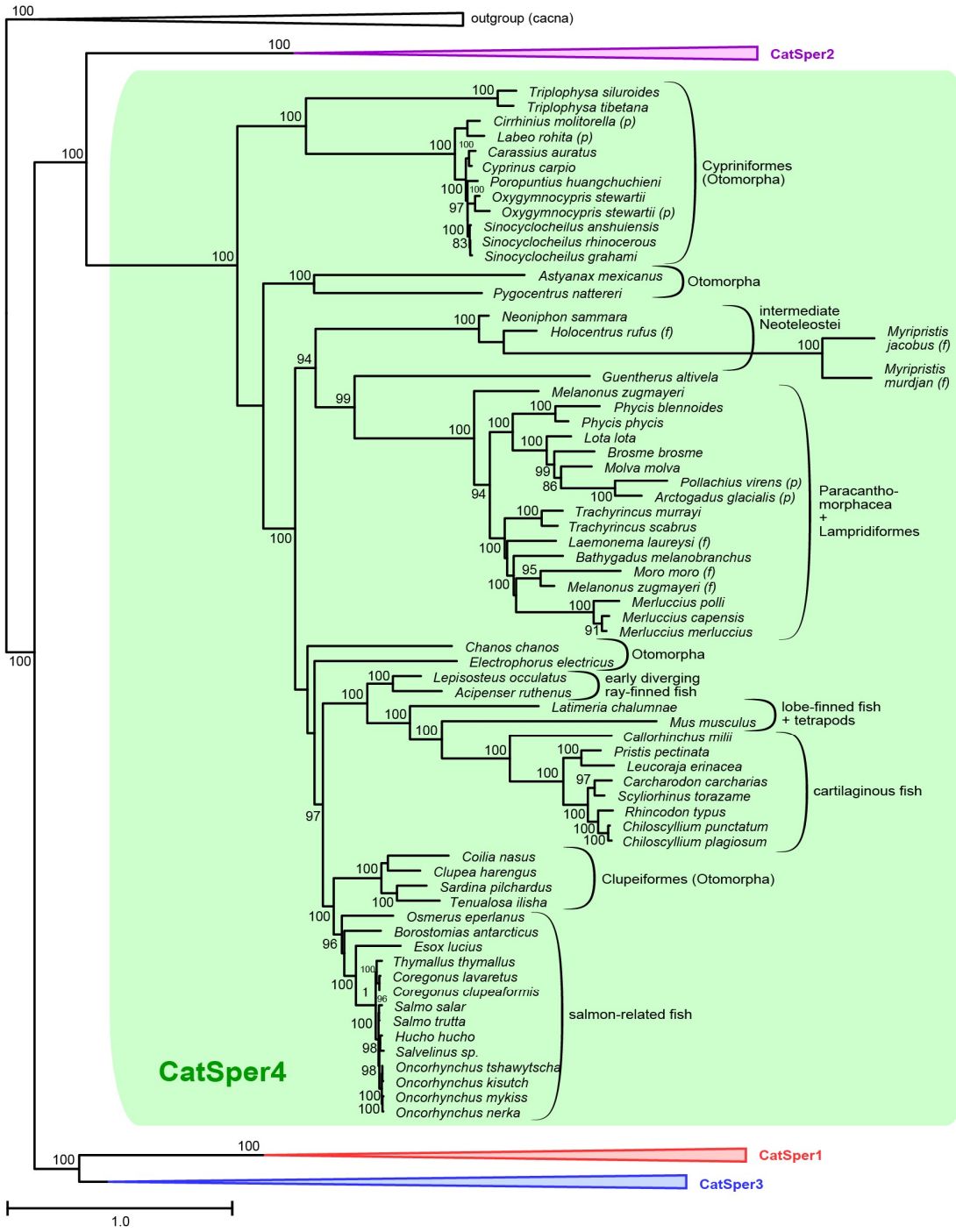

Appendix Figure 8: Phylogenic tree of new-found CatSper4 genes and known CatSper4 genes (such as *Mus musculus*, *Lepisosteus occulatus*), with cacna/Ca_V genes as outgroup, and CatSper1-3 (collapsed). Branch support values are given in %, if above 80%, at their respective node. Scale bar value (1.0) denotes the replacement rate of amino acids on every position of the sequences. Genes marked (f) are fragments (< 200 amino acids); genes marked (p) are pseudogenes.

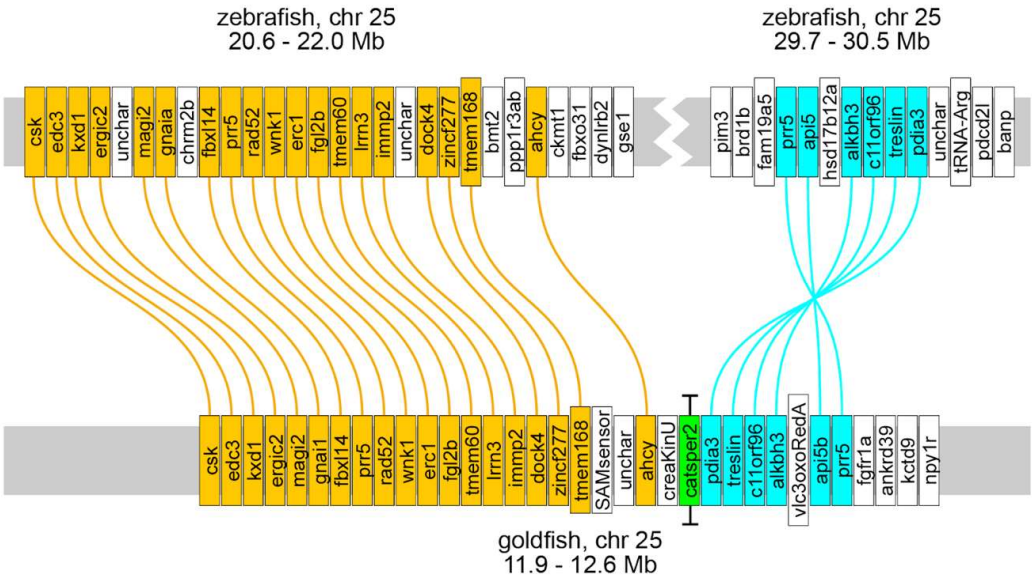

Appendix Figure 9: Synteny of genomic region of CatSper2 in goldfish and zebrafish. Conserved blocks of genes highlighted in yellow and cyan. Colored lines connect orthologous genes conserved between species. Goldfish CatSper2 is highlighted in green and flanked by black whiskers to indicate absence of orthologous genes. Genomic region from first to last gene is given in Mb for each chromosome (chr).

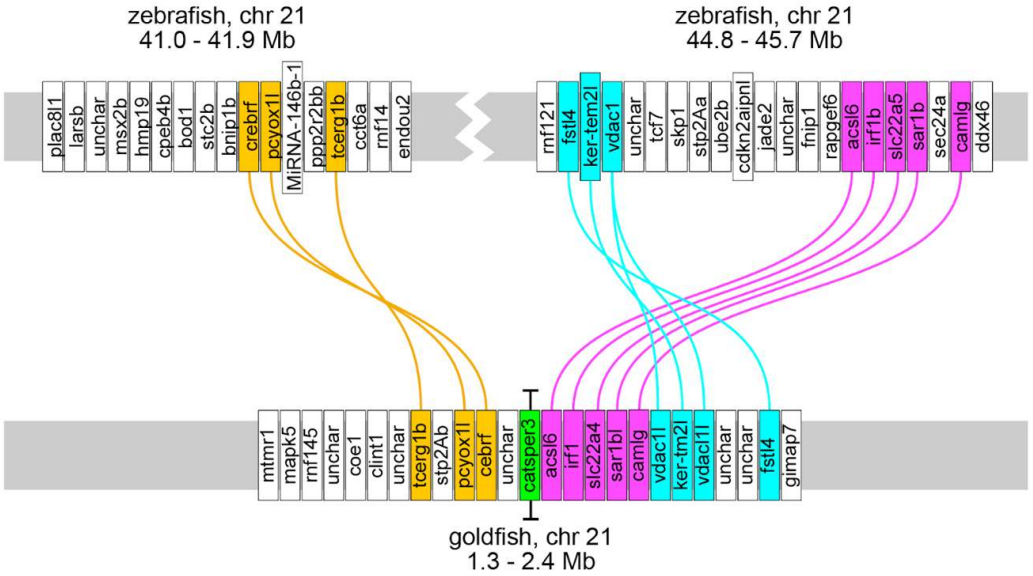

Appendix Figure 10: Synteny of genomic region of CatSper3 in goldfish and zebrafish. Conserved blocks of genes highlighted in yellow, magenta, and cyan. Colored lines connect orthologous genes conserved between species. Goldfish CatSper3 is highlighted in green and flanked by black whiskers to indicate absence of orthologues. Genomic region from first to last gene is given in Mb for each chromosome (chr).

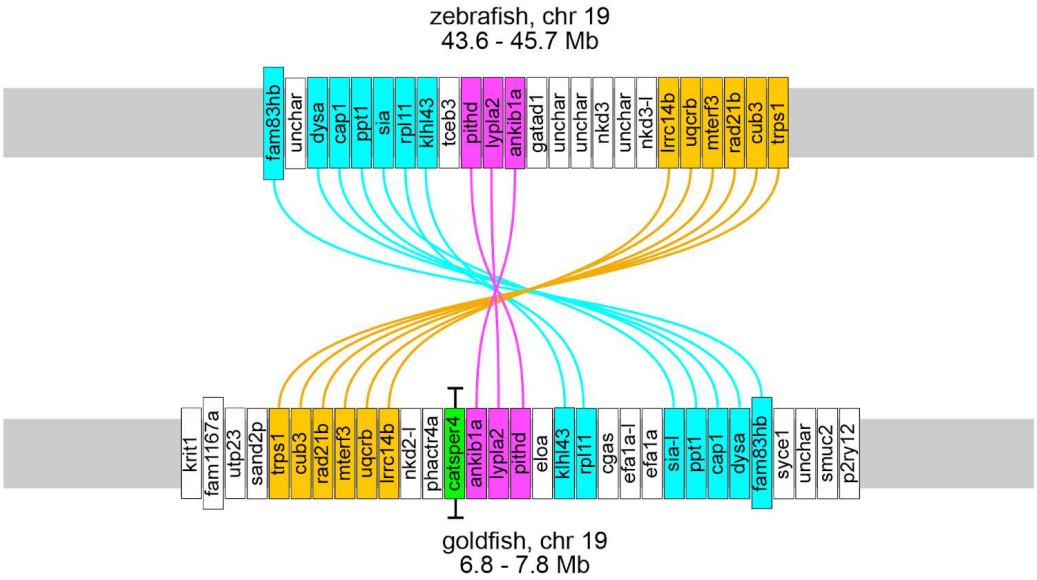

Appendix Figure 11: Synteny of genomic region of CatSper4 in goldfish and zebrafish. Conserved blocks of genes are highlighted in yellow, magenta, and cyan. Colored lines connect orthologous genes conserved between species. Goldfish CatSper4 is highlighted in green and flanked by black whiskers to indicate absence of orthologues. Genomic region from first to last gene is given in Mb for each chromosome (chr).

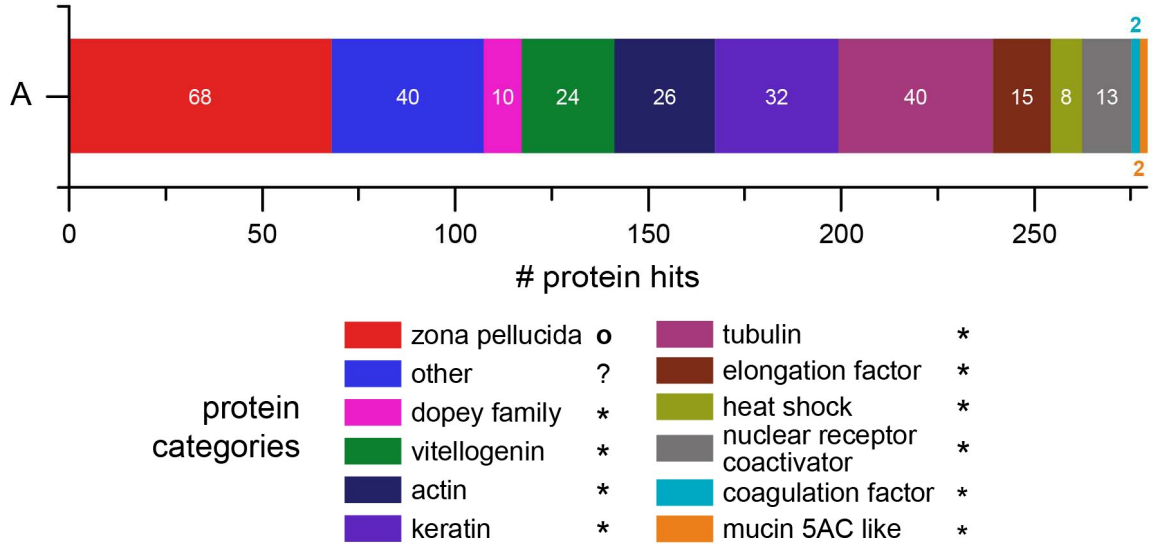

Appendix Figure 12: Categorization of protein hits found in whole-chorion samples of preparation by method A (whole ovaries, chorion obtained via trituration). Categories according to legend, symbols after the category name denote assignment: ? = potentially chorion-specific or chorion-associated protein; * = contaminant protein, originating from the oocyte itself or ovarian tissue; o = chorion-specific protein.

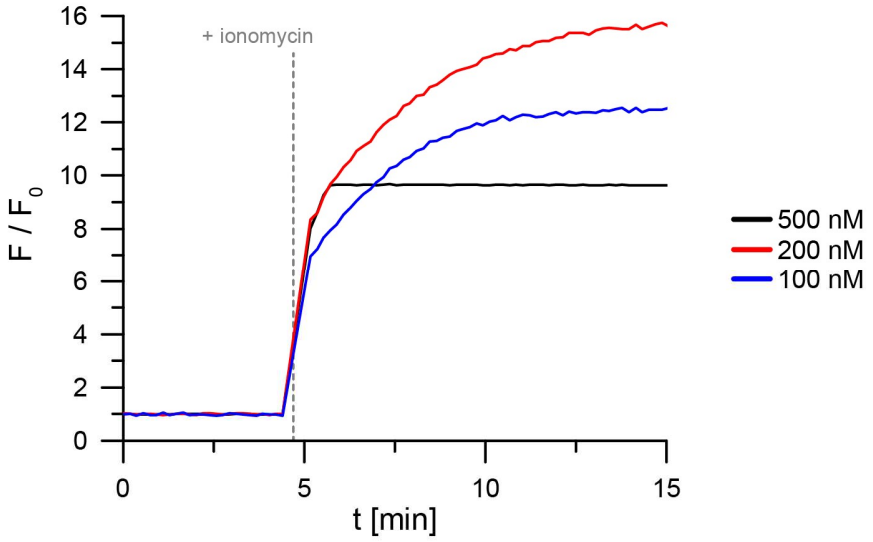

Appendix Figure 13: Fluorescence changes in CHO cells loaded with different concentrations of Calbryte520 in response to addition of ionomycin. Dye concentrations according to legend, loading time 80 min. The trace for 500 nM (black) cuts off due to saturation of the sensor.

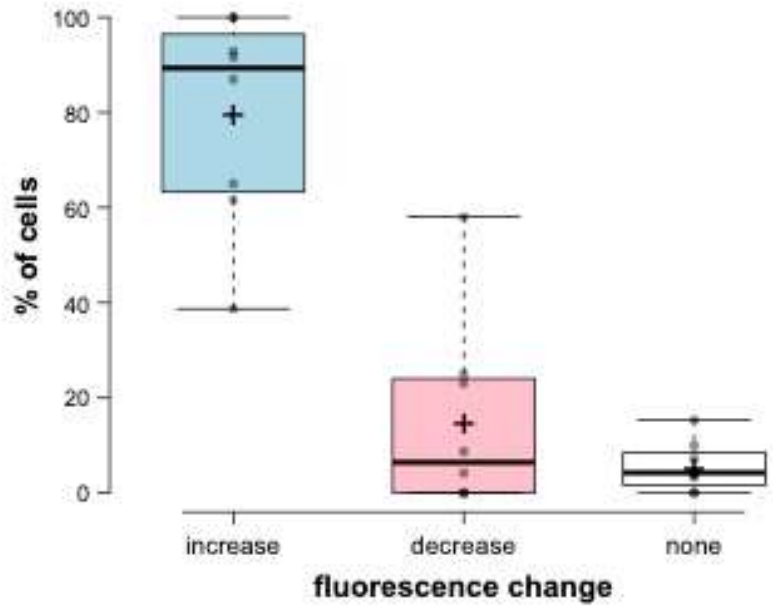

Appendix Figure 14: Boxplot showing percentages of sperm cells loaded with Calbryte520 that display a fluorescence increase, decrease, or no change, in response to activation with system water in the superfusion set-up. Data from eight experiments.

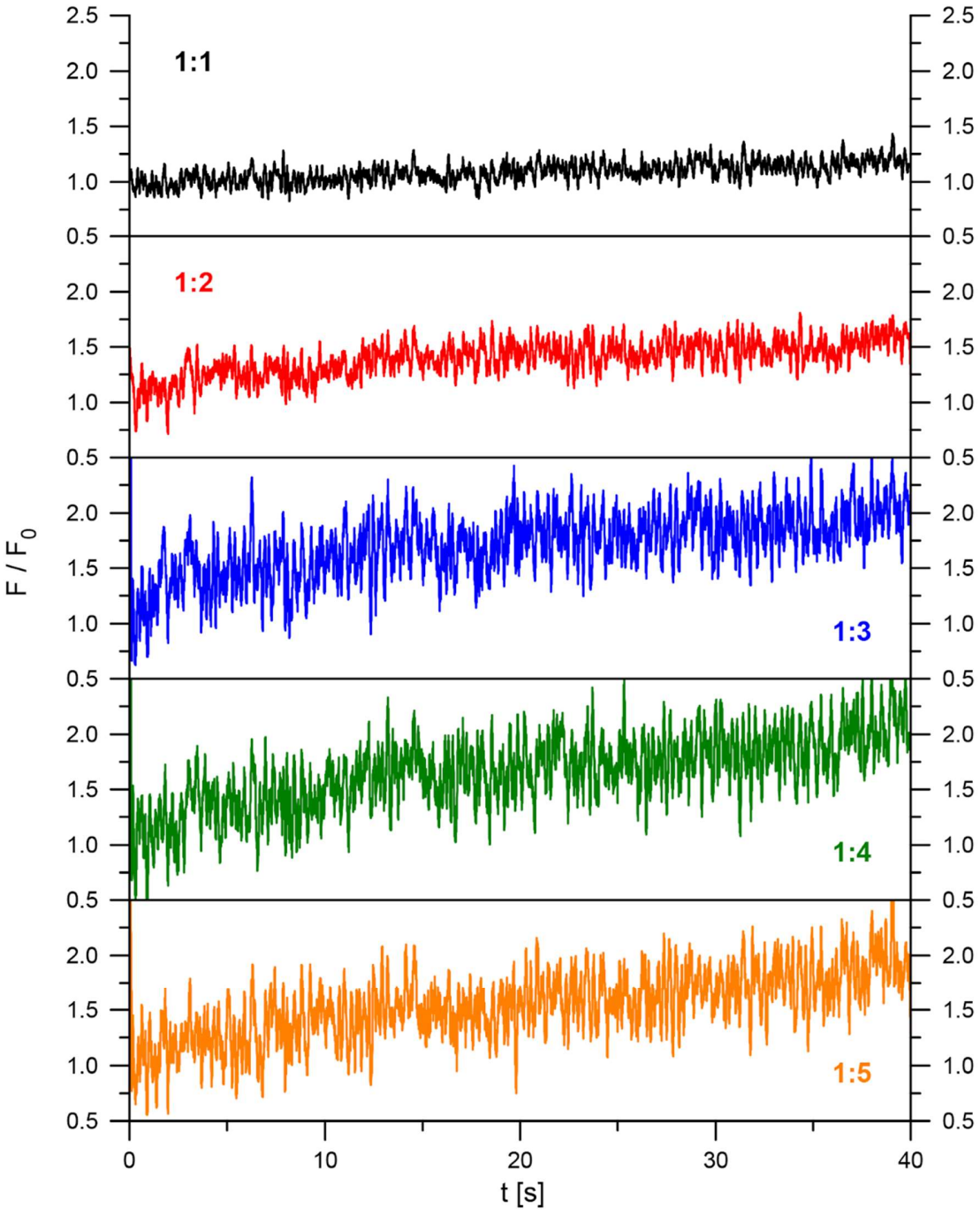

Appendix Figure 15: Fluorescence changes in zebrafish sperm loaded with Calbryte520, measured in a population measurement in the stopped-flow set-up. Immotile sperm in ES are mixed at ratios of 1:1, 1:2, 1:3, 1:4, or 1:5 with system water. Note that mixing ratios of 1:4 and 1:5 do not show further increases in fluorescence compared to 1:3.

6. References

Aird, Daniel, Michael G. Ross, Wei-Sheng Chen, Maxwell Danielsson, Timothy Fennell, Carsten Russ, David B. Jaffe, Chad Nusbaum, and Andreas Gnirke. 2011. "Analyzing and Minimizing PCR Amplification Bias in Illumina Sequencing Libraries." *Genome Biology* 12 (2): R18. https://doi.org/10.1186/gb-2011-12-2-r18.

Akbari, Arvand, Giovanni Battista Pipitone, Zahra Anvar, Mojtaba Jaafarinia, Maurizio Ferrari, Paola Carrera, and Mehdi Totonchi. 2019. "ADCY10 Frameshift Variant Leading to Severe Recessive Asthenozoospermia and Segregating with Absorptive Hypercalciuria." *Human Reproduction* 34 (6): 1155–64. https://doi.org/10.1093/humrep/dez048.

Alavi, Sayyed Mohammad Hadi, Jacky Cosson, Olga Bondarenko, and Otomar Linhart. 2019. "Sperm Motility in Fishes: (III) Diversity of Regulatory Signals from Membrane to the Axoneme." *Theriogenology* 136 (September): 143–65. https://doi.org/10.1016/j.theriogenology.2019.06.038.

Alvarez, Luis. 2017. "The Tailored Sperm Cell." *Journal of Plant Research* 130 (3): 455–64. https://doi.org/10.1007/s10265-017-0936-2.

Alvarez, Luis, Luru Dai, Benjamin M. Friedrich, Nachiket D. Kashikar, Ingo Gregor, René Pascal, and U. Benjamin Kaupp. 2012. "The Rate of Change in Ca^{2+} Concentration Controls Sperm Chemotaxis." *The Journal of Cell Biology* 196 (5): 653–63. https://doi.org/10.1083/jcb.201106096.

Amanze, D., and A. Iyengar. 1990. "The Micropyle: A Sperm Guidance System in Teleost Fertilization." *Development* 109 (2): 495–500.

Arppe, Riikka, Tuomas Näreoja, Sami Nylund, Leena Mattsson, Sami Koho, Jessica M. Rosenholm, Tero Soukka, and Michael Schäferling. 2014. "Photon Upconversion Sensitized Nanoprobes for Sensing and Imaging of pH." *Nanoscale* 6 (12): 6837–43. https://doi.org/10.1039/C4NR00461B.

Arsiccio, Andrea, Paolo Giorsello, Livio Marenco, and Roberto Pisano. 2020. "Considerations on Protein Stability During Freezing and Its Impact on the Freeze-Drying Cycle: A Design Space Approach." *Journal of Pharmaceutical Sciences* 109 (1): 464–75. https://doi.org/10.1016/j.xphs.2019.10.022.

Avella, Matteo A., Boris Baibakov, and Jurrien Dean. 2014. "A Single Domain of the ZP2 Zona Pellucida Protein Mediates Gamete Recognition in Mice and Humans." *The Journal of Cell Biology* 205 (6): 801–9. https://doi.org/10.1083/jcb.201404025.

Avella, Matteo A., Bo Xiong, and Jurrien Dean. 2013. "The Molecular Basis of Gamete Recognition in Mice and Humans." *MHR: Basic Science of Reproductive Medicine* 19 (5): 279–89. https://doi.org/10.1093/molehr/gat004.

Betancur-R, Ricardo, Richard E. Broughton, Edward O. Wiley, Kent Carpenter, J. Andrés López, Chenhong Li, Nancy I. Holcroft, et al. 2013. "The Tree of Life and a New Classification of Bony Fishes." *PLoS Currents* 5: ecurrents.tol.53ba26640df0ccaee75bb165c8c26288. https://doi.org/10.1371/currents.tol.53ba26640df0ccaee75bb165c8c26288.

Birney, Ewan, Michele Clamp, and Richard Durbin. 2004. "GeneWise and Genomewise." *Genome Research* 14 (5): 988–95. https://doi.org/10.1101/gr.1865504.

Boens, Noël, Wenwu Qin, Nikola Basarić, Angel Orte, Eva M. Talavera, and Jose M. Alvarez-Pez. 2006. "Photophysics of the Fluorescent pH Indicator BCECF." *The Journal of Physical Chemistry A* 110 (30): 9334–43. https://doi.org/10.1021/jp0615712.

Bönigk, Wolfgang, Astrid Loogen, Reinhard Seifert, Nachiket Kashikar, Clementine Klemm, Eberhard Krause, Volker Hagen, Elisabeth Kremmer, Timo Strünker, and U. Benjamin Kaupp. 2009. "An Atypical CNG Channel Activated by a Single cGMP Molecule Controls Sperm Chemotaxis." *Science Signaling* 2 (94): ra68–ra68. https://doi.org/10.1126/scisignal.2000516.

Bonsignorio, Daniele, Lucia Perego, Luca Del Giacco, and Franco Cotelli. 1996. "Structure and Macromolecular Composition of the Zebrafish Egg Chorion." *Zygote* 4 (02): 101–8.

Braasch, Ingo, Andrew R. Gehrke, Jeramiah J. Smith, Kazuhiko Kawasaki, Tereza Manousaki, Jeremy Pasquier, Angel Amores, et al. 2016. "The Spotted Gar Genome Illuminates Vertebrate Evolution and Facilitates Human-Teleost Comparisons." *Nature Genetics* 48 (4): 427–37. https://doi.org/10.1038/ng.3526.

Bradford, M. M. 1976. "A Rapid and Sensitive Method for the Quantitation of Microgram Quantities of Protein Utilizing the Principle of Protein-Dye Binding." *Analytical Biochemistry* 72 (May): 248–54. https://doi.org/10.1006/abio.1976.9999.

Brenker, Christoph, Normann Goodwin, Ingo Weyand, Nachiket D Kashikar, Masahiro Naruse, Miriam Krähling, Astrid Müller, U Benjamin Kaupp, and Timo Strünker. 2012. "The CatSper Channel: A Polymodal Chemosensor in Human Sperm." *The EMBO Journal* 31 (7): 1654–65. https://doi.org/10.1038/emboj.2012.30.

Brenker, Christoph, Yu Zhou, Astrid Müller, Fabio Andres Echeverry, Christian Trötschel, Ansgar Poetsch, Xiao-Ming Xia, et al. 2014. "The Ca2+-Activated K+ Current of Human Sperm Is Mediated by Slo3." Edited by Richard Aldrich. *eLife* 3 (March): e01438. https://doi.org/10.7554/eLife.01438.

Buffone, Mariano G., Eva V. Wertheimer, Pablo E. Visconti, and Dario Krapf. 2014. "Central Role of Soluble Adenylyl Cyclase and cAMP in Sperm Physiology." *Biochimica et Biophysica Acta (BBA) - Molecular Basis of Disease*, The role of soluble adenylyl cyclase in health and disease, 1842 (12, Part B): 2610–20. https://doi.org/10.1016/j.bbadis.2014.07.013.

Cai, Xinjiang, and David E. Clapham. 2008. "Evolutionary Genomics Reveals Lineage-Specific Gene Loss and Rapid Evolution of a Sperm-Specific Ion Channel Complex: CatSpers and CatSperβ." *PLOS ONE* 3 (10): e3569. https://doi.org/10.1371/journal.pone.0003569.

Cai, Xinjiang, and David E. Clapham. 2012. "Ancestral Ca2+ Signaling Machinery in Early Animal and Fungal Evolution." *Molecular Biology and Evolution* 29 (1): 91–100. https://doi.org/10.1093/molbev/msr149.

Cai, Xinjiang, Xiangbing Wang, and David E. Clapham. 2014. "Early Evolution of the Eukaryotic Ca2+ Signaling Machinery: Conservation of the CatSper Channel Complex." *Molecular Biology and Evolution* 31 (10): 2735–40. https://doi.org/10.1093/molbev/msu218.

Calvete, Oriol, Josefa González, Esther Betrán, and Alfredo Ruiz. 2012. "Segmental Duplication, Microinversion, and Gene Loss Associated with a Complex Inversion Breakpoint Region in Drosophila." *Molecular Biology and Evolution* 29 (7): 1875–89. https://doi.org/10.1093/molbev/mss067.

Carlisle, Jolie A., and Willie J. Swanson. 2021. "Molecular Mechanisms and Evolution of Fertilization Proteins." *Journal of Experimental Zoology Part B: Molecular and Developmental Evolution* 336 (8): 652–65. https://doi.org/10.1002/jez.b.23004.

Carter, S. B. 1967. "Haptotaxis and the Mechanism of Cell Motility." *Nature* 213 (5073): 256–60. https://doi.org/10.1038/213256a0.

Cavarocchi, Emma, Marjorie Whitfield, Ahmed Chargui, Laurence Stouvenel, Patrick Lorès, Charles Coutton, Christophe Arnoult, et al. 2021. "The Sodium/Proton Exchanger SLC9C1 (sNHE) Is Essential for Human Sperm Motility and Fertility." *Clinical Genetics* 99 (5): 684–93. https://doi.org/10.1111/cge.13927.

Chen, Yanqiu, Martin J. Cann, Tatiana N. Litvin, Vadim Iourgenko, Meeghan L. Sinclair, Lonny R. Levin, and Jochen Buck. 2000. "Soluble Adenylyl Cyclase as an Evolutionarily Conserved Bicarbonate Sensor." *Science* 289 (5479): 625–28. https://doi.org/10.1126/science.289.5479.625.

Chen, Ying, Hantsing Wang, Fang Wang, Chen Chen, Peng Zhang, Dandan Song, Tao Luo, Hong Xu, and Xuhui Zeng. 2020. "Sperm Motility Modulated by Trpv1 Regulates Zebrafish Fertilization." *Theriogenology* 151 (July): 41–51. https://doi.org/10.1016/j.theriogenology.2020.03.032.

Chen, Zelin, Yoshihiro Omori, Sergey Koren, Takuya Shirokiya, Takuo Kuroda, Atsushi Miyamoto, Hironori Wada, et al. 2019. "De Novo Assembly of the Goldfish (Carassius Auratus</Em>) Genome and the Evolution of Genes after Whole-Genome Duplication." *Science Advances* 5 (6): eaav0547. https://doi.org/10.1126/sciadv.aav0547.

Chow, Sue, David Hedley, and Ian Tannock. 1996. "Flow cytometric calibration of intracellular pH measurements in viable cells using mixtures of weak acids and bases." *Cytometry* 24 (4): 360–67. https://doi.org/10.1002/(SICI)1097-0320(19960801)24:4<360::AID-CYTO7>3.0.CO;2-J.

Chung, J. J., K. Miki, D. Kim, S. H. Shim, H. F. Shi, J. Y. Hwang, X. Cai, Y. Iseri, X. Zhuang, and D. E. Clapham. 2017. "CatSperzeta Regulates the Structural Continuity of Sperm Ca(2+) Signaling Domains and Is Required for Normal Fertility." *Elife* 6 (February). https://doi.org/10.7554/eLife.23082.

Chung, J. J., B. Navarro, G. Krapivinsky, L. Krapivinsky, and D. E. Clapham. 2011. "A Novel Gene Required for Male Fertility and Functional CATSPER Channel Formation in Spermatozoa." *Nat Commun* 2 (January): 153. https://doi.org/10.1038/ncomms1153.

Chung, Jean-Ju, Sang-Hee Shim, Robert A. Everley, Steven P. Gygi, Xiaowei Zhuang, and David E. Clapham. 2014. "Structurally Distinct Ca2+ Signaling Domains of Sperm Flagella Orchestrate Tyrosine Phosphorylation and Motility." *Cell* 157 (4): 808–22. https://doi.org/10.1016/j.cell.2014.02.056.

Cosson, J., P. Huitorel, and C. Gagnon. 2003. "How Spermatozoa Come to Be Confined to Surfaces." *Cell Motility* 54 (1): 56–63. https://doi.org/10.1002/cm.10085.

Cosson, Jacky. 2004. "The Ionic and Osmotic Factors Controlling Motility of Fish Spermatozoa." *Aquaculture International* 12 (1): 69–85. https://doi.org/10.1023/B:AQUI.0000017189.44263.bc.

"Danio_rerio - Ensembl Genome Browser 109." 2023. Danio_rerio - Ensembl. March 2, 2023. https://www.ensembl.org/Danio_rerio/Info/Annotation.

Dash, S., S. K. Das, J. Samal, and H. N. Thatoi. 2018. "Epidermal Mucus, a Major Determinant in Fish Health: A Review." *Iranian Journal of Veterinary Research* 19 (2): 72–81.

Denissenko, Petr, Vasily Kantsler, David J. Smith, and Jackson Kirkman-Brown. 2012. "Human Spermatozoa Migration in Microchannels Reveals Boundary-Following Navigation." *Proceedings of the National Academy of Sciences* 109 (21): 8007–10. https://doi.org/10.1073/pnas.1202934109.

Dohrmann, Martin, and Gert Wörheide. 2017. "Dating Early Animal Evolution Using Phylogenomic Data." *Scientific Reports* 7 (1): 3599. https://doi.org/10.1038/s41598-017-03791-w.

Einarson, S. 1993. "Effects of Temperature, Seawater Osmolality and Season on Oxygen Consumption and Osmoregulation of the Amphipod Gammarus Oceanicus." *Marine Biology* 117 (4): 599–606. https://doi.org/10.1007/BF00349771.

Eisner, D. A., N. A. Kenning, S. C. O'Neill, G. Pocock, C. D. Richards, and M. Valdeolmillos. 1989. "A Novel Method for Absolute Calibration of Intracellular pH Indicators." *Pflügers Archiv* 413 (5): 553–58. https://doi.org/10.1007/BF00594188.

Esposito, Gloria, Byjay S. Jaiswal, Fang Xie, Magda A. M. Krajnc-Franken, Tamara J. A. A. Robben, Ankie M. Strik, Cor Kuil, et al. 2004. "Mice Deficient for Soluble Adenylyl Cyclase Are Infertile Because of a Severe Sperm-Motility Defect." *Proceedings of the National Academy of Sciences* 101 (9): 2993–98. https://doi.org/10.1073/pnas.0400050101.

Fechner, S., L. Alvarez, W. Bonigk, A. Muller, T. K. Berger, R. Pascal, C. Trotschel, et al. 2015. "A K(+)-Selective CNG Channel Orchestrates Ca(2+) Signalling in Zebrafish Sperm." *Elife* 4. https://doi.org/10.7554/eLife.07624.

Fechner, Sylvia. 2012. "Charakterisierung K+-selektiver zyklisch Nukleotid-gesteuerter Ionenkanäle aus Danio rerio und Branchiostoma floridae." Bonn: Rheinischen Friedrich-Wilhelms-Universität Bonn.

Fitzpatrick, John L., Ariel F. Kahrl, and Rhonda R. Snook. 2022. "SpermTree, a Species-Level Database of Sperm Morphology Spanning the Animal Tree of Life." *Scientific Data* 9 (1): 30. https://doi.org/10.1038/s41597-022-01131-w.

Froese, R., D. Pauly, and Editors. 2020. "FishBase. World Wide Web Electronic Publication."

Fukuda, Nanaho, Kentaro Yomogida, Masaru Okabe, and Kazushige Touhara. 2004. "Functional Characterization of a Mouse Testicular Olfactory Receptor and Its Role in Chemosensing and in Regulation of Sperm Motility." *Journal of Cell Science* 117 (24): 5835–45. https://doi.org/10.1242/jcs.01507.

Furuta, Y., M. Kawai, K. Yahara, N. Takahashi, N. Handa, T. Tsuru, K. Oshima, et al. 2011. "Birth and Death of Genes Linked to Chromosomal Inversion." *Proc Natl Acad Sci U S A* 108 (4): 1501–6. https://doi.org/10.1073/pnas.1012579108.

Galindo, Blanca E., Victor D. Vacquier, and Willie J. Swanson. 2003. "Positive Selection in the Egg Receptor for Abalone Sperm Lysin." *Proceedings of the National Academy of Sciences* 100 (8): 4639–43. https://doi.org/10.1073/pnas.0830022100.

Gao, Z., D. M. Ruden, and X. Lu. 2003. "PKD2 Cation Channel Is Required for Directional Sperm Movement and Male Fertility." *Curr Biol* 13 (24): 2175–78. https://doi.org/10.1016/j.cub.2003.11.053.

Gauberg, Julia, Salsabil Abdallah, Wassim Elkhatib, Alicia N. Harracksingh, Thomas Piekut, Elise F. Stanley, and Adriano Senatore. 2020. "Conserved Biophysical Features of the CaV2 Presynaptic Ca2+ Channel Homologue from the Early-Diverging Animal Trichoplax Adhaerens." *Journal of Biological Chemistry* 295 (52): 18553–78. https://doi.org/10.1074/jbc.RA120.015725.

Gert, Krista R., and Andrea Pauli. 2020. "Chapter Five - Species-Specific Mechanisms during Fertilization." In *Current Topics in Developmental Biology*, edited by Florence L. Marlow, 140:121–44. Maternal Effect Genes in Development. Academic Press. https://doi.org/10.1016/bs.ctdb.2019.10.005.

Gonzales Jr, John M. 2012. "Preliminary Evaluation on the Effects of Feeds on the Growth and Early Reproductive Performance of Zebrafish (Danio Rerio)." *Journal of the American Association for Laboratory Animal Science* 51 (4): 412–17.

Goudet, Ghylène, Sylvie Mugnier, Isabelle Callebaut, and Philippe Monget. 2008. "Phylogenetic Analysis and Identification of Pseudogenes Reveal a Progressive Loss of Zona Pellucida Genes During Evolution of Vertebrates1." *Biology of Reproduction* 78 (5): 796–806. https://doi.org/10.1095/biolreprod.107.064568.

Griffin, Frederick J., Carol A. Vines, Murali C. Pillai, Ryuzo Yanagimachi, and Gary N. Cherr. 1996. "Sperm Motility Initiation Factor Is a Minor Component of the Pacific Herring Egg Chorion." *Development, Growth & Differentiation* 38 (2): 193–202.

Guindon, Stéphane, Jean-François Dufayard, Vincent Lefort, Maria Anisimova, Wim Hordijk, and Olivier Gascuel. 2010. "New Algorithms and Methods to Estimate Maximum-Likelihood Phylogenies: Assessing the Performance of PhyML 3.0." *Systematic Biology* 59 (3): 307–21. https://doi.org/10.1093/sysbio/syq010.

Gupta, Satish Kumar. 2021. "Human Zona Pellucida Glycoproteins: Binding Characteristics With Human Spermatozoa and Induction of Acrosome Reaction." *Frontiers in Cell and Developmental Biology* 9. https://www.frontiersin.org/articles/10.3389/fcell.2021.619868.

Hagedorn, M., J. Ricker, M. McCarthy, S. A. Meyers, T. R. Tiersch, Z. M. Varga, and F. W. Kleinhans. 2009. "Biophysics of Zebrafish (Danio Rerio) Sperm." *Cryobiology* 58 (1): 12–19. https://doi.org/10.1016/j.cryobiol.2008.09.013.

Hagenacker, T., D. Ledwig, and D. Büsselberg. 2008. "Feedback Mechanisms in the Regulation of Intracellular Calcium ([Ca2+]i) in the Peripheral Nociceptive System: Role of TRPV-1 and Pain Related Receptors." *Cell Calcium* 43 (3): 215–27. https://doi.org/10.1016/j.ceca.2007.05.019.

Hamamah, Samir, and Jean-Luc Gatti. 1998. "Role of the Ionic Environment and Internal pH on Sperm Activity." *Human Reproduction* 13 (suppl_4): 20–30. https://doi.org/10.1093/humrep/13.suppl_4.20.

Hart, Nathan H., Karen A. Becker, and Joseph S. Wolenski. 1992. "The Sperm Entry Site during Fertilization of the Zebrafish Egg: Localization of Actin." *Molecular Reproduction and Development* 32 (3): 217–28. https://doi.org/10.1002/mrd.1080320306.

Hart, Nathan H., and Michael Donovan. 1983. "Fine Structure of the Chorion and Site of Sperm Entry in the Egg of Brachydanio." *Journal of Experimental Zoology* 227 (2): 277–96. https://doi.org/10.1002/jez.1402270212.

Hisaoka, K. K., and C. F. Firlit. 1962. "Ovarian Cycle and Egg Production in the Zebrafish, Brachydanio Rerio." *Copeia* 1962 (4): 788. https://doi.org/10.2307/1440680.

Ho, Han-Chen, and Susan S. Suarez. 2003. "Characterization of the Intracellular Calcium Store at the Base of the Sperm Flagellum That Regulates Hyperactivated Motility." *Biology of Reproduction* 68 (5): 1590–96. https://doi.org/10.1095/biolreprod.102.011320.

Hoo, Jing Ying, Yatinesh Kumari, Mohd Farooq Shaikh, Seow Mun Hue, and Bey Hing Goh. 2016. "Zebrafish: A Versatile Animal Model for Fertility Research." *BioMed Research International* 2016 (July): e9732780. https://doi.org/10.1155/2016/9732780.

Howe, Kerstin, Matthew D. Clark, Carlos F. Torroja, James Torrance, Camille Berthelot, Matthieu Muffato, John E. Collins, et al. 2013. "The Zebrafish Reference Genome Sequence and Its Relationship to the Human Genome." *Nature* 496: 498. https://doi.org/10.1038/nature12111 https://www.nature.com/articles/nature12111#supplementary-information.

Ingermann, R. L., C. L. F. Schultz, M. K. Kanuga, and J. G. Wilson-Leedy. 2011. "Metabolism of Motile Zebrafish Sperm." *Comparative Biochemistry and Physiology Part A: Molecular & Integrative Physiology* 158 (4): 461–67. https://doi.org/10.1016/j.cbpa.2010.12.008.

Ishimoto, Kenta. 2017. "Guidance of Microswimmers by Wall and Flow: Thigmotaxis and Rheotaxis of Unsteady Squirmers in Two and Three Dimensions." *Physical Review E* 96 (4): 043103. https://doi.org/10.1103/PhysRevE.96.043103.

Jaiswal, Deepika, Vertika Singh, U. S. Dwivedi, Sameer Trivedi, and Kiran Singh. 2014. "Chromosome Microarray Analysis: A Case Report of Infertile Brothers with CATSPER Gene Deletion." *Gene* 542 (2): 263–65. https://doi.org/10.1016/j.gene.2014.03.055.

Jekosch, Kerstin. 2004. "The Zebrafish Genome Project: Sequence Analysis and Annotation." In *Methods in Cell Biology*, 77:225–39. The Zebrafish: Genetics, Genomics, and Informatics. Academic Press. https://doi.org/10.1016/S0091-679X(04)77012-0.

Katoh, Kazutaka, Kazuharu Misawa, Kei-ichi Kuma, and Takashi Miyata. 2002. "MAFFT: A Novel Method for Rapid Multiple Sequence Alignment Based on Fast Fourier Transform." *Nucleic Acids Research* 30 (14): 3059–66. https://doi.org/10.1093/nar/gkf436.

Katoh, Kazutaka, and Daron M. Standley. 2013. "MAFFT Multiple Sequence Alignment Software Version 7: Improvements in Performance and Usability." *Molecular Biology and Evolution* 30 (4): 772–80. https://doi.org/10.1093/molbev/mst010.

Kaupp, U. B., and T. Strünker. 2017. "Signaling in Sperm: More Different than Similar." *Trends in Cell Biology* 27 (2): 101–9. https://doi.org/10.1016/j.tcb.2016.10.002.

Kendall, William Converse. 1921. *Peritoneal Membranes, Ovaries, and Oviducts of Salmonoid Fishes and Their Significance in Fish-Cultural Practices*. U.S. Government Printing Office.

Kierszenbaum, Abraham L, Eugene Rivkin, and Laura L Tres. 2007. "Molecular Biology of Sperm Head Shaping." *Soc Reprod Fertil Suppl.*, no. 65: 33–43.

Kleinboelting, Silke, Ana Diaz, Sebastien Moniot, Joop van den Heuvel, Michael Weyand, Lonny R. Levin, Jochen Buck, and Clemens Steegborn. 2014. "Crystal Structures of Human Soluble Adenylyl Cyclase Reveal Mechanisms of Catalysis and of Its Activation through Bicarbonate." *Proceedings of the National Academy of Sciences* 111 (10): 3727–32. https://doi.org/10.1073/pnas.1322778111.

Kobayashi, Makito, Peter W. Sorensen, and Norm E. Stacey. 2002. "Hormonal and Pheromonal Control of Spawning Behavior in the Goldfish." *Fish Physiology and Biochemistry* 26 (1): 71–84. https://doi.org/10.1023/A:1023375931734.

Körschen, H. G., H. Hamzeh, R. Pascal, L. Alvarez, W. Bönigk, N. Kaur, L. R. Levin, et al. 2021. "External Fertilization Is Orchestrated by a pH-Regulated Soluble Adenylyl Cyclase Controlling Sperm Motility and Chemotaxis." bioRxiv. https://doi.org/10.1101/2021.06.18.448929.

Köttgen, Michael, Alexis Hofherr, Weizhe Li, Kristy Chu, Stacey Cook, Craig Montell, and Terry Watnick. 2011. "Drosophila Sperm Swim Backwards in the Female Reproductive Tract and Are Activated via TRPP2 Ion Channels." *PLOS ONE* 6 (5): e20031. https://doi.org/10.1371/journal.pone.0020031.

Koulen, Peter, Yiqiang Cai, Lin Geng, Yoshiko Maeda, Sayoko Nishimura, Ralph Witzgall, Barbara E. Ehrlich, and Stefan Somlo. 2002. "Polycystin-2 Is an Intracellular Calcium Release Channel." *Nature Cell Biology* 4 (3): 191–97. https://doi.org/10.1038/ncb754.

Kumar, Sudhir, Glen Stecher, Michael Suleski, and S. Blair Hedges. 2017. "TimeTree: A Resource for Timelines, Timetrees, and Divergence Times." *Molecular Biology and Evolution* 34 (7): 1812–19. https://doi.org/10.1093/molbev/msx116.

Laemmli, U. K. 1970. "Cleavage of Structural Proteins during the Assembly of the Head of Bacteriophage T4." *Nature* 227 (5259): 680–85. https://doi.org/10.1038/227680a0.

Lage, Hermann. 2003. "ABC-Transporters: Implications on Drug Resistance from Microorganisms to Human Cancers." *International Journal of Antimicrobial Agents*, Efflux pumps and antibiotic resistance of microorganisms, 22 (3): 188–99. https://doi.org/10.1016/S0924-8579(03)00203-6.

Li, Xi-Yin, Xiao-Juan Zhang, Zhi Li, Wei Hong, Wei Liu, Jun Zhang, and Jian-Fang Gui. 2014. "Evolutionary History of Two Divergent Dmrt1 Genes Reveals Two Rounds of Polyploidy Origins in Gibel Carp." *Molecular Phylogenetics and Evolution* 78 (September): 96–104. https://doi.org/10.1016/j.ympev.2014.05.005.

Lieschke, Graham J., and Peter D. Currie. 2007. "Animal Models of Human Disease: Zebrafish Swim into View." *Nature Reviews Genetics* 8 (5): 353–67. https://doi.org/10.1038/nrg2091.

Lin, Shiyi, Meng Ke, Yuqi Zhang, Zhen Yan, and Jianping Wu. 2021. "Structure of a Mammalian Sperm Cation Channel Complex." *Nature* 595 (7869): 746–50. https://doi.org/10.1038/s41586-021-03742-6.

Lindemann, Charles B., and Kathleen A. Lesich. 2016. "Functional Anatomy of the Mammalian Sperm Flagellum." *Cytoskeleton* 73 (11): 652–69. https://doi.org/10.1002/cm.21338.

Lishko, P. V., Y. Kirichok, D. Ren, B. Navarro, J. J. Chung, and D. E. Clapham. 2012. "The Control of Male Fertility by Spermatozoan Ion Channels." *Annu Rev Physiol* 74: 453–75. https://doi.org/10.1146/annurev-physiol-020911-153258.

Lishko, Polina V., Inna L. Botchkina, and Yuriy Kirichok. 2011. "Progesterone Activates the Principal Ca2+ Channel of Human Sperm." *Nature* 471 (7338): 387–91. https://doi.org/10.1038/nature09767.

Lissabet, Jorge Félix Beltrán, Lisandra Herrera Belén, Manuel Lee-Estevez, Jennie Risopatrón, Iván Valdebenito, Elías Figueroa, and Jorge G. Farías. 2020. "The CatSper Channel Is Present and Plays a Key Role in Sperm Motility of the Atlantic Salmon (Salmo Salar)." *Comparative Biochemistry and Physiology Part A: Molecular & Integrative Physiology* 241 (March): 110634. https://doi.org/10.1016/j.cbpa.2019.110634.

Liu, Jin, Jingsheng Xia, Kwang-Hyun Cho, David E. Clapham, and Dejian Ren. 2007. "CatSperβ, a Novel Transmembrane Protein in the CatSper Channel Complex." *Journal of Biological Chemistry* 282 (26): 18945–52. https://doi.org/10.1074/jbc.M701083200.

Liu, Xingjun, Hai Wang, and Zhiyuan Gong. 2006. "Tandem-Repeated Zebrafish Zp3 Genes Possess Oocyte-Specific Promoters and Are Insensitive to Estrogen Induction." *Biol Reprod* 74 (6): 1016–25. https://doi.org/10.1095/biolreprod.105.049403.

Lübke, Joachim. 1993. "Photoconversion of Diaminobenzidine with Different Fluorescent Neuronal Markers into a Light and Electron Microscopic Dense Reaction Product." *Microscopy Research and Technique* 24 (1): 2–14. https://doi.org/10.1002/jemt.1070240103.

Luconi, M, and E Baldi. 2003. "How Do Sperm Swim? Molecular Mechanisms Underlying Sperm Motility." *Cellular and Molecular Biology (Noisy-Le-Grand, France)* 49 (3): 357–69.

Mansour, Ragaa T., Mohamed A. Aboulghar, Gamal I. Serour, Amal M. Abbas, and Inas Elattar. 1995. "The Life Span of Sperm Motility and Pattern in Cumulus Coculture." *Fertility and Sterility* 63 (3): 660–62. https://doi.org/10.1016/S0015-0282(16)57442-1.

Meißlitzer-Ruppitsch, Claudia, Monika Vetterlein, Herbert Stangl, Susanne Maier, Josef Neumüller, Michael Freissmuth, Margit Pavelka, and Adolf Ellinger. 2008. "Electron Microscopic Visualization of Fluorescent Signals in Cellular Compartments and Organelles by Means of DAB-Photoconversion." *Histochemistry and Cell Biology* 130 (2): 407–19. https://doi.org/10.1007/s00418-008-0429-4.

Mengerink, Kathryn J., and Victor D. Vacquier. 2001. "Glycobiology of Sperm–Egg Interactions in Deuterostomes." *Glycobiology* 11 (4): 37R-43R. https://doi.org/10.1093/glycob/11.4.37R.

Mihaljevic, Ivan, Marta Popovic, Roko Zaja, and Tvrtko Smital. 2016. "Phylogenetic, Syntenic, and Tissue Expression Analysis of Slc22 Genes in Zebrafish (Danio Rerio)." *BMC Genomics* 17 (1): 626. https://doi.org/10.1186/s12864-016-2981-y.

Miki, Kiyoshi, and David E. Clapham. 2013. "Rheotaxis Guides Mammalian Sperm." *Current Biology* 23 (6): 443–52. https://doi.org/10.1016/j.cub.2013.02.007.

Miller, Melissa R., Samuel J. Kenny, Nadja Mannowetz, Steven A. Mansell, Michal Wojcik, Sarah Mendoza, Robert S. Zucker, Ke Xu, and Polina V. Lishko. 2018. "Asymmetrically Positioned Flagellar Control Units Regulate Human Sperm Rotation." *Cell Reports* 24 (10): 2606–13. https://doi.org/10.1016/j.celrep.2018.08.016.

Miller, Melissa R., Steven A. Mansell, Stuart A. Meyers, and Polina V. Lishko. 2015. "Flagellar Ion Channels of Sperm: Similarities and Differences between Species." *Cell Calcium*, SI: Organellar Channels & Transporters, 58 (1): 105–13. https://doi.org/10.1016/j.ceca.2014.10.009.

Mold, D. E., I. F. Kim, C. M. Tsai, D. Lee, C. Y. Chang, and R. C. C. Huang. 2001. "Cluster of Genes Encoding the Major Egg Envelope Protein of Zebrafish." *Molecular Reproduction and Development* 58 (1): 4–14. https://doi.org/10.1002/1098-2795(200101)58:1<4::aid-mrd2>3.0.co;2-p.

Mold, David E., Amy E. Dinitz, and Divya R. Sambandan. 2009. "Regulation of Zebrafish Zona Pellucida Gene Activity in Developing Oocytes." *Biol Reprod* 81 (1): 101–10. https://doi.org/10.1095/biolreprod.108.071720.

Molière, Adrian, Katharina B. Beer, and Ann M. Wehman. 2022. "Dopey Proteins Are Essential but Overlooked Regulators of Membrane Trafficking." *Journal of Cell Science* 135 (7): jcs259628. https://doi.org/10.1242/jcs.259628.

Moran, Yehu, Maya Gur Barzilai, Benjamin J. Liebeskind, and Harold H. Zakon. 2015. "Evolution of Voltage-Gated Ion Channels at the Emergence of Metazoa." *Journal of Experimental Biology* 218 (4): 515–25. https://doi.org/10.1242/jeb.110270.

Morisawa, Masaaki, and Keiji Suzuki. 1980. "Osmolality and Potassium Ion: Their Roles in Initiation of Sperm Motility in Teleosts." *Science* 210 (4474): 1145–47. https://doi.org/10.1126/science.7444445.

Mundt, Nadine, Marc Spehr, and Polina V Lishko. 2018. "TRPV4 Is the Temperature-Sensitive Ion Channel of Human Sperm." Edited by Leon D Islas. *eLife* 7 (July): e35853. https://doi.org/10.7554/eLife.35853.

Nigam, Sanjay K., Kevin T. Bush, Gleb Martovetsky, Sun-Young Ahn, Henry C. Liu, Erin Richard, Vibha Bhatnagar, and Wei Wu. 2015. "The Organic Anion Transporter (OAT) Family: A Systems Biology Perspective." *Physiological Reviews* 95 (1): 83–123. https://doi.org/10.1152/physrev.00025.2013.

Nomura, Mamoru, and Victor D. Vacquier. 2006. "Proteins Associated with Soluble Adenylyl Cyclase in Sea Urchin Sperm Flagella." *Cell Motility* 63 (9): 582–90. https://doi.org/10.1002/cm.20147.

Nowicka-Bauer, Karolina, and Monika Szymczak-Cendlak. 2021. "Structure and Function of Ion Channels Regulating Sperm Motility—An Overview." *International Journal of Molecular Sciences* 22 (6): 3259. https://doi.org/10.3390/ijms22063259.

Oren-Benaroya, R., R. Orvieto, A. Gakamsky, M. Pinchasov, and M. Eisenbach. 2008. "The Sperm Chemoattractant Secreted from Human Cumulus Cells Is Progesterone." *Human Reproduction* 23 (10): 2339–45. https://doi.org/10.1093/humrep/den265.

Palumbi, S. R. 2009. "Speciation and the Evolution of Gamete Recognition Genes: Pattern and Process." *Heredity* 102 (1): 66–76. https://doi.org/10.1038/hdy.2008.104.

Pitnick, Scott S., Dave J. Hosken, and Tim R. Birkhead. 2008. *Sperm Biology: An Evolutionary Perspective*. Academic Press.

Publicover, Stephen John, Laura Cecilia Giojalas, Maria Eugenia Teves, Gisela Sofia Mendes, Machado de Oliveira, Aduen Andres Morales Garcia, Christopher Lowther Robert Barratt, and Claire Victoria Harper. 2008. "Ca2+ Signalling in the Control of Motility and Guidance in Mammalian Sperm." *Frontiers in Bioscience* 13: 5623–37.

Pujolar, J. M., and G. H. Pogson. 2011. "Positive Darwinian Selection in Gamete Recognition Proteins of Strongylocentrotus Sea Urchins." *Molecular Ecology* 20 (23): 4968–82. https://doi.org/10.1111/j.1365-294X.2011.05336.x.

Qi, H., M. M. Moran, B. Navarro, J. A. Chong, G. Krapivinsky, L. Krapivinsky, Y. Kirichok, I. S. Ramsey, T. A. Quill, and D. E. Clapham. 2007. "All Four CatSper Ion Channel Proteins Are Required for Male Fertility and Sperm Cell Hyperactivated Motility." *Proc Natl Acad Sci U S A* 104 (4): 1219–23. https://doi.org/10.1073/pnas.0610286104.

Rafati, Nima, Junfeng Chen, Amaury Herpin, Mats E. Pettersson, Fan Han, Chungang Feng, Ola Wallerman, et al. 2020. "Reconstruction of the Birth of a Male Sex Chromosome Present in Atlantic Herring." *Proceedings of the National Academy of Sciences* 117 (39): 24359–68. https://doi.org/10.1073/pnas.2009925117.

Rahman, N., J. Buck, and L. R. Levin. 2013. "pH Sensing via Bicarbonate-Regulated 'Soluble' Adenylyl Cyclase (sAC)." *Front Physiol* 4 (November): 343. https://doi.org/10.3389/fphys.2013.00343.

Ramírez-Gómez, Héctor Vicente, Vilma Jimenez Sabinina, Martín Velázquez Pérez, Carmen Beltran, Jorge Carneiro, Christopher D Wood, Idan Tuval, Alberto Darszon, and Adán Guerrero. 2020. "Sperm Chemotaxis Is Driven by the Slope of the Chemoattractant Concentration Field." Edited by Naama Barkai, Raymond E Goldstein, Jörn Dunkel, and Robert Austin. *eLife* 9 (March): e50532. https://doi.org/10.7554/eLife.50532.

Rangwala, S. H., A. Kuznetsov, V. Ananiev, A. Asztalos, E. Borodin, V. Evgeniev, V. Joukov, et al. 2021. "Accessing NCBI Data Using the NCBI Sequence Viewer and Genome Data Viewer (GDV)." *Genome Res* 31 (1): 159–69. https://doi.org/10.1101/gr.266932.120.

Ren, Dejian, Betsy Navarro, Gloria Perez, Alexander C. Jackson, Shyuefang Hsu, Qing Shi, Jonathan L. Tilly, and David E. Clapham. 2001. "A Sperm Ion Channel Required for Sperm Motility and Male Fertility." *Nature* 413 (6856): 603–9. https://doi.org/10.1038/35098027.

Ricoult, Sébastien G., Timothy E. Kennedy, and David Juncker. 2015. "Substrate-Bound Protein Gradients to Study Haptotaxis." *Frontiers in Bioengineering and Biotechnology* 3. https://www.frontiersin.org/articles/10.3389/fbioe.2015.00040.

Robbins, Nathan, Sheryl E. Koch, Michael Tranter, and Jack Rubinstein. 2012. "The History and Future of Probenecid." *Cardiovascular Toxicology* 12 (1): 1–9. https://doi.org/10.1007/s12012-011-9145-8.

Romero, F., and T. Nishigaki. 2019a. "Comparative Genomic Analysis Suggests That the Sperm-Specific Sodium/Proton Exchanger and Soluble Adenylyl Cyclase Are Key Regulators of CatSper among the Metazoa." *Zoological Lett* 5: 25. https://doi.org/10.1186/s40851-019-0141-3.

Romero, Francisco, and Takuya Nishigaki. 2019b. "Comparative Genomic Analysis Suggests That the Sperm-Specific Sodium/Proton Exchanger and Soluble Adenylyl Cyclase Are Key Regulators of CatSper among the Metazoa." *Zoological Letters* 5 (1): 25. https://doi.org/10.1186/s40851-019-0141-3.

Roskov, Y., G. Ower, T. Orrell, D. Nicolson, N. Bailly, P.M. Kirk, T. Bourgoin, et al. 2021. "Species 2000 & ITIS Catalogue of Life, 25th March 2019. Digital Resource at Www.Catalogueoflife.Org/Col. Species 2000: Naturalis, Leiden, the Netherlands." 2021. http://www.catalogueoflife.org/col.

Sáez-Espinosa, Paula, Cristina Franco-Esclapez, Laura Robles-Gómez, Willian T. A. F. Silva, Alejandro Romero, Simone Immler, and María José Gómez-Torres. 2022. "Morphological and Ultrastructural Alterations of Zebrafish (Danio Rerio) Spermatozoa after Motility Activation." *Theriogenology* 188 (August): 108–15. https://doi.org/10.1016/j.theriogenology.2022.05.025.

Saggiorato, Guglielmo, Luis Alvarez, Jan F. Jikeli, U. Benjamin Kaupp, Gerhard Gompper, and Jens Elgeti. 2017. "Human Sperm Steer with Second Harmonics of the Flagellar Beat." *Nature Communications* 8 (1): 1415. https://doi.org/10.1038/s41467-017-01462-y.

Scalzitti, Nicolas, Anne Jeannin-Girardon, Pierre Collet, Olivier Poch, and Julie D. Thompson. 2020. "A Benchmark Study of Ab Initio Gene Prediction Methods in Diverse Eukaryotic Organisms." *BMC Genomics* 21 (1): 293. https://doi.org/10.1186/s12864-020-6707-9.

Scannell, Devin R., Kevin P. Byrne, Jonathan L. Gordon, Simon Wong, and Kenneth H. Wolfe. 2006. "Multiple Rounds of Speciation Associated with Reciprocal Gene Loss in Polyploid Yeasts." *Nature* 440 (7082): 341–45. https://doi.org/10.1038/nature04562.

Schindelin, Johannes, Ignacio Arganda-Carreras, Erwin Frise, Verena Kaynig, Mark Longair, Tobias Pietzsch, Stephan Preibisch, et al. 2012. "Fiji: An Open-Source Platform for Biological-Image Analysis." *Nature Methods* 9 (7): 676–82. https://doi.org/10.1038/nmeth.2019.

Schneider, Caroline A., Wayne S. Rasband, and Kevin W. Eliceiri. 2012. "NIH Image to ImageJ: 25 Years of Image Analysis." *Nature Methods* 9 (7): 671–75. https://doi.org/10.1038/nmeth.2089.

Schwarz, Jan, and Michael Sixt. 2016. "Quantitative Analysis of Dendritic Cell Haptotaxis." *Methods in Enzymology* 570: 567–81. https://doi.org/10.1016/bs.mie.2015.11.004.

Seifert, Reinhard, Melanie Flick, Wolfgang Bönigk, Luis Alvarez, Christian Trötschel, Ansgar Poetsch, Astrid Müller, et al. 2015. "The CatSper Channel Controls Chemosensation in Sea Urchin Sperm." *The EMBO Journal* 34 (3): 379–92. https://doi.org/10.15252/embj.201489376.

Siu, Karen K., Vitor Hugo B. Serrão, Ahmed Ziyyat, and Jeffrey E. Lee. 2021. "The Cell Biology of Fertilization: Gamete Attachment and Fusion." *Journal of Cell Biology* 220 (10): e202102146. https://doi.org/10.1083/jcb.202102146.

Smith, P. K., R. I. Krohn, G. T. Hermanson, A. K. Mallia, F. H. Gartner, M. D. Provenzano, E. K. Fujimoto, N. M. Goeke, B. J. Olson, and D. C. Klenk. 1985. "BCA Protein Assay." *Anal Biochem* 150: 76–85.

Solzin, Johannes, Annika Helbig, Qui Van, Joel E. Brown, Eilo Hildebrand, Ingo Weyand, and U. Benjamin Kaupp. 2004. "Revisiting the Role of H+ in Chemotactic Signaling of Sperm." *Journal of General Physiology* 124 (2): 115–24. https://doi.org/10.1085/jgp.200409030.

Spargo, Scott C., and Rory M. Hope. 2003. "Evolution and Nomenclature of the Zona Pellucida Gene Family." *Biology of Reproduction* 68 (2): 358–62. https://doi.org/10.1095/biolreprod.102.008086.

Stout, Carla C., Milton Tan, Alan R. Lemmon, Emily Moriarty Lemmon, and Jonathan W. Armbruster. 2016. "Resolving Cypriniformes Relationships Using an Anchored Enrichment Approach." *BMC Evolutionary Biology* 16 (1): 244. https://doi.org/10.1186/s12862-016-0819-5.

Strünker, T., L. Alvarez, and U. B. Kaupp. 2015. "At the Physical Limit — Chemosensation in Sperm." *Current Opinion in Neurobiology* 34: 110–16. http://dx.doi.org/10.1016/j.conb.2015.02.007.

Strünker, Timo, Normann Goodwin, Christoph Brenker, Nachiket D. Kashikar, Ingo Weyand, Reinhard Seifert, and U. Benjamin Kaupp. 2011. "The CatSper Channel Mediates Progesterone-Induced Ca2+ Influx in Human Sperm." *Nature* 471 (7338): 382–86. https://doi.org/10.1038/nature09769.

Swanson, Willie J., and Victor D. Vacquier. 2002. "The Rapid Evolution of Reproductive Proteins." *Nature Reviews Genetics* 3 (2): 137–44. https://doi.org/10.1038/nrg733.

Takai, H., and M. Morisawa. 1995. "Change in Intracellular K+ Concentration Caused by External Osmolality Change Regulates Sperm Motility of Marine and Freshwater Teleosts." *Journal of Cell Science* 108 (3): 1175–81.

The UniProt Consortium. 2021. "UniProt: The Universal Protein Knowledgebase in 2021." *Nucleic Acids Research* 49 (D1): D480–89. https://doi.org/10.1093/nar/gkaa1100.

Thomas, Paul, and Stanley Meizel. 1988. "An Influx of Extracelluar Calcium Is Required for Initiation of the Human Sperm Acrosome Reaction Induced by Human Follicular Fluid." *Gamete Research* 20 (4): 397–411. https://doi.org/10.1002/mrd.1120200402.

Treangen, Todd J., and Steven L. Salzberg. 2012. "Repetitive DNA and Next-Generation Sequencing: Computational Challenges and Solutions." *Nature Reviews Genetics* 13 (1): 36–46. https://doi.org/10.1038/nrg3117.

Tresguerres, Martin, Scott K. Parks, Eric Salazar, Lonny R. Levin, Greg G. Goss, and Jochen Buck. 2010. "Bicarbonate-Sensing Soluble Adenylyl Cyclase Is an Essential Sensor for Acid/Base Homeostasis." *Proceedings of the National Academy of Sciences* 107 (1): 442–47. https://doi.org/10.1073/pnas.0911790107.

Tsaur, S C, and C I Wu. 1997. "Positive Selection and the Molecular Evolution of a Gene of Male Reproduction, Acp26Aa of Drosophila." *Molecular Biology and Evolution* 14 (5): 544–49. https://doi.org/10.1093/oxfordjournals.molbev.a025791.

Tsien, R. Y. 1981. "A Non-Disruptive Technique for Loading Calcium Buffers and Indicators into Cells." *Nature* 290 (5806): 527–28. https://doi.org/10.1038/290527a0.

Tyler, Albert. 1953. "Prolongation of Life-Span of Sea Urchin Spermatozoa, and Improvement of the Fertilization-Reaction, by Treatment of Spermatozoa and Eggs with Metal-Chelating Agents (Amino Acids, Versene, Dedtc, Oxine, Cupron)." *The Biological Bulletin*, April. https://doi.org/10.2307/1538796.

Vyklicka, Lenka, and Polina V. Lishko. 2020. "Dissecting the Signaling Pathways Involved in the Function of Sperm Flagellum." *Current Opinion in Cell Biology* 63 (April): 154–61. https://doi.org/10.1016/j.ceb.2020.01.015.

Wachten, D., J. F. Jikeli, and U. B. Kaupp. 2017. "Sperm Sensory Signaling." *Cold Spring Harb Perspect Biol* 9 (7). https://doi.org/10.1101/cshperspect.a028225.

Wang, Haikun, Jin Liu, Kwang-Hyun Cho, and Dejian Ren. 2009. "A Novel, Single, Transmembrane Protein CATSPERG Is Associated with CATSPER1 Channel Protein." *Biol Reprod* 81 (3): 539–44. https://doi.org/10.1095/biolreprod.109.077107.

Wang, Huafeng, Luke L. McGoldrick, and Jean-Ju Chung. 2021. "Sperm Ion Channels and Transporters in Male Fertility and Infertility." *Nature Reviews Urology* 18 (1): 46–66. https://doi.org/10.1038/s41585-020-00390-9.

Wang, Yajun, and Wei Ge. 2004. "Developmental Profiles of Activin betaA, betaB, and Follistatin Expression in the Zebrafish Ovary: Evidence for Their Differential Roles during Sexual Maturation and Ovulatory Cycle." *Biology of Reproduction* 71 (6): 2056–64. https://doi.org/10.1095/biolreprod.104.032649.

Ward, Cynthia R., and Gregory S. Kopf. 1993. "Molecular Events Mediating Sperm Activation." *Developmental Biology* 158 (1): 9–34. https://doi.org/10.1006/dbio.1993.1165.

Ward, Gary E., Charles J. Brokaw, David L. Garbers, and Victor D. Vacquier. 1985. "Chemotaxis of Arbacia Punctulata Spermatozoa to Resact, a Peptide from the Egg Jelly Layer." *The Journal of Cell Biology* 101 (6): 2324–29.

Wassarman, Paul M., and Eveline S. Litscher. 2018. "Chapter Ten - The Mouse Egg's Zona Pellucida." In *Current Topics in Developmental Biology*, edited by Eveline S. Litscher and Paul M. Wassarman, 130:331–

56. Extracellular Matrix and Egg Coats. Academic Press. https://doi.org/10.1016/bs.ctdb.2018.01.003.

Westerfield, M. 2007. *THE ZEBRAFISH BOOK, 5th Edition; A Guide for the Laboratory Use of Zebrafish (Danio Rerio)*. 5th ed. Eugene: Univ. of Oregon Press.

Wieder, E. D., H. Hang, and M. H. Fox. 1993. "Measurement of Intracellular pH Using Flow Cytometry with Carboxy-SNARF-1." *Cytometry* 14 (8): 916–21. https://doi.org/10.1002/cyto.990140810.

Wilson-Leedy, J. G., M. K. Kanuga, and R. L. Ingermann. 2009. "Influence of Osmolality and Ions on the Activation and Characteristics of Zebrafish Sperm Motility." *Theriogenology* 71 (7): 1054–62. https://doi.org/10.1016/j.theriogenology.2008.11.006.

Wilson-Leedy, Jonas G., and Rolf L. Ingermann. 2007. "Development of a Novel CASA System Based on Open Source Software for Characterization of Zebrafish Sperm Motility Parameters." *Theriogenology* 67 (3): 661–72. https://doi.org/10.1016/j.theriogenology.2006.10.003.

Wobig, Lea, Thérèse Wolfenstetter, Sylvia Fechner, Wolfgang Bönigk, Heinz G. Körschen, Jan F. Jikeli, Christian Trötschel, et al. 2020. "A Family of Hyperpolarization-Activated Channels Selective for Protons." *Proceedings of the National Academy of Sciences* 117 (24): 13783. https://doi.org/10.1073/pnas.2001214117.

Wu, Tianli, Yunying Cheng, Zhilong Liu, Wenjing Tao, Shuqing Zheng, and Deshou Wang. 2018. "Bioinformatic Analyses of Zona Pellucida Genes in Vertebrates and Their Expression in Nile Tilapia." *Fish Physiology and Biochemistry* 44 (2): 435–49. https://doi.org/10.1007/s10695-017-0434-4.

Yanagimachi, R., G. Cherr, T. Matsubara, T. Andoh, T. Harumi, C. Vines, M. Pillai, et al. 2013. "Sperm Attractant in the Micropyle Region of Fish and Insect Eggs." *Biol Reprod* 88 (2): 47. https://doi.org/10.1095/biolreprod.112.105072.

Yanagimachi, R., Gary N. Cherr, Muralidharan C. Pillai, and John D. Baldwin. 1992. "Factors Controlling Sperm Entry into the Micropyles of Salmonid and Herring Eggs." *Development, Growth & Differentiation* 34 (4): 447–61.

Yanagimachi, Ryuzo, Tatsuo Harumi, Hajime Matsubara, Wei Yan, Shuiqiao Yuan, Noritaka Hirohashi, Tomohiro Iida, et al. 2017. "Chemical and Physical Guidance of Fish Spermatozoa into the Egg through the Micropyle†,‡." *Biol Reprod* 96 (4): 780–99. https://doi.org/10.1093/biolre/iox015.

Yang, Ziheng. 1994. "Statistical Properties of the Maximum Likelihood Method of Phylogenetic Estimation and Comparison With Distance Matrix Methods." *Systematic Biology* 43 (3): 329–42. https://doi.org/10.1093/sysbio/43.3.329.

Yuan, Shiaulou, Lu Zhao, Martina Brueckner, and Zhaoxia Sun. 2015. "Intraciliary Calcium Oscillations Initiate Vertebrate Left-Right Asymmetry." *Current Biology* 25 (5): 556–67. https://doi.org/10.1016/j.cub.2014.12.051.

Zang, Liqing, Vincenzo Torraca, Yasuhito Shimada, and Norihiro Nishimura. 2022. "Editorial: Zebrafish Models for Human Disease Studies." *Frontiers in Cell and Developmental Biology* 10. https://www.frontiersin.org/articles/10.3389/fcell.2022.861941.

Zempo, Buntaro, Natsuko Tanaka, Eriko Daikoku, and Fumihito Ono. 2021. "High-Speed Camera Recordings Uncover Previously Unidentified Elements of Zebrafish Mating Behaviors Integral to Successful Fertilization." *Scientific Reports* 11 (1): 20228. https://doi.org/10.1038/s41598-021-99638-6.

Zhang, Linli, Shuai Wang, Wei Chen, Bing Hu, Shakeeb Ullah, Qian Zhang, Yuan Le, et al. 2014. "Fine Structure of Zebrafish (Danio Rerio) Spermatozoa." *Pak Vet J*.

Zhang, Tiantian, Anna Isayeva, Serean L. Adams, and David M. Rawson. 2005. "Studies on Membrane Permeability of Zebrafish (Danio Rerio) Oocytes in the Presence of Different Cryoprotectants." *Cryobiology* 50 (3): 285–93. https://doi.org/10.1016/j.cryobiol.2005.02.007.